DEVELOPMENT OF A NANOPARTICLE-BASED SYSTEM FOR IMAGING AND TARGETED THERAPEUTIC DELIVERY TO TUMOR CELLS

By

Ralph Adam Smith

Dissertation

Submitted to the Faculty of the

Graduate School of Vanderbilt University

in partial fulfillment of the requirements

for the degree of

DOCTOR OF PHILOSOPHY

in

Biomedical Engineering

May, 2006

Nashville, Tennessee

Approved:

Todd Giorgio

Frederick Haselton

E. Duco Jansen

J. Oliver McIntyre

Ian Tomlinson

TABLE OF CONTENTS

Page

LIST OF FIGURES

LIST OF TABLES

CHAPTER I

INTRODUCTION

1.1 Significance

Selective targeting of damaged or diseased cells is a concept with great potential to revolutionize the manner in which effective therapies are administered. Many current treatments are administered systematically, allowing the therapy equal access to both target and nontarget cells throughout the entire body. The introduction of contrast agents for clinical imaging and biosensing approaches is similarly constrained by ubiquitous systemic delivery, resulting in high background noise and reduced sensitivity. Targeting of imaging approaches and/or therapies to specific cell types, however, has the potential to deliver high concentrations to specific tissues, enabling sensitive detection and diagnostics as well as therapies that minimize collateral damage to nontarget cells. Several targeting strategies, including magnetic and ligand-receptor interactions, have been employed to achieve this goal both *in vitro* and *in vivo* (1). Many recent studies have focused specifically on ligand-receptor interactions (2) or structural modification by enzymes (3,4) to achieve specific action. The work presented here describes a hybrid approach designed to impart increased target sensitivity and to overcome the limitations of single-modality targeting methods.

Nanoparticles confer multiple advantages to tissue-specific targeting not available with molecular structures alone. Prominent among these is the flexibility offered by physical characteristics of the nanoparticle base. As particle size strongly affects tissue

biodistribution, the small physical size of the NP base allows the construct to retain much of the interstitial mobility that is characteristic of molecular structures. However, fine control over optical and chemical properties (for imaging and biosensing applications) and surface chemistry (for attachment of active molecules) is possible in the synthesis of nanoparticles, allowing the formulation of a multitude of populations with distinct characteristics (2,3). The attachment of multiple bioactive molecules and the capability for colocalization of different targeting agents further extends the capability of the nanoparticle format, enabling the creation of multifunctional nanoprobes and multivalent target interaction. The combination of optical properties and differing surface chemistries results in a modular format, enabling the development of nanoprobes that can be customized to suit the specific target, imaging or sensing format, or treatment modality.

Beyond the physical and chemical characteristics of the construct, appropriate selection of the target antigen is vital to the success of any targeting approach. As targeted constructs typically interact directly with surface proteins, the efficacy of tissue-specific delivery is strongly modulated by the relative concentration of the target. Ideal candidate molecules are expressed only on target cells or within the target tissue. While appropriate for *in vitro* applications in which experimental conditions can be tightly controlled, this caveat is predictably demanding when applied to complex *in vivo* systems. In these instances, the target antigens are often overexpressed in target tissue relative to normal tissues. This differential expression affords the opportunity for successful selective targeting. However, target expression, especially *in vivo*, can be modulated by a number of environmental factors including cytokine exposure and

physical cellular damage. Due to these constraints, and others, prior knowledge of target expression is required to reliably select suitable targeting agents and to predict the success of any targeting approach. Further quantitative evaluation of native and modulated expression of a particular target antigen can be instrumental in assessing the improvement in therapeutic index provided by a specific approach. Chapter 2 of this dissertation describes the analysis of one such target receptor in an *in vitro* environment and explores the advantages of quantitative target analysis relevant to targeted delivery.

Once the target antigen has been selected, appropriate targeting elements must be implemented to mediate specific interaction with the target site. Often, small molecule and peptide ligands have been employed to mediate these specific environmental interactions. However, conjugation of molecules to the particle surface can alter both the activity of the ligand and the characteristics of the base particle, often in unpredictable ways. Thus, incorporation of these ligands into nanoparticle constructs has not yet seen widespread application. Nonetheless, new conjugation approaches enable the synthesis of nanoparticle constructs that retain both the bioactivity of the attached ligands and the properties of the underlying nanostructure. Chapter 3 details the synthesis and in vitro analysis of one such construct and highlights the utility of specific ligand interactions in targeting nanoparticles to cellular proteins.

One historic drawback to the use of molecular targeting agents, even when operating with ideal target receptors, is target binding specificity. Previous approaches using a range of small molecule and peptide targeting agents have been plagued by nonspecific interaction with nontarget tissues and specific binding to nontarget tissues that express the antigen target. One approach to limit these interactions is modification

of the construct surface with PEG polymers. The effectiveness of PEG in reducing nonspecific interactions has been well documented, and has been utilized in several commercial therapies (*e.g.* Neulasta™, PEG-INTRON®, Somavert®). One variation of this approach (described in detail in Chapter 4) is the application of a cleavable passive PEG "mask" to the targeting construct. In the absence of specific enzymatic activity, the targeting construct appears as a PEGylated nanoparticle with low nonspecific recognition. Specific proteolytic modification can then be harnessed to unmask the construct, thus removing the passivating PEG layer and activating the previously concealed targeting system.

To achieve maximal target selectivity of the envisioned proximity activated targeting (PAT) construct (described in the *Future Work* section of this document), *both* targeting elements (specific enzyme activity and target protein expression) must be simultaneously present to effect specific interaction of the ligand with the target tissue. In this system, initial proteolytic cleavage and liberation of the passivating PEG layer enables access to the peptide targeting agent previously concealed near the NP surface. Once unmasked, the targeting ligand can then participate in specific binding interactions with target proteins in the area. Thus, the colocalization of two distinct, but separate, targeting mechanisms greatly reduces the probability of construct interaction with nontarget sites.

The approaches developed in this work have the potential to establish a NP targeting system with the sensitivity, efficacy, and modularity previously unavailable in similar targeting strategies. The multi-layer targeting strategy employed in this system integrates the advantages of multiple targeting approaches while implementing measures

to overcome their various limitations. The ease of detection (via fluorescence) make the model system described here a powerful and readily accessible detection alternative. In addition, the inherent construct modularity enables customization of the targeting system to adapt to different targets, detection modalities, and delivery strategies. These advancements have the potential to provide a versatile system capable of providing features for targeted binding, imaging, biosensing, and therapeutic payload delivery in a single nanoscale particle.

1.2 Specific Aims

Aim I – Characterize peptide and receptor properties and interactions in *in vitro* cellular models.

I have completed a detailed quantitative study of the CD13 (aminopeptidase N) protein on the surface of HT-1080 cells *in vitro*. Cell surface proteins were labeled with fluorescently tagged mAbs and results quantified via flow cytometry. Native receptor density as well as the kinetic cellular response to sublethal radiation doses and endogenous cytokines TNF-α and TGF-β1 were measured and quantified to provide a more complete portrait of the CD13 protein under neoplastic conditions.

Aim II – Characterize NP-linked ligand binding to target cellular receptors in *in vitro* tissue models.

I have synthesized a mobile NP construct capable of specific binding to proteins on the surface of tumor cells. The effects of surface modification on NPs were studied, including the effects of PEG coating and ligand attachment. To enable specific targeting, a peptide (CNGRC) recognizing the CD13 receptor was conjugated to the NP surface.

NP-ligand binding was visually assessed by fluorescence microscopy, with subsequent quantitative analysis flow cytometry. A new method was also developed and applied to calibrate flow cytometry fluorescence measurements for quantitative analysis of NP binding to the cell surface.

Aim III – Investigate NP-linked tumor-specific cleavable construct in *in vitro* models.

I have developed a NP construct capable of modification by enzymes in the local tumor environment. Successful synthesis and specific cleavage of a PEG-peptide$_{MMP7}$-PEG proximity activated (PA) proteolytic peptide construct was demonstrated in an *in vitro* environment. Based on this evidence, a NP-PA construct capable of specific cleavage by the MMP-7 enzyme was developed, synthesized, and characterized. Quantitative measurements and analysis of construct performance were assessed by gel electrophoresis and fluorescence spectroscopy.

1.3 Background and Significance

Despite the substantial resources allotted to cancer study and prevention each year, an estimated 1.3 million people in the United States will be diagnosed in 2004, with over 560,000 deaths attributable to the disease (5). On top of the immense cost to human life, the NIH estimates $64,200,000,000 in direct medical costs for cancer treatment in 2004 (5). The continued prevalence of cancer diagnosis and death, as well as the soaring medical costs associated with cancer management, demand new efforts to develop novel detection and treatment strategies. Current anti-tumor chemotherapeutic agents are plagued by inherent shortcomings, including rapid clearance of the agents from the blood circulation, poor distribution to tumor sites, and toxic side effects on normal tissues. We

employ several elements of nanoscale particle design to overcome limitations of conventional cancer detection, reporting, and treatment, and to facilitate strategies to significantly reduce morbidity associated with the disease.

1.3.1 Treatment Strategies are Limited by Tissue Biodistribution

The *in vivo* distribution pattern of macromolecules and NPs is a major obstacle limiting the design and implementation of particulate drug delivery systems. NP delivery *in vivo* is limited on both circulation and a tissue levels. Particle diameter variation within the nanoscale range strongly affects both the blood circulation time as well as the bioavailability of particles within the body (6-8). Mechanical filtration in the pulmonary capillary beds and the superficial and juxtamedullary glomerular tissue of the kidney limits the maximum particle diameter to less than 3μm, although particle trapping is significant with diameters above 1μm (9). Endocytosis or other removal by immune or humoral response also modulates circulation duration and must be considered in particle design (10,11). To achieve systemic interrogation, the construct must be capable of cardiovascular extravasation and subsequent tissue transport of at least 50% of the average intercapillary distance. Thus, construct mobility must be on the order of 50μm or less for most tissues.

1.3.2 Smaller Particles for Ubiquitous Tissue Delivery

Particle diameter strongly modulates tissue biodistribution. Generally, particles in the nanoscale range are preferable, as their small diameter allows transport through size restrictive structures in all physiological compartments. *In vitro*, particle size

significantly affects cellular and tissue uptake, and in some cells only submicron size particles are taken up efficiently but not larger size microparticles (12). *In vivo*, structures as large as 70nm have been observed to passively move through the interstitial space. Furthermore, the diffusion of nanoscale structures 10-20nm in size in tumor tissue of varying densities is sufficient to move the structures from 400-800μm over the course of one hour (13).

Semiconductor QD nanocrystals coated with an amphiphilic polymer vary in diameter from 2 to 7nm, while PEG surface modification contributes an additional 7 to 21nm to the QD diameter, depending on molecular weight (14). Thus, total construct diameter is predicted to range from 9 to 28nm. Molecular flexibility and relatively low surface concentration of the PEG, however, provide a deformable layer surrounding the rigid nanocrystal core, decreasing the effective particle diameter and improving biotransport through size restrictive structures. The overall diameter of PAT NPs presumably allows their implementation as a versatile delivery construct, capable of significant interstitial mobility and intracellular trafficking.

1.3.3 Therapeutic Efficacy is Limited by Nonspecific Delivery of Therapeutics

For more than five decades, chemotherapy has been the main modality for systemic treatment of advanced and metastatic cancers (15). However, therapeutic approaches to cancer treatment are often limited by intrinsic or acquired multidrug resistance of tumor cells and toxicity caused by nonspecific delivery of chemotherapeutics to normal cells (16). Administration of bolus systemic doses of highly potent drugs to overcome these obstacles often triggers side-effects so intense that

patients must discontinue therapy before the drugs have a chance to eradicate the cancer (17). The current generation of targeted therapies has not yet solved this issue, as highly specific targeting of existing tumors and emerging neoplasia through a single recognition mechanism has not generally been successful (18,19). Nonspecific binding and specific binding to nontarget tissues compromise the therapeutic index of small molecule, ubiquitous cancer targeting ligands and limit their applicability and efficiency as primary chemotherapeutic agents.

1.3.4 Enhanced Specific Delivery Towards Improved Treatment/Outcomes

Increased distribution of therapeutics to target areas can occur by direct injection of the therapeutic construct into the tumor volume or by increased specific targeting of the construct to the tumor. Enhanced delivery and distribution of therapeutics within the tumor volume can be achieved by both passive and active targeting principles.

Passive targeting reduces the nonspecific interaction with nontarget sites such as the RES, while active targeting involves increasing the affinity of the delivery system for the target site. PAT delivery systems are intended to minimize undesirable interactions with nontarget tissues via a passivating hydrophilic PEG surface coating. This coating serves to limit recognition and clearance by the RES and other nontarget cells as well as to protect the inner construct and payload from enzymatic degradation. PAT systems also employ two levels of active targeting (cleavage by MMP-7 and specific targeting of the CD13 receptor by the NGR peptide) to maximize specific binding to target tissue. This two-layer targeted system increases the effective sensitivity of the construct by keeping the passive PEG coating intact and revealing the targeting ligand only in the

immediate proximity of the tumor (Figure 1.1). Thus, PAT constructs are expected to achieve greater target selectivity over both conventional and single-modality targeted chemotherapeutics.

1.3.5 Prior Evidence of Molecular Targeting of Nanoparticles

Enhanced targeting of intravascularly delivered NPs has been reported in several recent publications. Passive targeting of QDs in mice is detailed by the work of Ballou *et al.* (20). This study suggests that manipulation of NP surface coating can control both serum lifetime and the pattern of tissue deposition *in vivo*. In particular, long-chain PEG surface coatings (MW = 5 kDa) were found to be superior to shorter PEGs at reducing nonspecific uptake of NPs by the RES and binding to nontarget tissues such as the liver, lungs, and spleen. However, Ballou *et al.* incorporate no active targeting measures into the NPs studied here, nor do they demonstrate a propensity for these NPs to accumulate preferentially in tumor tissue.

Oyewumi *et al.* offered additional evidence of passive targeting by studying the biodistribution and tumor retention of folate-PEG coated NPs (21). These particles were shown to exhibit prolonged blood retention properties indicating reduced uptake by the RES. Additionally, significant NP retention was seen in the liver, spleen, and lungs. However, it is unclear whether this accumulation was due to mechanical filtration or nonspecific interaction as the NPs utilized were on the order of 100nm in diameter. Biodistribution studies indicate that any tumor accumulation was likely due to passive targeting, as the active targeting component (folate ligand) demonstrated no benefit over passive PEG coatings.

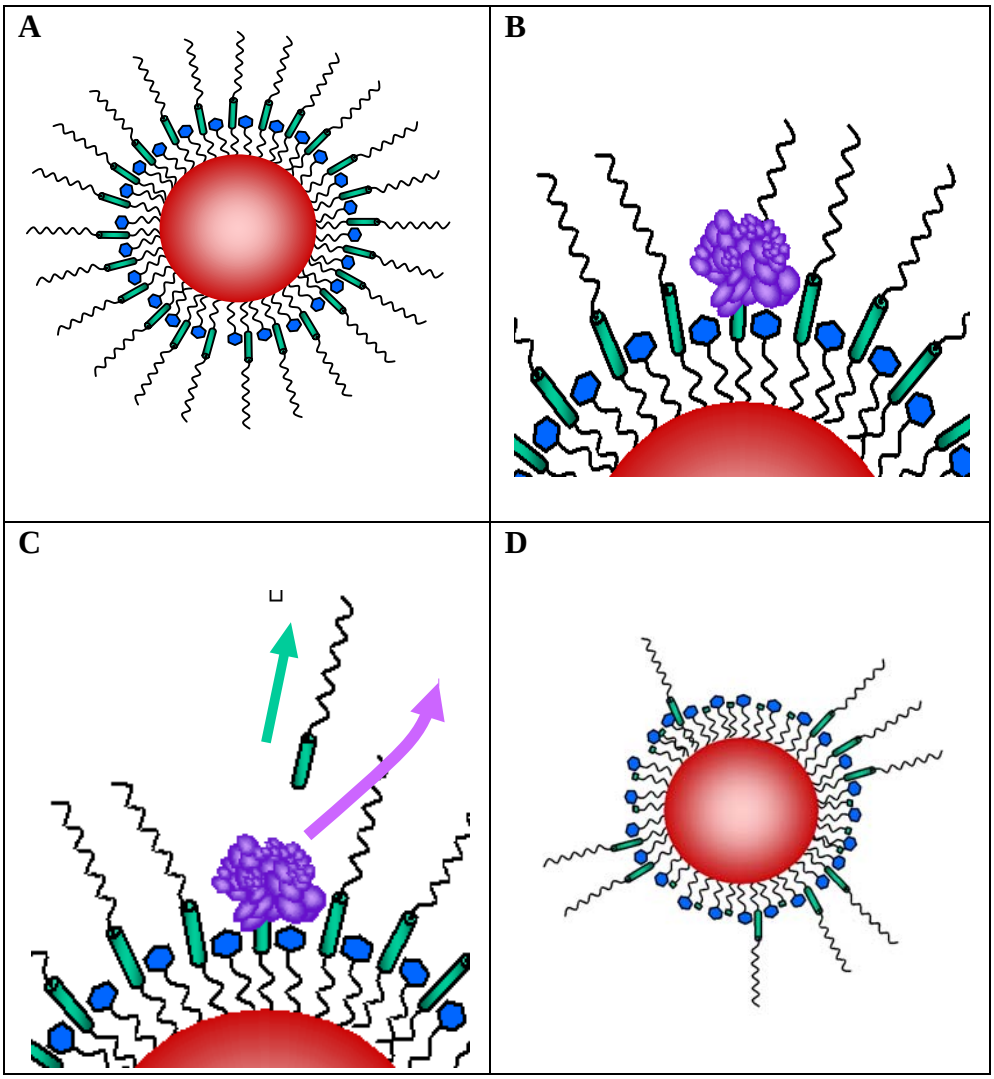

Figure 1.1. Representative structure of PAT nanoparticle. **A.** A PEG coating conceals the targeting ligand (blue) and passivates the surface of the native particle. **B.** Proteolytic action of MMP-7 (purple), secreted by tumor, cleaves the peptide bridge (green) revealing the targeting ligand. **C.** MMP-7 and cleavage fragments diffuse away. **D.** Ligand-targeted construct is revealed only in proximity to tumor, enabling specific binding to target sites.

Active targeting and gene delivery of 40-50nm cationic NPs was studied in the work of Hood *et al* (22). This work reports selective targeting to receptor-positive cells *in vitro* as well as to tumor vasculature *in vivo* resulting in significant reduction of tumor volume after treatment with targeted NPs. This work, however, provides no measurements detailing the *delivery* of NPs to target or nontarget sites. Hood *et al.* relied on gene expression and tumor regression as a measure of success; they did not attempt to offer qualitative observations or to quantify the delivery or biodistribution of their targeted NPs.

Effective targeting and tissue biodistribution can be improved through incorporation of both passive and active targeting components. Gao *et al.* showed that QDs can be successfully targeted to cancer cells under *in vivo* conditions (23). NPs used in this study contained both a PEG coating and an active targeting mAb ligand. Targeted NPs exhibited increased performance over NPs with only a PEG coating as they extravasated, and were delivered to and retained by tumor xenografts *in vivo*. However, nonspecific liver and spleen uptake was still apparent with these particles. It is unclear whether this accumulation resulted from mechanical filtration due to the relatively large size of the mAb targeting ligand (~150 kDa), immune recognition and clearance of the mAb ligand, or through some other unknown mechanism.

Ruoslahti *et al.* further demonstrated both active and passive targeting principles in a single NP with a coating of coadsorbed targeting peptide and PEG (24). These NPs successfully targeted vascular sites *in vivo* (active targeting) while significantly reducing uptake by the RES and accumulation in the liver and spleen (passive targeting). However, only qualitative visual data garnered from tissue sections was presented to

support these claims. Furthermore, the particles were targeted only to vascular tissue and failed to accumulate in the tumor volume. No negative control or blocking data was presented, leaving concerns regarding nonspecific binding due to the targeting peptide as well as the stability of the NPs under *in vivo* conditions.

NP targeting described in the literature predominantly focuses on easily accessible tissues such as blood and lymph vessels, liver, spleen, kidney, and lung. Active targeting of NPs to deep tissues (including tumors) is not widely reported beyond particle accumulation due to passive targeting and leaky tumor vasculature.

1.3.6 Prior Evidence of Successful Implementation of Tumor-Specific Cleavable Constructs

Compounds cleavable by tumor-specific enzymes have been incorporated into many structures ranging from *in vivo* imaging constructs to chemically modified drug structures.

The development of tumor-specific molecular imaging constructs cleavable by MMPs has been reported by Zucker *et al.* (25), Bremer *et al.* (26,27), and McIntyre *et al* (28,29). The latter study reports the synthesis of a proteolytic beacon for *in vivo* imaging of the MMP-7 enzyme. McIntyre *et al.* found that this structure was successfully cleaved by MMP-7 in *in vitro* assays as well as *in vivo* in mouse xenograft tumors expressing the MMP-7 enzyme. Cleavage was shown to be specific for the MMP-7 enzyme, with a resulting k_{cat}/K_m at least 13-fold larger than for other MMP enzymes tested. The basis of the MMP-7 specific peptide substrate utilized by McIntyre *et al.* (RPLALWRS) is

employed in the current studies described in this dissertation as the cleavable portion of the NP delivery system.

Multiple studies have reported the incorporation of tumor-specific cleavage into the structural design of drug molecules in the form of prodrugs. In one such reference, Liu *et al.* describe a doxorubicin prodrug capable of specific cleavage and activation by the tumor-associated enzyme legumain (30). Doxorubicin was successfully modified with a legumain-cleavable peptide substrate to form a prodrug with significantly reduced toxicity. The cytotoxicity of this structure could be recovered by cleavage of the arginyl peptide by tumor-associated legumain. The work of Liu *et al.* demonstrates the feasibility of tumor-specific enzyme interaction as a means of modifying the physical structure of delivered drugs, and possibly of delivered NP and particulate drug carriers.

Incorporation of tumor-specific cleavable linkers into structures for drug delivery has been documented by Suzawa *et al* (31,32). Immunoconjugates of the antitumor drug adriamycin (ADM) were synthesized by conjugation to a targeting mAb through a cleavable PEG-dipeptidyl linker. Specific cleavage of this linker was demonstrated as well as antigen-specific targeting of the conjugate to the cell surface (via the attached mAb). While this study does report specific cleavage of the dipeptidyl linker by model enzymes, it does not demonstrate release of active drug at the cell surface or by enzymes released by cells *in vitro*. It is unclear whether this construct can be cleaved by tumor-specific enzymes or at enzyme levels produced by tumors *in vivo*. Furthermore, concerns remain as to whether the ADM released by construct cleavage exhibits sufficient cytotoxicity compared to unconjugated ADM.

Literature citations of tumor-specific cleavable constructs focus mainly on molecular imaging of enzyme activity and drug activation *in vivo*. Incorporation of these constructs into NPs or their application to target NP-based therapeutic delivery systems has not yet been reported in the literature.

1.3.7 Novel Aspects and Improvements upon Prior Efforts

We have assessed NP accumulation and specific delivery in *in vitro* systems based on established fluorescence and cell viability protocols, coupled with quantitative imaging modalities. The PAT construct described here combines the successes of prior targeting efforts, producing a novel bionanoparticle that offers inherent desirable advantages in the realm targeted therapeutics and biosensing.

The strength of this approach lies in the ability to integrate detection, imaging, and treatment characteristics into a single particle. The nanocrystal base of the construct is a flexible platform that affords opportunities for attachment of a range of molecular structures ranging from specific targeting ligands to small molecule chemotherapeutics. Furthermore, the relatively large surface area of the nanocrystal base (when compared to single molecules) allows the attachment of multiple copies of both the targeting ligand and therapeutic molecule, or of multiple distinct targeting mechanisms. This characteristic confers multivalent binding capability to the NP construct as well as the ability to deliver multiple therapeutic molecules in a single package. Envisioned, but not studied here, are extensions to the NP construct to enable high sensitivity, high resolution *in vivo* imaging of emerging neoplasia and established tumors.

Previous studies have outlined the importance of both passive and active processes on the success of specific targeting. The PAT construct contains elements to maximize each of these targeting processes. A passivating PEG barrier is employed to minimize nonspecific interaction and specific interaction to nontarget tissues. Two independent recognition mechanisms have also been described for integration into the PAT particle to maximize active targeting of the construct: local MMP-7 secretion and expression of the target receptor on the cellular surface. The requirement for local proteolytic cleavage to reveal the targeting ligand allows the PEG barrier to remain intact until the particle encounters a target area, presumably enabling the construct to actively target only in areas of increased MMP-7 enzyme concentration.

Most targeted applications focus mainly on vascular or other easily accessible targets. The nanoparticle system described here should interrogate all potential target body compartments via a single administration route. To achieve this aim, the NP construct must exhibit efficient extravasation and interstitial transport. Based on prior evidence, NP diameter is a strong modulator of these characteristics. The overall diameter of the NP construct is chosen to minimize rapid, nonspecific clearance of the NPs while maximizing extravasation and interstitial transport of the constructs. Small particle size and enhanced biodistribution characteristics proffer the ability to treat established primary tumors, emerging neoplasia, and distant metastases.

Once an effective strategy is developed for the treatment of a single type of tumorigenic target, tumor phenotype or physiology often prohibits adaptation of the therapy for treatment of other malignancies. The NP delivery system described here contains multiple levels of modularity to enable an array of NP constructs to significantly

impact cancer therapy. The current strategy is modular in four dimensions: (1) different tumor-specific small molecule targeting ligands can be employed, (2) different peptide substrates for enzymatic activity can replace the MMP-7 peptide, (3) a range of therapeutic molecules can be delivered and (4) different nanoparticle, nanocrystal or molecular structures can be used as the core of the construct. Thus, the ideal component can be chosen from all four categories to create a NP delivery system tailored to the purposes of the specific application.

1.3.8 Imaging of NP accumulation in target cell populations

The intense fluorescence and photostability of QD nanocrystals allows high-sensitivity detection of NP accumulation *in vitro*. These fluorescence characteristics enable high-resolution fluorescence microscopy and confocal microscopy imaging of labeled cells and internal cell structures as well as quantitative fluorescence measurements via fluorescence spectroscopy and flow cytometry.

The use of high-resolution fluorescence imaging allows determination of the intracellular fate of targeted NPs in *in vitro* systems and visualization of NP surface binding and internalization. Fluorescence spectroscopy and flow cytometry enables quantitative analysis and validation of NP accumulation and binding. Quantitative fluorescence measurements also provide kinetic NP binding and proteolytic cleavage measurements to further characterize the efficiency of the NP construct.

1.3.9 Overcoming nonspecific delivery of therapeutic agents

Due, in part, to the historic difficulties encountered in specific targeting, no single targeting strategy has been able embody the "magic bullet" concept envisioned by Paul Ehrlich at the turn of the 20th century. Obstacles such as nonspecific binding and specific binding to nontarget tissues continue to plague most single-modality targeting strategies. The relative lack of effective targeted therapies in the marketplace reveals the need for new and innovative approaches to this problem and presents an opportunity to make a significant contribution to this effort.

Autonomous unmasking of the targeting ligand only in the proximity of a cellular target is the critical feature of the PAT construct. Upon administration, PAT NPs exhibit a passive, non-immunogenic PEG barrier. Previous studies have shown PEG conjugation to increase particle circulation time by minimizing nonspecific clearance by the RES as well as nonspecific retention of particles in the liver and spleen (20,33). This behavior is expected to extend to particles in the interstitial space as well, although the body of evidence regarding interstitial NP transport and recognition is limited.

Local proteolytic cleavage removes the passivating PEG layer to reveal a site-specific targeting ligand, enabling active targeting of the NP to target cellular receptors. The independent action of the recognition mechanisms built into the PAT NP ensures that both enzymatic activity and target receptor expression must be present to elicit active targeting of the construct. This independent dual-layered targeting approach combines successful elements of previous studies to maximize site-specific targeting of the PAT NP while keeping side effects caused by nonspecific interactions to a minimum.

1.3.10 Background and Significance: *Aim I – Characterize peptide and receptor properties and interactions in in vitro cellular models.*

The role of the CD13 receptor in biological processes

CD13 is a zinc-binding protease belonging to the family of proteins known as ectoenzymes. This enzyme is constitutively expressed in a variety of tissues, with its functional role dependent on location. CD13 is highly expressed in the intestinal brush border where it participates in the final hydrolysis of ingested proteins (34). It is also expressed in the kidney, and to a lesser extent in the spleen and brain, among other tissues. Functions in these tissues range from degradation of neuropeptides and cytokines to antigen processing (35).

CD13 has been shown to take on a different role in tumor physiology. Under neoplastic conditions, CD13 is reported to react with leukemic blasts of most acute myeloblastic leukemias (36,37), and has been utilized extensively as a marker for leukemia typing (38,39). This protein has been shown to promote tumor invasion and migration by active degradation and rearrangement of ECM components and promotion of angiogenesis. CD13 has also been implicated as an auxiliary adhesion molecule, mediating cell-cell contact in melanoma colonies and adherence of metastatic breast and prostate carcinomas (40,41).

NGR binding and differential expression of CD13 isoforms *in vivo*

The NGR motif has been identified via phage display as a tumor-homing tripeptide sequence selectively targeting tumor vasculature *in vivo* (42,43). Additional studies identified CD13 as the receptor for this peptide motif (44). Although CD13

expression has been reported in a variety of tissues, Curnis *et al.* have exhibited the existence of at least two distinct isoforms of this antigen (45). Further investigation confirmed that the isoform found in tumorigenic cells and angiogenic blood vessels functions as a receptor for the NGR motif, while the isoform expressed in normal counterparts of these cells does not appreciably bind NGR conjugates. CD13 overexpression has been measured in both tumor cells and angiogenic blood vessels (46,47), providing an appealing and accessible target for directed therapy.

Receptor expression in response to environmental factors

Mammalian cells express a wide variety of surface molecules ranging from enzymes to integrins, with a spectrum of expression profiles. Some of these molecules are constitutively synthesized, while the expression of others can be increased, decreased, or induced *de novo* in response to various stimuli (48). One study measured marked differences in surface expression of a host of surface molecules after exposure to endogenous factors including the proinflammatory cytokines IL-1β and TNF-α as well as to the well-characterized PKC activator PMA (49). Exogenous factors such as ionizing radiation (50,51) and chemotherapeutics (52,53) have also been shown to strongly modulate gene and receptor expression in both *in vitro* and *in vivo* environments. Cells in this "activated" state often exhibit large changes in the expression profiles of a number of surface receptors, leading to a functional state distinct from that seen under normal physiologic conditions.

1.3.11 Background and Significance: *Aim II – Characterize NP-linked ligand binding to target cellular receptors in in vitro tissue models.*

Strategies to link functional molecular targeting ligands to the NP surface

Immobilization of functional proteins and peptides to solid supports has recently become an area of active research. The use of NPs for this purpose has the inherent advantage of a large surface area to volume ratio (compared to molecular agents), allowing conjugation of a large number of active molecules. Surface conjugation is further facilitated by the availability of multiple functional groups (typically carboxylic acid groups) on the surface of the QD, which can be utilized in a number of well-characterized linking strategies. Stable covalent conjugation of bioactive molecules such as enzymes (54,55), mAbs (56), peptides (57), and DNA (58,59) to the surface of NPs has been reported. Many copies of small-molecule or short peptide ligands or DNA probes can be attached to the surface enabling multivalent QD-target binding.

Quantifying cellular binding of NP-linked targeting ligand

Due to the intense fluorescence characteristics of the QDs utilized as the NP base, detection of cell-associated NPs is uncomplicated. Similar strategies have been outlined for the fluorescence quantification of mAb binding to cell surface receptors (60,61). The crux of these strategies is the measurement and quantitation of fluorescence changes in response to ligand binding. Qualitative measurements can be made by visualization using fluorescence microscopy. Total quantitative fluorescence measurements can be performed on a macroscopic level by simple spectroscopic detection using a fluorescence plate reader, or on the level of individual cells by flow cytometry. Fluorescence

measurements are then converted to the level of ligand binding through the use of calibration methods.

1.3.12 Background and Significance: *Aim III -- Investigate NP-linked tumor-specific cleavable construct in in vitro models.*

Synthesis of the PA construct

Synthesis of the PA construct proceeds via established and well-characterized synthesis routes. PEG molecules exhibiting a range of functional groups reactive toward the N- and C-terminal groups on the MMP-7 peptide can be readily purchased (Nektar Therapeutics). Reactions proceed to completion using excess PEG, ensuring virtually complete conjugation of available MMP-7 target peptides.

Purification of the PA construct can proceed via several pathways. Perhaps the fastest and simplest of these approaches is size exclusion chromatography. As the individual components and intermediates have significantly smaller molecular weights than the final construct, size exclusion chromatography is expected to render a sufficiently pure product. More sophisticated strategies such as HPLC and dialysis are available, but these approaches often require nontrivial time investments to optimize the separation parameters.

Strategies to link PA constructs to the NP surface

Immobilization of PA constructs to the NP surface can be accomplished under the same conditions and linking strategies employed for targeting molecules (Aim II). These

constructs employ the same functional groups as the targeting peptide molecules, allowing simultaneous and stoichiometric conjugation of both moieties to the NP surface.

Measurement of PA construct cleavage

Due to the nature of the cleavage product (LWRS-[Ahx]-C-PEG_{3400}), detection of PA construct cleavage is nontrivial. Total protein assays assessed by spectroscopic detection of fluorogenic amino acids (*i.e.* tryptophan) or traditional staining techniques may not be suitable due to the low amino acid content of the cleaved portion of the construct (5 amino acids, ~16% of the cleavage product by weight). MALDI-TOF sampling can detect the generation and verify the molecular weight of cleavage products, although this method does not allow direct quantitation of cleavage extent (62).

Alternatively, the PA construct can be labeled with a fluorescent molecule (*e.g.* FITC or a FITC analog) to enable fluorogenic identification of cleavage products. Construct cleavage can be visualized qualitatively by changes in electrophoretic mobility of either the free molecule (in the case of non-QD conjugated construct), or of the entire QD construct (in the case of NP-linked PA construct), as well as by the generation of a distinct fluorescent band representing the labeled cleavage product. Quantification of NP-linked PA construct cleavage can be assessed through a combination of the methods described above, or via spectroscopic measurement of liberated labeled cleavage products.

MMP-7 expression in physiological and pathophysiological states

MMP-7 expression in both normal and neoplastic tissue has been well-characterized (63-65). It is notable that MMP-7 is produced predominantly by cells of

epithelial origin, whereas most other MMPs are generally expressed by the underlying stromal cells including those residing in connective tissues or by migratory cells of the immune system (29). Thus, in adenocarcinomas (the most common adult tumor type to arise from cells of epithelial origin) MMP-7 is expressed in the malignant epithelial component rather than in the surrounding stromal tissue. Additionally, overexpression of MMP-7 has been reported in many tumors relative to the normal surrounding tissues (66,67).

For tumor systems in which MMP-7 activity is known to modulate the course of the disease, MMP-7 is secreted even in the earliest stages. Small, benign "precancerous" lesions, for example, exhibit MMP-7 secretion well before these lesions would be clinically detectable (68,69). Furthermore, analysis of MMP-7 expression in human neoplasia revealed that the mRNA appeared in the surrounding normal tissue in only a few isolated cases (70). The larger and more progressed these tumors become, the higher the MMP-7 levels tend to be. This focused source of abundant extracellular MMP-7 is expected to provide ample activity for the *in vivo* application of PA NPs to cancer targeting.

The role of MMP-7 in biological processes

MMPs (including MMP-7) are a family of enzymes that have a role in tissue breakdown and remodeling during both normal (*e.g.* angiogenesis, gut innate immunity) and pathological (*e.g.* inflammation, tumorigenesis, metastasis) processes. MMP-7 has been specifically implicated as an important facilitator of tissue remodeling due to its ability to cleave a variety of known substrates, including many ECM proteins and the latent forms of other MMPs (70). In fact, overexpression of MMP-7 has been directly

correlated with enhanced tumorigenicity and tumor cell invasion using *in vitro* model systems (67). It has been shown to be important in the progression of a number of tumors, notably those originating in the colon or in the breast (29). Furthermore, MMP-7 has proven to have diagnostic and prognostic value, as expression is associated with poor outcome in esophageal (71), colon (72), and pancreatic (73) cancers. The overexpression and significance of MMP-7 in the tumor cascade make this enzyme an attractive target for site-directed drug delivery vehicles.

QD toxicity

In vivo application of QD probes requires a comprehensive examination of both the short- and long-term toxicity of the QD core materials as well as any structures exhibited on the surface of the molecule; these studies are beyond the scope of this work. Most i*n vitro* applications require only short-term toxicity studies on cultured cells, as experiments are often completed in a matter of hours or days.

Recent publications have examined the toxicity of QDs in both *in vitro* and *in vivo* environments. Some studies have reported that QDs applied to immortalized cell lines *in vitro* results in no significant measures of toxicity (74,75). In primary cultures and i*n vivo* applications, QD toxicity was detected; however, QDs could be rendered nontoxic with appropriate surface coatings (76,77). Long-term, degradation of QDs may result in liberation of the core materials of the particle. However, as the studies described here do not occur over these time frames, short-term toxicity studies are expected to be sufficient to predict the response of cultured cells *in vitro*.

1.4 References

1. Torchilin VP. Drug targeting. Eur J Pharm Sci 2000;11 Suppl 2:S81-91.

2. Vyas SP, Singh A, Sihorkar V. Ligand-receptor-mediated drug delivery: an emerging paradigm in cellular drug targeting. Crit Rev Ther Drug Carrier Syst 2001;18(1):1-76.

3. Tietze LF, Feuerstein T. Enzyme and proton-activated prodrugs for a selective cancer therapy. Curr Pharm Des 2003;9(26):2155-75.

4. Rooseboom M, Commandeur JN, Vermeulen NP. Enzyme-catalyzed activation of anticancer prodrugs. Pharmacol Rev 2004;56(1):53-102.

5. Society AC. Cancer Facts & Figures 2004. Atlanta, GA: American Cancer Society; 2004.

6. Ishida O, Maruyama K, Sasaki K, Iwatsuru M. Size-dependent extravasation and interstitial localization of polyethyleneglycol liposomes in solid tumor-bearing mice. Int J Pharm 1999;190(1):49-56.

7. Kong G, Braun RD, Dewhirst MW. Hyperthermia enables tumor-specific nanoparticle delivery: effect of particle size. Cancer Res 2000;60(16):4440-5.

8. Schiffelers RM, Bakker-Woudenberg IA, Snijders SV, Storm G. Localization of sterically stabilized liposomes in Klebsiella pneumoniae-infected rat lung tissue: influence of liposome characteristics. Biochim Biophys Acta 1999;1421(2):329-39.

9. Sugibayashi K. Biomedical Applications of Magnetic Drug Carriers in Cancer Chemotherapy. Polymeric Nanospheres and Microparticles: CRC Press; 1986. p 95-133.

10. Rolland A, Merdrignac G, Gouranton J, Bourel D, Le Verge R, Genetet B. Flow cytometric quantitative evaluation of phagocytosis by human mononuclear and polymorphonuclear cells using fluorescent nanoparticles. J Immunol Methods 1987;96(2):185-93.

11. Vyas SP, Malaiya A. In vivo characterization of indomethacin magnetic polymethyl methacrylate nanoparticles. J Microencapsul 1989;6(4):493-9.

12. Panyam J, Labhasetwar V. Biodegradable nanoparticles for drug and gene delivery to cells and tissue. Adv Drug Deliv Rev 2003;55(3):329-47.

13. Pluen A, Boucher Y, Ramanujan S, McKee TD, Gohongi T, di Tomaso E, Brown EB, Izumi Y, Campbell RB, Berk DA and others. Role of tumor-host interactions in interstitial diffusion of macromolecules: cranial vs. subcutaneous tumors. Proc Natl Acad Sci U S A 2001;98(8):4628-33.

14. Illum L, Church AE, Butterworth MD, Arien A, Whetstone J, Davis SS. Development of systems for targeting the regional lymph nodes for diagnostic imaging: in vivo behaviour of colloidal PEG-coated magnetite nanospheres in the rat following interstitial administration. Pharm Res 2001;18(5):640-5.

15. Chabner B. Cancer Chemotherapy. Principles and Practice. Philadelphia: J.B. Lippincott; 1990.

16. Frei EI. Combination chemotherapy, dose and schedule. Cancer Medicine. 4 ed; 1997. p 817-837.

17. Brannon-Peppas L, Blanchette JO. Nanoparticle and targeted systems for cancer therapy. Adv Drug Deliv Rev 2004;56(11):1649-59.

18. Kim R, Toge T. Changes in therapy for solid tumors: potential for overcoming drug resistance in vivo with molecular targeting agents. Surg Today 2004;34(4):293-303.

19. Bogenrieder T, Herlyn M. Axis of evil: molecular mechanisms of cancer metastasis. Oncogene 2003;22(42):6524-36.

20. Ballou B, Lagerholm BC, Ernst LA, Bruchez MP, Waggoner AS. Noninvasive imaging of quantum dots in mice. Bioconjug Chem 2004;15(1):79-86.

21. Oyewumi MO, Yokel RA, Jay M, Coakley T, Mumper RJ. Comparison of cell uptake, biodistribution and tumor retention of folate-coated and PEG-coated gadolinium nanoparticles in tumor-bearing mice. J Control Release 2004;95(3):613-26.

22. Hood JD, Bednarski M, Frausto R, Guccione S, Reisfeld RA, Xiang R, Cheresh DA. Tumor regression by targeted gene delivery to the neovasculature. Science 2002;296(5577):2404-7.

23. Gao X, Cui Y, Levenson RM, Chung LW, Nie S. In vivo cancer targeting and imaging with semiconductor quantum dots. Nat Biotechnol 2004;22(8):969-76.

24. Akerman ME, Chan WC, Laakkonen P, Bhatia SN, Ruoslahti E. Nanocrystal targeting in vivo. Proc Natl Acad Sci U S A 2002;99(20):12617-21.

25. Zucker S, Cao J. Imaging metalloproteinase activity in vivo. Nat Med 2001;7(6):655-6.

26. Bremer C, Tung CH, Weissleder R. Molecular imaging of MMP expression and therapeutic MMP inhibition. Acad Radiol 2002;9 Suppl 2:S314-5.

27. Bremer C, Tung CH, Weissleder R. In vivo molecular target assessment of matrix metalloproteinase inhibition. Nat Med 2001;7(6):743-8.

28. McIntyre JO, Matrisian LM. Molecular imaging of proteolytic activity in cancer. J Cell Biochem 2003;90(6):1087-97.

29. McIntyre JO, Fingleton B, Wells KS, Piston DW, Lynch CC, Gautam S, Matrisian LM. Development of a novel fluorogenic proteolytic beacon for in vivo detection and imaging of tumour-associated matrix metalloproteinase-7 activity. Biochem J 2004;377(Pt 3):617-28.

30. Liu C, Sun C, Huang H, Janda K, Edgington T. Overexpression of legumain in tumors is significant for invasion/metastasis and a candidate enzymatic target for prodrug therapy. Cancer Res 2003;63(11):2957-64.

31. Suzawa T, Nagamura S, Saito H, Ohta S, Hanai N, Yamasaki M. Synthesis and HPLC analysis of enzymatically cleavable linker consisting of poly(ethylene glycol) and dipeptide for the development of immunoconjugate. J Control Release 2000;69(1):27-41.

32. Suzawa T, Nagamura S, Saito H, Ohta S, Hanai N, Kanazawa J, Okabe M, Yamasaki M. Enhanced tumor cell selectivity of adriamycin-monoclonal antibody conjugate via a poly(ethylene glycol)-based cleavable linker. J Control Release 2002;79(1-3):229-42.

33. Greenwald RB. PEG drugs: an overview. J Control Release 2001;74(1-3):159-71.

34. Olsen J, Kokholm K, Noren O, Sjostrom H. Structure and expression of aminopeptidase N. Adv Exp Med Biol 1997;421:47-57.

35. Firla B, Arndt M, Frank K, Thiel U, Ansorge S, Tager M, Lendeckel U. Extracellular cysteines define ectopeptidase (APN, CD13) expression and function. Free Radic Biol Med 2002;32(7):584-95.

36. Griffin JD, Ritz J, Nadler LM, Schlossman SF. Expression of myeloid differentiation antigens on normal and malignant myeloid cells. J Clin Invest 1981;68(4):932-41.

37. Sakai K, Hattori T, Sagawa K, Yokoyama M, Takatsuki K. Biochemical and functional characterization of MCS-2 antigen (CD13) on myeloid leukemic cells and polymorphonuclear leukocytes. Cancer Res 1987;47(21):5572-6.

38. Dixon J, Kaklamanis L, Turley H, Hickson ID, Leek RD, Harris AL, Gatter KC. Expression of aminopeptidase-n (CD 13) in normal tissues and malignant neoplasms of epithelial and lymphoid origin. J Clin Pathol 1994;47(1):43-7.

39. Riemann D, Kehlen A, Langner J. CD13--not just a marker in leukemia typing. Immunol Today 1999;20(2):83-8.

40. Saiki I, Fujii H, Yoneda J, Abe F, Nakajima M, Tsuruo T, Azuma I. Role of aminopeptidase N (CD13) in tumor-cell invasion and extracellular matrix degradation. Int J Cancer 1993;54(1):137-43.

41. Menrad A, Speicher D, Wacker J, Herlyn M. Biochemical and functional characterization of aminopeptidase N expressed by human melanoma cells. Cancer Res 1993;53(6):1450-5.

42. Pasqualini R, Koivunen E, Ruoslahti E. Alpha v integrins as receptors for tumor targeting by circulating ligands. Nat Biotechnol 1997;15(6):542-6.

43. Arap W, Pasqualini R, Ruoslahti E. Cancer treatment by targeted drug delivery to tumor vasculature in a mouse model. Science 1998;279(5349):377-80.

44. Pasqualini R, Koivunen E, Kain R, Lahdenranta J, Sakamoto M, Stryhn A, Ashmun RA, Shapiro LH, Arap W, Ruoslahti E. Aminopeptidase N is a receptor for tumor-homing peptides and a target for inhibiting angiogenesis. Cancer Res 2000;60(3):722-7.

45. Curnis F, Arrigoni G, Sacchi A, Fischetti L, Arap W, Pasqualini R, Corti A. Differential binding of drugs containing the NGR motif to CD13 isoforms in tumor vessels, epithelia, and myeloid cells. Cancer Res 2002;62(3):867-74.

46. van Hensbergen Y, Broxterman HJ, Rana S, van Diest PJ, Duyndam MC, Hoekman K, Pinedo HM, Boven E. Reduced growth, increased vascular area, and reduced response to cisplatin in CD13-overexpressing human ovarian cancer xenografts. Clin Cancer Res 2004;10(3):1180-91.

47. van Hensbergen Y, Broxterman HJ, Hanemaaijer R, Jorna AS, van Lent NA, Verheul HM, Pinedo HM, Hoekman K. Soluble aminopeptidase N/CD13 in malignant and nonmalignant effusions and intratumoral fluid. Clin Cancer Res 2002;8(12):3747-54.

48. Albelda SM, Buck CA. Integrins and other cell adhesion molecules. Faseb J 1990;4(11):2868-80.

49. Mutin M, Dignat-George F, Sampol J. Immunologic phenotype of cultured endothelial cells: quantitative analysis of cell surface molecules. Tissue Antigens 1997;50(5):449-58.

50. Smith RA, Giorgio TD. Quantitation and kinetics of CD51 surface receptor expression: implications for targeted delivery. Ann Biomed Eng 2004;32(5):635-44.

51. Giannopoulou E, Katsoris P, Hatziapostolou M, Kardamakis D, Kotsaki E, Polytarchou C, Parthymou A, Papaioannou S, Papadimitriou E. X-rays modulate extracellular matrix in vivo. Int J Cancer 2001;94(5):690-8.

52. Kerbel RS, Yu J, Tran J, Man S, Viloria-Petit A, Klement G, Coomber BL, Rak J. Possible mechanisms of acquired resistance to anti-angiogenic drugs: implications for the use of combination therapy approaches. Cancer Metastasis Rev 2001;20(1-2):79-86.

53. Novelli F, Allione A, Bernabei P, Rigamonti L, Forni G. Antiblastic chemotherapy drugs up-modulate interferon-gamma receptor expression on human malignant T cells. Cancer Detect Prev 1997;21(2):191-5.

54. Rossi LM, Quach AD, Rosenzweig Z. Glucose oxidase-magnetite nanoparticle bioconjugate for glucose sensing. Anal Bioanal Chem 2004;380(4):606-13.

55. Phadtare S, Vinod VP, Mukhopadhyay K, Kumar A, Rao M, Chaudhari RV, Sastry M. Immobilization and biocatalytic activity of fungal protease on gold nanoparticle-loaded zeolite microspheres. Biotechnol Bioeng 2004;85(6):629-37.

56. Tang DP, Yuan R, Chai YQ, Zhong X, Liu Y, Dai JY, Zhang LY. Novel potentiometric immunosensor for hepatitis B surface antigen using a gold nanoparticle-based biomolecular immobilization method. Anal Biochem 2004;333(2):345-50.

57. Liu J, Zhang Q, Remsen EE, Wooley KL. Nanostructured materials designed for cell binding and transduction. Biomacromolecules 2001;2(2):362-8.

58. Zhang D, Chen Y, Chen HY, Xia XH. Silica-nanoparticle-based interface for the enhanced immobilization and sequence-specific detection of DNA. Anal Bioanal Chem 2004;379(7-8):1025-30.

59. Wang M, Sun C, Wang L, Ji X, Bai Y, Li T, Li J. Electrochemical detection of DNA immobilized on gold colloid particles modified self-assembled monolayer electrode with silver nanoparticle label. J Pharm Biomed Anal 2003;33(5):1117-25.

60. Serke S, van Lessen A, Huhn D. Quantitative fluorescence flow cytometry: a comparison of the three techniques for direct and indirect immunofluorescence. Cytometry 1998;33(2):179-87.

61. Lenkei R, Gratama JW, Rothe G, Schmitz G, D'Hautcourt J L, Arekrans A, Mandy F, Marti G. Performance of calibration standards for antigen quantitation with flow cytometry. Cytometry 1998;33(2):188-96.

62. Rosche F, Schmidt J, Hoffmann T, Pauly RP, McIntosh CH, Pederson RA, Demuth HU. Kinetic analysis of enzymatic and nonenzymatic degradation of peptides by MALDI-TOFMS. Methods Mol Biol 2000;146:251-72.

63. Wilson CL, Heppner KJ, Rudolph LA, Matrisian LM. The metalloproteinase matrilysin is preferentially expressed by epithelial cells in a tissue-restricted pattern in the mouse. Mol Biol Cell 1995;6(7):851-69.

64. Crawford HC, Matrisian LM. Mechanisms controlling the transcription of matrix metalloproteinase genes in normal and neoplastic cells. Enzyme Protein 1996;49(1-3):20-37.

65. Khasigov PZ, Podobed OV, Ktzoeva SA, Gatagonova TM, Grachev SV, Shishkin SS, Berezov TT. Matrix metalloproteinases of normal human tissues. Biochemistry (Mosc) 2001;66(2):130-40.

66. Khasigov PZ, Podobed OV, Gracheva TS, Salbiev KD, Grachev SV, Berezov TT. Role of matrix metalloproteinases and their inhibitors in tumor invasion and metastasis. Biochemistry (Mosc) 2003;68(7):711-7.

67. Rudolph-Owen LA, Chan R, Muller WJ, Matrisian LM. The matrix metalloproteinase matrilysin influences early-stage mammary tumorigenesis. Cancer Res 1998;58(23):5500-6.

68. Crawford HC, Scoggins CR, Washington MK, Matrisian LM, Leach SD. Matrix metalloproteinase-7 is expressed by pancreatic cancer precursors and regulates acinar-to-ductal metaplasia in exocrine pancreas. J Clin Invest 2002;109(11):1437-44.

69. Hulboy DL, Gautam S, Fingleton B, Matrisian LM. The influence of matrix metalloproteinase-7 on early mammary tumorigenesis in the multiple intestinal neoplasia mouse. Oncol Rep 2004;12(1):13-7.

70. Wilson CL, Matrisian LM. Matrilysin: an epithelial matrix metalloproteinase with potentially novel functions. Int J Biochem Cell Biol 1996;28(2):123-36.

71. Yamamoto H, Adachi Y, Itoh F, Iku S, Matsuno K, Kusano M, Arimura Y, Endo T, Hinoda Y, Hosokawa M and others. Association of matrilysin expression with recurrence and poor prognosis in human esophageal squamous cell carcinoma. Cancer Res 1999;59(14):3313-6.

72. Adachi Y, Yamamoto H, Itoh F, Arimura Y, Nishi M, Endo T, Imai K. Clinicopathologic and prognostic significance of matrilysin expression at the invasive front in human colorectal cancers. Int J Cancer 2001;95(5):290-4.

73. Yamamoto H, Itoh F, Iku S, Adachi Y, Fukushima H, Sasaki S, Mukaiya M, Hirata K, Imai K. Expression of matrix metalloproteinases and tissue inhibitors of metalloproteinases in human pancreatic adenocarcinomas: clinicopathologic and prognostic significance of matrilysin expression. J Clin Oncol 2001;19(4):1118-27.

74. Wu X, Liu H, Liu J, Haley KN, Treadway JA, Larson JP, Ge N, Peale F, Bruchez MP. Immunofluorescent labeling of cancer marker Her2 and other cellular targets with semiconductor quantum dots. Nat Biotechnol 2003;21(1):41-6.

75. Jaiswal JK, Mattoussi H, Mauro JM, Simon SM. Long-term multiple color imaging of live cells using quantum dot bioconjugates. Nat Biotechnol 2003;21(1):47-51.

76. Hoshino A, Fujioka K, Oku T, Suga M, Sasaki YF, Ohta T, Yasuhara M, Suzuki K, Yamamoto K. Physiochemical properties and cellular toxicity of nanocrystal quantum dots depend on their surface modification. Nano Lett 2004;4(11):2163-2169.

77. Derfus AM, Chan WCW, Bhatia SN. Probing the Cytotoxicity of Quantum Dots. Nano Lett 2004;4(1):11-18.

CHAPTER II

A QUANTITATIVE ANALYSIS OF THE CD13 PROTEIN ON THE SURFACE OF HT-1080 CELLS

RA Smith and TD Giorgio

Department of Biomedical Engineering
Vanderbilt University, Nashville, TN

Correspondence:
Todd D. Giorgio
Vanderbilt University
Box 351620, Station B
Nashville, TN 37235
615-322-3756 (voice)
615-343-7919 (fax)
todd.d.giorgio@vanderbilt.edu

Key terms: aminopeptidase N, CD13, flow cytometry, irradiation, NGR, quantitative, TNF-α, TGF-β1

Note: this work was not submitted for publication. Although important in the framework of this research, the results described here are not substantive enough for a complete publication.

2.1 Abstract

The CD13 protein is important in many functions ranging from degradation of neuropeptides to rearrangement of the basement membrane. Due to its prominent overexpression in many cancers, CD13 has also gained interest as an attractive ligand for directed therapy studies. While the function and performance of several CD13-specific targeting molecules has been examined both *in vitro* and *in vivo*, studies are often carried out without quantitative assessment of the target protein. A lack of this data complicates further quantitative analysis and precludes a full understanding of the overall efficiency of specific targeting. We performed a quantitative evaluation of CD13 on the surface of HT-1080 cells, a cell line utilized in several receptor-based studies, and compared this resting (unstimulated) value to that of cells stimulated in various manners. Unstimulated HT-1080 cells strongly express CD13 at a level of 3,840,000 ± 70,000 (mean ± SD) antibody binding capacity (ABC)/cell (n = 4). Following low-dose irradiation with 3Gy, receptor expression increases, peaking at a value of 6,300,000 ± 220,000 (n = 3). The effects of TNF-α and TGF-β1 incubation were also monitored, with both cytokines resulting in marked increases in maximal CD13 expression relative to unstimulated controls to 7,250,000 ± 280,000 (n = 3) and 4,700,000 ± 270,000 (n = 3), respectively. Our results yield detailed information not available with experimental targeting data alone, and highlight the importance of conducting quantitative receptor analysis in conjunction with targeted delivery experiments.

2.2 Introduction

Prototypical targeted therapeutic vectors have inherent advantages over traditional techniques in the areas of dose, safety, and overall efficacy. In practice, however, these vehicles generally fail to realize their potential and suffer from poor targeting efficiencies and ineffective delivery (1). One approach to improving the efficacy of these delivery devices is the addition of targeting complexes to the vector, thus promoting specific receptor-mediated binding and endocytosis of the construct. Recent efforts have utilized this and other approaches in an attempt to improve the delivery and target specificity of genes and drugs to specific cell types (2,3,4,5). For example, peptide and other tumor-specific sequences have been utilized to target unique receptors on the surface of diseased cells, allowing the delivery of a relatively high concentration of drugs or genetic material to specific areas, increasing the efficiency and effectiveness of treatment (6-9). Molecular agents have also been included in several commercial therapies, including Herceptin, Glivec, and Avestin, to achieve site-specific delivery to target tissues *in vivo*.

Ligands including the Asn-Gly-Arg (NGR) motif in particular have been used to target treatments such as gene therapy and chemotherapy to the cell surface (10-12). Phage display studies identified this ligand as a tumor-homing tripeptide sequence selectively targeting tumor vasculature *in vivo* (13,14). Further studies revealed the target of this sequence as the CD13 protein (15). CD13 is expressed in a variety of tissues, with functions ranging from degradation of neuropeptides to rearrangement of the extracellular matrix (16,17). Additional studies have discovered at least two distinct isoforms of this protein. These experiments confirm that the isoform found in tumorigenic cells and angiogenic blood vessels functions as a receptor for the NGR motif, while that expressed

in the normal counterparts of these cells does not appreciably bind NGR conjugates (18). CD13 overexpression has been measured in both tumor cells and angiogenic blood vessels (19,20), providing an appealing and accessible target for directed therapy.

Previous studies have shown that expression levels of cellular receptors and other proteins are strongly modulated by exposure to ionizing radiation (21,22,23) and various cytokines (24), although the extent of modulation is highly dependent on the protein-cell line pair. Innate or inducible expression, as well as up- or down-regulation of these proteins may prove to be an important marker and target for tumor cells. Furthermore, the phage display technique has uncovered a growing library of additional peptide sequences for molecular targeting to tumors and other specific cell types (25-28). While these peptide sequences, along with other modalities, may be able to increase targeting efficiency, their intrinsic mechanism is governed by interaction with cell surface receptors. Due to this constraint, a quantitative analysis of the relevant receptors is central to understanding and evaluating the effectiveness of the targeting moiety.

Many studies have demonstrated the successful application of NGR-modified genes, drugs, and imaging agents to specifically target several cancer cell lines and vascular cells (29-31). These NGR-directed delivery vehicles are designed to interact with specific surface proteins (CD13) to achieve effective site-specific binding. This close surface association may modulate construct internalization and intracellular processing. In fact, studies have shown that internalization is enhanced by high cell surface densities of integrin receptors (32). Thus, these targeted constructs can be expected to be highly dependent on surface receptor concentration to achieve maximal

efficacy, and it is likely that cell types with varying numbers of these receptors would have differing intrinsic susceptibilities to targeted therapy.

The correlation between relative receptor number and success of targeted delivery has been demonstrated in previous studies using traditional FACS analysis, although absolute quantitative measurement of the receptor number was not performed (33-35). The FACS measurements employed in these studies yields only uncalibrated fluorescence values for whole cells, revealing the limitations of traditional FACS analysis. Thus, it is not possible to translate the results of most previous targeting studies into meaningful measures intrinsically associated with cellular characteristics. These results allow only a *qualitative* comparison between cell lines.

Advances in quantitative flow cytometry, however, have allowed the power of this technology to be extended for use in quantitative experiments including surface receptor quantitation (36,37). Standardized products such as the Quantum Simply Cellular (QSC) kit, among others, allow quantitative cellular measurements to be performed in a consistent manner by using calibrated microspheres. With this quantitative data, targeting effects can be combined with quantitative receptor measures to distinguish differences in performance and intracellular trafficking of targeting systems. This additional analysis can presumably identify subcellular mechanisms suitable for modulation to optimize the biological impact from targeting materials and methods.

A quantitative evaluation of the receptor number on the target cell surface is essential for a comprehensive interpretation of targeted gene or drug delivery, as well as other receptor-based experiments. A lack of this quantitative data precludes further

important analyses and modeling and makes direct comparisons between cell lines and targeting systems much less compelling. Quantitative methods, such as the one employed in this work, are invaluable resources in understanding the mechanism(s) responsible for limiting intracellular delivery and trafficking of drugs or gene therapies. This information could prove to be a critical factor in the development of improved delivery strategies for existing therapies or in the design of new and effective therapies altogether.

2.3 Materials and Methods

2.3.1 Cell culture

HT-1080 cells (human fibrosarcoma, ATCC CCL-121) were maintained and subcultured in complete culture medium consisting of minimum essential medium (MEM) supplemented with 10% fetal bovine serum, 2mM glutamine, 1.5 g/L sodium bicarbonate, 0.1mM non-essential amino acids, 1mM sodium pyruvate, and 1% antibiotics of penicillin-streptomycin-amphotericin. All cells were maintained at 37°C, 5% CO_2, and 95% humidity for the duration of the study.

For immunolabeling assays, cells were grown in 12-well plates (Becton-Dickinson) containing 1ml/well supplemented medium. Before harvest, adherent cells were washed with Ca^{++}/Mg^{++} free phosphate buffered saline (PBS). PBS was aspirated and 1ml of non-enzymatic cell dissociation solution (Sigma) was then added until the cells detached. Cells were immediately transferred into labeled cytometer tubes and 1mL supplemented MEM was added to stop the dissociation reaction. Cells were then pelleted

by centrifugation at 900×g and counted (Coulter Counter). For each cell type, 1×10^6 cells were removed and used for the remainder of the immunolabeling protocol.

2.3.2 Monoclonal Antibodies

Mouse IgG1 WM15 clone R-phycoerythrin (R-PE) labeled anti-human CD13 monoclonal antibody (mAb; Becton Dickinson) was purchased and used to screen HT-1080 cells. All antibody measurements were administered at the stock concentration delivered by the manufacturer. Conjugation to R-PE allowed straightforward detection using the FL2 channel of a FACSCalibur flow cytometer (Becton Dickinson). The same lot of antibody was used in all studies.

2.3.3 Cell irradiation

Irradiation was performed at room temperature using a Mark 1 irradiator with a Cs 137 source (JL Shepherd and Associates). Subconfluent monolayers (~60% confluence) in 12-well plates (Becton-Dickinson) were irradiated with 3Gy at a dose rate of ~1Gy/min. Immediately following radiation exposure, cells were returned to 37°C, 5% CO_2, and 95% humidity. Cells were then harvested by incubation in non-enzymatic cell dissociation solution (Sigma) at 1, 3, 6, 12, 24, and 48 hours post-irradiation and the immunolabeling and quantification assays were followed as described below.

2.3.4 Cytokine incubation

HT-1080 cells were seeded in 12-well tissue culture plates for exposure to either TNF-α or TGF-β1. To achieve consistent final cell concentrations, individual wells were

seeded at varying cell densities depending on the incubation duration for each sample: 1-day samples were seeded at ~50% confluence, 3-day samples at ~25% confluence, and 6 day samples at ~10% confluence. Subconfluent monolayers were incubated in complete culture medium as previously described, supplemented with either 100ng/ml TNF-α (Sigma) or 10ng/ml TGF-β1 (Sigma). Culture medium was changed every 24h to ensure relatively constant cytokine concentrations during the course of the experiment. Cells were then harvested by incubation in non-enzymatic cell dissociation solution at 1, 3, and 6 days and assayed for CD13 expression.

2.3.5 Immunolabeling assay

For initial studies, mAbs were utilized at the manufacturer's recommended dilution (20μL/10^6 cells) in PBS in a direct immunofluorescence assay. Cells (approximately $1x10^6$) were preincubated for 5 min in PBS supplemented with 1% bovine serum albumin to block nonspecific binding. Cells were then incubated with 80μl of mAb solution for 45 min at 4°C. After washing twice with fresh PBS cells were suspended in 1ml PBS for flow cytometric analysis. Saturating mAb conditions were confirmed by increasing the mAb concentration until no additional fluorescence (as measured by flow cytometry) was seen with increasing dose. The initial mAb concentration was found to be sufficient to saturate all available CD13 sites on the cell surface.

2.3.6 Flow cytometry calibration

Flow cytometry fluorescence measurements were calibrated by utilizing standardized Quantum Simply Cellular microspheres (QSC; Bangs Labs). This assay is based on the linear relationship between measured mean fluorescence intensity (MFI) and surface receptor expression level measured as antibody binding capacity (ABC). The QSC kit contains four uniform microsphere populations of the same size with various known binding capacities to mouse monoclonal IgG antibodies (2693, 27795, 439497, and 681322 ABC), along with a blank population that has no specific binding capacity for mouse IgG.

1 drop (~50μl) of QSC microspheres was incubated with the manufacturer's suggested concentration of mAb in PBS for 60 min at room temperature. The sample was then washed twice, analyzed by flow cytometry, and the results used to calculate a standard curve by plotting the MFI for each microsphere population (FL2 intensity) against its known ABC level. Saturation of the IgG binding sites on the surface of the microspheres was confirmed by treatment with increased concentrations of mAb until no additional fluorescence was measured. The original mAb concentration was sufficient to saturate all mAb binding sites on the QSC microspheres.

2.3.7 Surface protein quantification

CD13 quantification was performed by determining the mean fluorescence of both control and mAb treated cell populations. The control fluorescence was then subtracted from the fluorescence of the treated cells to determine the fluorescence shift

caused by mAb binding. This fluorescence shift was compared to the regression curve obtained from the QSC microspheres to determine the ABC level of the cell population.

2.3.8 Flow cytometric analysis

All samples were analyzed on a FACSCalibur (Becton Dickinson) that delivers an excitation beam at 488nm with an argon laser. Cell or microsphere controls were measured and gates were drawn to define whole cell and sphere populations. Further data collection was then based on these gates. All samples (cells and QSC microspheres) were collected using identical instrument settings to allow direct comparison of measured values. For each sample, 20,000 gated events were collected by list-mode data, consisting of forward scatter, side scatter, and fluorescence emissions FL1 (530 nm), FL2 (585 nm), and FL3 (650 nm). WinList software (Verity Software House) was utilized to determine the linear mean (MFI; mean FL2 intensity) of each cell and QSC microsphere population.

2.3.9 Statistics

Statistical significance of experimental populations was assessed using an upaired t-test and determined by SigmaStat (Jandel Scientific Software). Differences were termed significant for $p < 0.05$.

2.4 Results

HT-1080 cells express the CD13 protein on their surface at relatively high levels. Flow cytometry was utilized to quantify changes in cell-associated fluorescence after

addition of anti-CD13/R-PE mAb (Figure 2.1). A distinct increase in FL2 emission intensity was observed after treatment with the labeled mAb, indicating strong interaction of the mAb with the cell surface. Control, untreated HT-1080 cells had a mean FL2 intensity of 1.3 arbitrary units (a.u.), while cells treated with the anti-CD13/R-PE mAb had a mean intensity of 922.4 a.u. This shift of 921.1 a.u. suggests significant antibody-cell surface interaction that can be quantified by the calibration method applied in this work.

The QSC assay yields a linear relationship relating fluorescence changes to surface receptor concentration. To perform receptor quantitation, QSC microspheres were incubated with anti-CD13/RP-E mAb and analyzed by flow cytometry utilizing the same settings used in cell experiments. Mean fluorescence measurements were obtained for each microsphere population and data was used to calculate a standard curve relating FL2 fluorescence intensity and the known ABC of each microsphere population (Figure 2.2). The standard curve demonstrates the linear relationship between receptor concentration and fluorescence intensity obtained from these values.

Flow cytometry results, coupled with the QSC assay, can be used to quantify mAb binding to the cell surface. The standard curve obtained from the QSC microspheres was used to relate the measured FL2 shift of mAb treated cell samples to the corresponding ABC level. The calibrated CD13 expression levels for the HT-1080 cells studied here are a direct linear transformation of the uncalibrated fluorescence values shown in Figure 2.1. These cells exhibit a fluorescence shift of 921.1 a.u. as a result of anti-CD13/R-PE binding, correlating to a mean CD13 expression level of 3,840,000 ± 70,000 ABC/cell (n = 4).

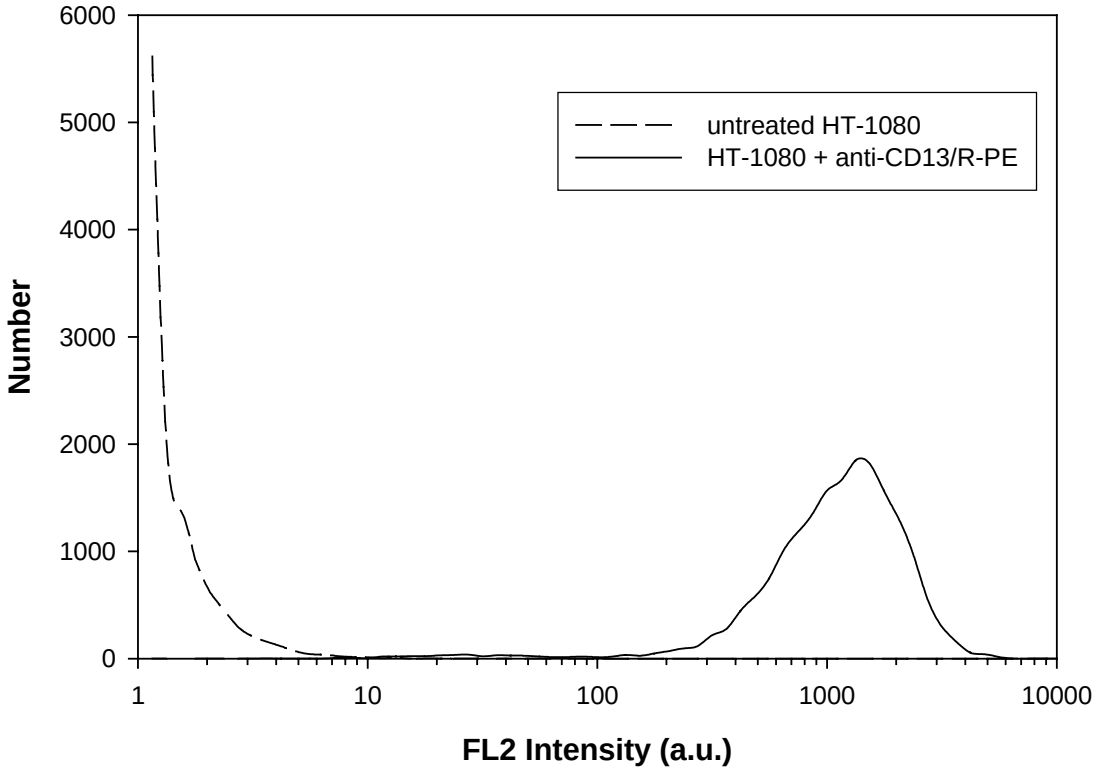

Figure 2.1. Incubation of HT-1080 cells with anti-CD13/R-PE mAb results in a significant shift in fluorescence intensity in the FL2 measurement range. Control, untreated HT-1080 cells (dashed line) generate low autofluorescence in the FL2 wavelength range when measured by flow cytometry. Incubation of the cells with R-PE labeled mAb (solid line) produces a unimodal cell population with an average FL2 intensity more than 1000-fold greater than that of untreated HT-1080 cells, presumably correlated with high expression levels of the CD13 antigen on the cell surface.

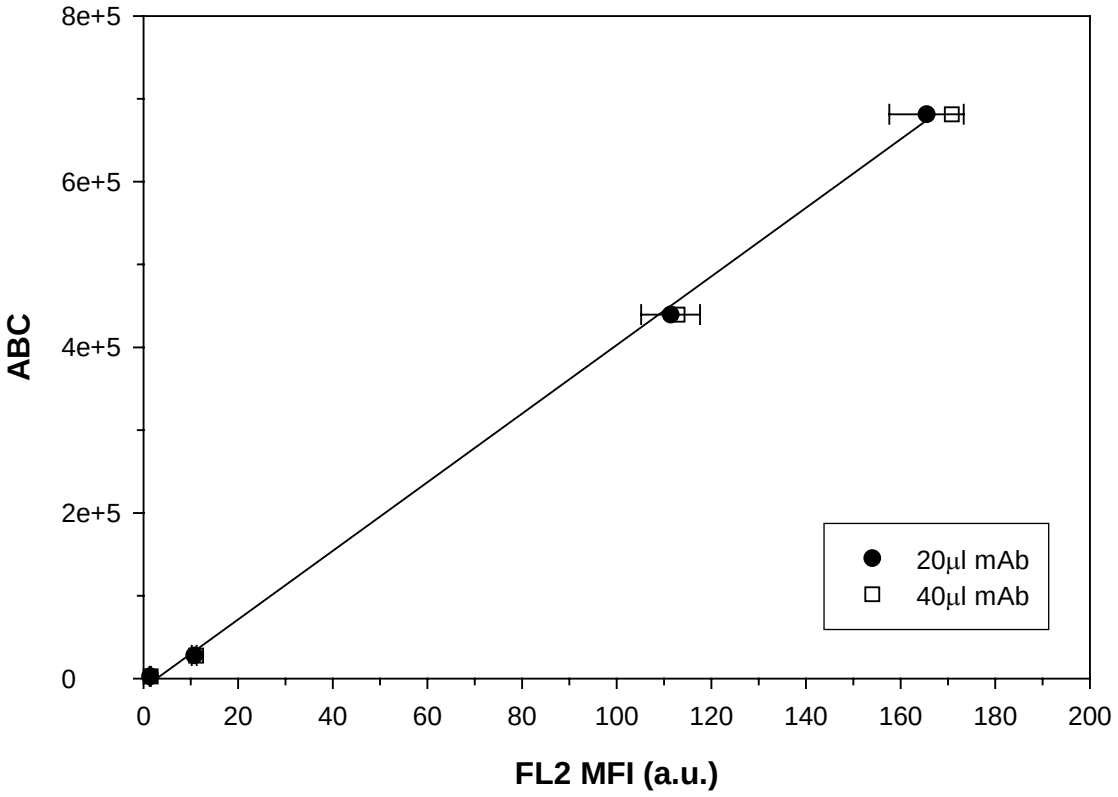

Figure 2.2. The correlation relating mean fluorescence intensity (MFI) measured by flow cytometry to antigen expression levels (measured as ABC) results in a highly linear relationship. QSC microspheres were incubated with the manufacturer's recommended mAb concentration (20µl mAb, solid circles). A standard curve (solid line) produced from the relationship between MFI and ABC yielded a linear relationship ($R^2 = 0.9992$) enabling a straightforward and accurate conversion of raw MFI data to ABC/cell. Insignificant modulation of the MFI:ABC relationship resulted from doubling the manufacturer's recommended mAb concentration (40µl; open squares), suggesting that the microspheres were saturated at the 20µl dose. n = 3 for each mAb concentration. Error bars for the 40µl concentration have been suppressed to ease visualization.

Low-level radiation exposure results in an extensive increase in CD13 expression on the surface of HT-1080 cells. An increase in CD13 surface expression was detected by flow cytometry up to 48 hours after low dose irradiation (Figure 2.3). CD13 expression decreased transiently within 1h of irradiation at 3Gy, followed by the induction of a prolonged significant increase beginning 6h after irradiation. Receptor concentration in irradiated cells continued to rise up to 24 hr after stimulation, reaching a mean value of 6,300,000 ± 220,000 ABC/cell (n = 3). This rise in CD13 expression appears to peak at times >24 hr, as expression begins to decrease slightly at the 48h mark to 5,670,000 ± 110,000 ABC/cell (n = 3).

Exposure to the cytokines TNF-α and TGF-β1 modulates CD13 expression on HT-1080 cells. Both compounds had statistically significant effects, although incubation with TNF-α resulted in markedly increased protein levels over both resting and TGF-β1 stimulated HT-1080 cells (Figure 2.4). After 24h, both cytokines caused a small but measurable increase in CD13 expression compared to control, unstimulated cells. Effects of TGF-β1 appear to peak after this timepoint, reaching a maximum CD13 value of 4,700,000 ± 270,000 ABC/cell, as no statistically significant increases are measured with continued incubation. HT-1080 cells maintained these increased CD13 levels for the duration of the experiment. TNF-α modulation continues to increase after 24h, elevating CD13 levels to 7,250,000 ± 280,000 ABC/cell at 48h. This effect peaks after the 48h timepoint, with CD13 expression falling to 6,210,000 ± 260,000 ABC/cell after 72h.

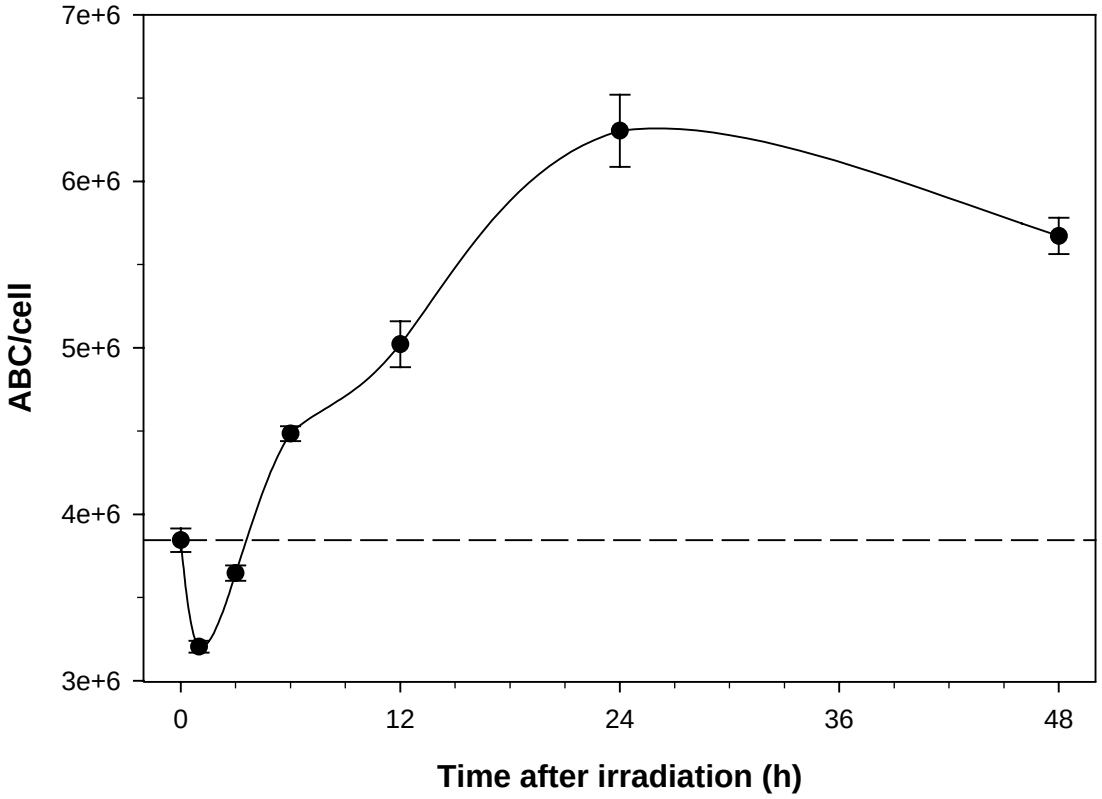

Figure 2.3. CD13 expression on HT-1080 cells increases significantly following low-dose irradiation with 3Gy, as assessed by quantitative flow cytometry. Functional protein surface concentration decreased transiently within 1h of irradiation, followed by the induction of a prolonged significant increase phase beginning at 6h post-irradiation. Increased CD13 levels continue to rise up to 24h post-irradiation, reaching a peak value of 6,303,200 ± 216,800 ABC/cell (a 64% increase over unirradiated cells). Values are mean ± standard deviation of three independent measurements (dotted line = CD13 expression of control, untreated HT-1080 cells). All values are statistically different ($p < 0.05$) from unstimulated HT-1080 cells (t=0).

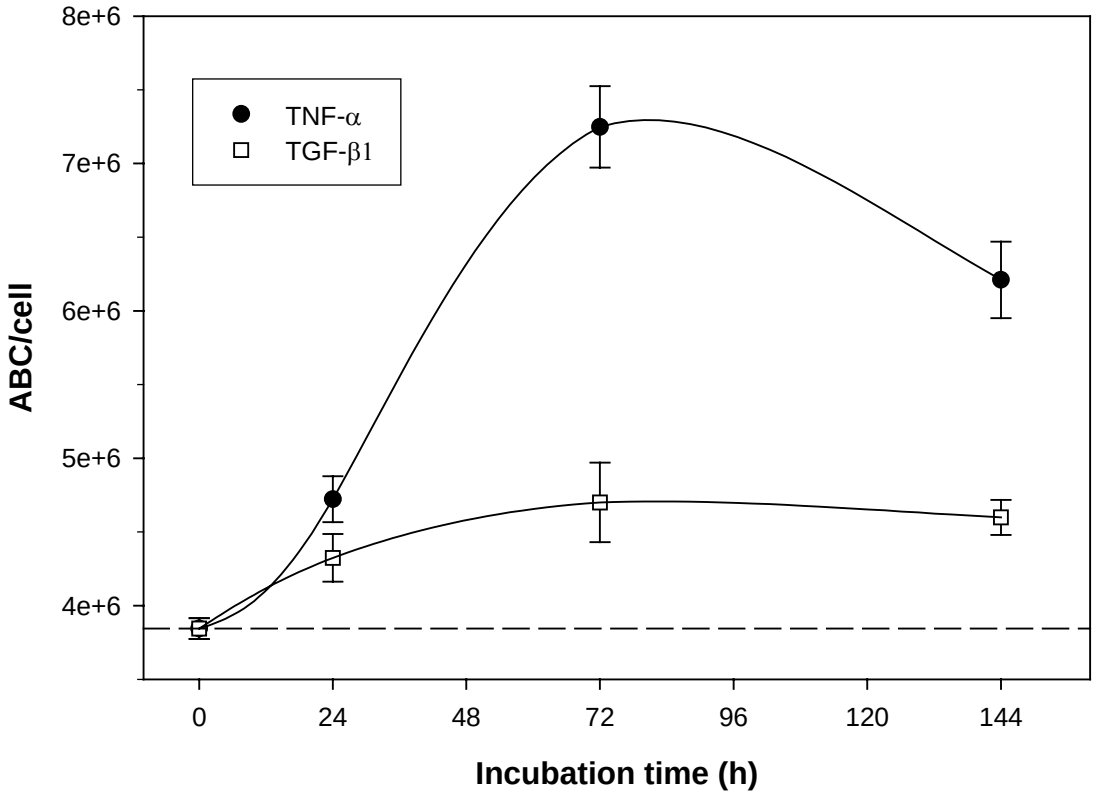

Figure 2.4. Cytokine exposure results in significant modulation of CD13 expression on HT-1080 cells. Incubation with 10ng/ml TGF-β1 (open squares) resulted in a modest, but statistically significant increase (22%) in CD13 expression, peaking at 4,700,000 ± 269,900 ABC/cell after 72h. 100ng.ml TNF-α (solid circles) had a much larger modulatory effect, increasing CD13 levels to 7,248,100 ± 276,400 ABC/cell (an 89% increase) after 72h. Elevated CD13 expression levels were measured for both cytokines for the duration of the study (up to 144h incubation). Values are mean ± standard deviation of three independent measurements (dotted line = CD13 expression of control, untreated HT-1080 cells). Values for all timepoints are statistically significant from control (t=0) and between treatments ($p < 0.05$).

2.5 Discussion

Although the importance of receptor concentration in modulating specific drug or gene targeting is well defined, few targeting studies have included direct target quantification. Methods such as Western blotting and immunoprecipitation are typically used to confirm the presence of proteins on the surface of specific cell types (33,38). While such methods can confirm the surface presentation of specific proteins, they are not robust tools for quantitative assessments. Traditional FACS analysis is also employed in a number of studies to verify the presence of specific proteins on the cell surface (33-35). Although FACS analysis is intrinsically quantitative, uncalibrated results yield only a qualitative estimate of receptor presentation and complicate comparisons among instruments and reagents. The methods used in the current study enable robust comparison of receptor presentations among multiple cell types and for various experimental and assessment conditions.

Our studies (Figure 2.1), using traditional FACS analysis, confirm the presence and relatively high expression of CD13 on the surface of HT-1080 cells, in agreement with previous reports of high CD13 levels on these cells (39). Fluorescence intensities in this system were well above the values measured in our previous quantitative studies for CD51 surface presentation on HeLa and other cell types (40), necessitating adjustment of fluorescence gain settings to accurately measure the labeled cell population. Large differences in fluorescence intensity distribution require optimization of FACS instrument settings that compromise comparisons in the absence of quantitative calibrations.

While fluorescence shifts measured by flow cytometry indicate functional protein presence on the cell surface and enable qualitative comparisons, they are not a direct measure of the number of receptors present on the cell surface. Fluorescence intensity in this system is modulated by multiple of factors, ranging from the particular fluorophore used to specific instrument settings. For example, fluorescence shifts measured in this study are far lower than those measured in our previous quantitative studies of receptor expression (~920 a.u. as compared to ~1400 a.u.) (40). However, the smaller fluorescence shifts measured in the current study correlate to significantly higher expression values due to the specific, optimized, instrument settings utilized during data acquisition. Thus, direct comparisons of raw fluorescence data are not necessarily accurate indicators of target surface number, especially across multiple systems, instruments, and reagents. To ensure portability and reproducibility, FACS fluorescence intensity data must be correlated to physical values unaffected by experimental conditions.

In the current study, fluorescence intensity measurements are standardized to enable conversion of measured intensity to the corresponding number of surface receptors. The high degree of response linearity (in Figure 2.2) suggests that this calibration is free from artifacts, and provides a straightforward and reliable conversion. However, the fluorescence of some HT-1080 cells following mAb treatment (Figure 2.1) is outside the range established by the QSC standard curve (Figure 2.2). The use of calibrated R-PE fluorescence standards, a common practice in flow cytometry, confirms the linear fluorescence response of this flow cytometer well beyond the established range. The fluorescence intensities of these standards span the measurable range, yielding a

linear relationship between fluorophore concentration and fluorescence intensity (MFI) to values approaching 10,000 MFI (data not shown).

The ABC values obtained in this study indicate that CD13 is very highly expressed on the surface of HT-1080 cells (3,840,000 ± 70,000 ABC/cell), but not outside the measurement range established for cellular proteins. Previous studies have shown that integrins and other proteins are highly expressed on many cell types *in vitro*, including expression levels of various surface markers from the low thousands to the low millions per cell (41). The optimized methods used in this work yield functional protein quantitations on the cell surface that are more precise than many other techniques, reducing uncertainty in interpretation and subsequent calculational use of these values.

Stimulation of HT-1080 cells with low dose ionizing radiation (3Gy) produced a significant increase in CD13 presentation on the cell surface (Figure 2.3). This type of radiation-induced expression has been utilized in targeting to tumor endothelial cells and has been demonstrated to improve the efficacy of chemotherapy (42). However, the lack of quantitative characterization of the endothelial cell response to x-ray complicates the application and limits optimization of increased targeting efficacy. Elucidation of the kinetic and quantitative effects enables accurate identification of the temporal treatment strategy for optimum access to radiation-upregulated receptors and prediction of the likely success of the application. The magnitude (64% increase) and duration (>48 hr) of the response measured in this and other (40) studies demonstrates the potential of radiation-induced tumor targeting as a strong potential candidate for therapeutic applications. This result is particularly important in cases where standard treatment involves combination therapies such as radiation followed by administration of

chemotherapeutics (43). Combination therapies utilizing elements directly targeted to tumor cells have the potential to improve the therapeutic index of conventional, nontargeted materials, but only if the pharmacokinetics of receptor availability are used to optimize the approach.

CD13 presentation on the HT-1080 surface was also modulated by cell exposure to cytokines. Both TNF-α and TGF-β1 produced measurable increases in CD13 expression on the cell surface. This response ranged from a modest but significant increase (22%) with TGF-β1 incubation, to a strong modulation (89% increase) by TNF-α. This result is consistent with previous reports of cytokine modulation of an array of cellular proteins (41,44). This work is the first quantitative assessment of CD13 surface presentation modulated by TNF-α and TGF-β1 cytokines.

Cytokine modulation of target expression is especially important in cases where these bioactive molecules are themselves utilized as therapeutic molecules. Several studies have highlighted the utility of TNF-α as an antitumor agent (10,45,46). These studies include several attempts at specific targeting to proteins expressed on the cell surface, including CD13. Our results reveal that TNF-α significantly increases CD13 expression in our *in vitro* system. However, as shown in other studies, these effects can be either positive (increasing protein presentation) or negative (decreasing protein presentation) (41). Thus, TNF-α (or other cytokines) delivered as therapeutic agents may have a direct effect on the efficiency of subsequent targeting through modulation of cell surface target presentation. Knowledge of these interactions is likely to be critical in the development of effective therapeutic strategies and targeting approaches.

The role of cytokine modulation of cell surface receptor presentation in cancer biology is another application that can benefit from quantitative understanding. The secondary effects on increased CD13 presentation on the cell surface is beyond the scope of this work, but conceivably contributes to the characteristics associated with a proliferative cell phenotype. This study enables the quantitative comparison of CD13 modulation by cytokine exposure in primary cells as a tool to explore the differential effects of this response.

As evidenced by this study, receptor concentration can range widely, even within the same cell line when stimulated with various factors and to different degrees. The wide range in CD13 expression levels measured within a given cell type subjected to various experimental conditions underscores the importance of quantitative receptor analysis in conjunction with targeted therapies. The range in possible receptor concentrations is an important consideration in the design of targeted drug delivery vectors and the methods used for their evaluation and characterization. Interaction with cell surface receptors is a prevalent strategy for specific cellular delivery in both *in vitro* and *in vivo* targeting studies. Thus, direct receptor quantitation represents an important step in evaluating the fundamental efficiency of any receptor-targeting element.

Many of the so-called “next generation” delivery systems are or will be designed to target specific cell surface markers, and therefore will be strongly dependent on receptor concentration for effective binding of the construct. The effectiveness of these specific targeted vehicles, in turn, can only be determined with knowledge of the target availability (*i.e.* receptor concentration), and factors modulating target expression (*e.g.* irradiation, cytokine exposure). However, surface interactions alone cannot dictate the

success or failure of targeted drug or gene delivery. Other events, characteristic of the therapeutic mechanism(s), such as intracellular signaling, cytosolic processing, and entry into the nucleus, are also important factors governing therapeutic efficacy. Nonetheless, binding mediated by surface receptors is the first step in the delivery pathway, acting as a gateway for all subsequent intracellular events.

Quantitative evaluation methods such as the one employed here can be important tools in understanding subcellular events associated with molecular targeting. However, interpretation of any quantitative technique can be complicated by several issues involving instrumentation, reagent selection, and methodology-specific factors such as antibody/antigen binding valency. We have taken steps to minimize these difficulties in the current study, and have assessed the validity of our results using multiple, redundant techniques. Ultimately, the accuracy of these results depends on immunofluorescence methods that are widely accepted and generally applicable for both research and clinical understanding.

A growing body of evidence points to the fundamental role cell surface proteins play in determining the physiological activity and experimental response of individual cell phenotypes. This response, in turn, plays a crucial role in governing the effectiveness of many specifically targeted gene and drug delivery vectors. A detailed analysis of these surface reactions can be extremely valuable in understanding the intracellular process(es) responsible for limiting delivery of active drugs and genes to specific cells, as interactions with surface receptors serve as the gateway to these events. Quantitative information promises to extend the power and efficacy of current studies by allowing a more thorough understanding of the importance of specific cell surface

proteins in physiological and disease processes. This information can then be employed in the development of new therapies or the creation of more effective targeting strategies for therapies in existence today.

2.6 Acknowledgements

This work was supported by the National Institutes of Health (Grant number R21CA091299). We also thank the laboratory of Dr. Dennis Hallahan (Vanderbilt University, Department of Radiation Oncology) for expertise and equipment for cell irradiation.

2.7 References

1. Chen EX, Siu LL. Development of molecular targeted anticancer agents: successes, failures and future directions. Curr Pharm Des 2005;11(2):265-72.

2. Hart SL, Arancibia-Carcamo CV, Wolfert MA, Mailhos C, O'Reilly NJ, Ali RR, Coutelle C, George AJ, Harbottle RP, Knight AM and others. Lipid-mediated enhancement of transfection by a nonviral integrin-targeting vector. Hum Gene Ther 1998;9(4):575-85.

3. Schneider H, Harbottle RP, Yokosaki Y, Jost P, Coutelle C. Targeted gene delivery into alpha9beta1-integrin-displaying cells by a synthetic peptide. FEBS Lett 1999;458(3):329-32.

4. Vyas SP, Singh A, Sihorkar V. Ligand-receptor-mediated drug delivery: an emerging paradigm in cellular drug targeting. Crit Rev Ther Drug Carrier Syst 2001;18(1):1-76.

5. Torchilin VP. Drug targeting. Eur J Pharm Sci 2000;11 Suppl 2:S81-91.

6. Hallahan DE, Geng L, Cmelak AJ, Chakravarthy AB, Martin W, Scarfone C, Gonzalez A. Targeting drug delivery to radiation-induced neoantigens in tumor microvasculature. J Control Release 2001;74(1-3):183-91.

7. Hu Z, Garen A. Intratumoral injection of adenoviral vectors encoding tumor-targeted immunoconjugates for cancer immunotherapy. Proc Natl Acad Sci U S A 2000;97(16):9221-5.

8. Hu Z, Sun Y, Garen A. Targeting tumor vasculature endothelial cells and tumor cells for immunotherapy of human melanoma in a mouse xenograft model. Proc Natl Acad Sci U S A 1999;96(14):8161-6.

9. Schatzlein AG, Rutherford C, Corrihons F, Moore BD. Phage derived peptides for targeting of doxorubicin conjugates to solid tumours. J Control Release 2001;74(1-3):357-62.

10. Corti A, Ponzoni M. Tumor vascular targeting with tumor necrosis factor alpha and chemotherapeutic drugs. Ann N Y Acad Sci 2004;1028:104-12.

11. Holle L, Song W, Hicks L, Holle E, Holmes L, Wei Y, Li J, Wagner T, Yu X. In vitro targeted killing of human endothelial cells by co-incubation of human serum and NGR peptide conjugated human albumin protein bearing alpha (1-3) galactose epitopes. Oncol Rep 2004;11(3):613-6.

12. Mizuguchi H, Koizumi N, Hosono T, Utoguchi N, Watanabe Y, Kay MA, Hayakawa T. A simplified system for constructing recombinant adenoviral

vectors containing heterologous peptides in the HI loop of their fiber knob. Gene Ther 2001;8(9):730-5.

13. Arap W, Pasqualini R, Ruoslahti E. Cancer treatment by targeted drug delivery to tumor vasculature in a mouse model. Science 1998;279(5349):377-80.

14. Pasqualini R, Koivunen E, Ruoslahti E. Alpha v integrins as receptors for tumor targeting by circulating ligands. Nat Biotechnol 1997;15(6):542-6.

15. Pasqualini R, Koivunen E, Kain R, Lahdenranta J, Sakamoto M, Stryhn A, Ashmun RA, Shapiro LH, Arap W, Ruoslahti E. Aminopeptidase N is a receptor for tumor-homing peptides and a target for inhibiting angiogenesis. Cancer Res 2000;60(3):722-7.

16. Olsen J, Kokholm K, Noren O, Sjostrom H. Structure and expression of aminopeptidase N. Adv Exp Med Biol 1997;421:47-57.

17. Firla B, Arndt M, Frank K, Thiel U, Ansorge S, Tager M, Lendeckel U. Extracellular cysteines define ectopeptidase (APN, CD13) expression and function. Free Radic Biol Med 2002;32(7):584-95.

18. Curnis F, Arrigoni G, Sacchi A, Fischetti L, Arap W, Pasqualini R, Corti A. Differential binding of drugs containing the NGR motif to CD13 isoforms in tumor vessels, epithelia, and myeloid cells. Cancer Res 2002;62(3):867-74.

19. van Hensbergen Y, Broxterman HJ, Rana S, van Diest PJ, Duyndam MC, Hoekman K, Pinedo HM, Boven E. Reduced growth, increased vascular area, and reduced response to cisplatin in CD13-overexpressing human ovarian cancer xenografts. Clin Cancer Res 2004;10(3):1180-91.

20. van Hensbergen Y, Broxterman HJ, Hanemaaijer R, Jorna AS, van Lent NA, Verheul HM, Pinedo HM, Hoekman K. Soluble aminopeptidase N/CD13 in malignant and nonmalignant effusions and intratumoral fluid. Clin Cancer Res 2002;8(12):3747-54.

21. Wick W, Wick A, Schulz JB, Dichgans J, Rodemann HP, Weller M. Prevention of irradiation-induced glioma cell invasion by temozolomide involves caspase 3 activity and cleavage of focal adhesion kinase. Cancer Res 2002;62(6):1915-9.

22. Hallahan DE, Staba-Hogan MJ, Virudachalam S, Kolchinsky A. X-ray-induced P-selectin localization to the lumen of tumor blood vessels. Cancer Res 1998;58(22):5216-20.

23. Giannopoulou E, Katsoris P, Hatziapostolou M, Kardamakis D, Kotsaki E, Polytarchou C, Parthymou A, Papaioannou S, Papadimitriou E. X-rays modulate extracellular matrix in vivo. Int J Cancer 2001;94(5):690-8.

24. Kim LT, Yamada KM. The regulation of expression of integrin receptors. Proc Soc Exp Biol Med 1997;214(2):123-31.

25. Zhang J, Spring H, Schwab M. Neuroblastoma tumor cell-binding peptides identified through random peptide phage display. Cancer Lett 2001;171(2):153-64.

26. Ruoslahti E. Targeting tumor vasculature with homing peptides from phage display. Semin Cancer Biol 2000;10(6):435-42.

27. Pasqualini R, Ruoslahti E. Organ targeting in vivo using phage display peptide libraries. Nature 1996;380(6572):364-6.

28. Rajotte D, Ruoslahti E. Membrane dipeptidase is the receptor for a lung-targeting peptide identified by in vivo phage display. J Biol Chem 1999;274(17):11593-8.

29. Yokoyama Y, Ramakrishnan S. Addition of an aminopeptidase N-binding sequence to human endostatin improves inhibition of ovarian carcinoma growth. Cancer 2005;104(2):321-31.

30. Zarovni N, Monaco L, Corti A. Inhibition of tumor growth by intramuscular injection of cDNA encoding tumor necrosis factor alpha coupled to NGR and RGD tumor-homing peptides. Hum Gene Ther 2004;15(4):373-82.

31. Dirksen A, Langereis S, de Waal BF, van Genderen MH, Meijer EW, de Lussanet QG, Hackeng TM. Design and synthesis of a bimodal target-specific contrast agent for angiogenesis. Org Lett 2004;6(26):4857-60.

32. Ruoslahti E, Pierschbacher MD. New perspectives in cell adhesion: RGD and integrins. Science 1987;238(4826):491-7.

33. Takayama K, Ueno H, Pei XH, Nakanishi Y, Yatsunami J, Hara N. The levels of integrin alpha v beta 5 may predict the susceptibility to adenovirus-mediated gene transfer in human lung cancer cells. Gene Ther 1998;5(3):361-8.

34. Romanov VI, Goligorsky MS. RGD-recognizing integrins mediate interactions of human prostate carcinoma cells with endothelial cells in vitro. Prostate 1999;39(2):108-18.

35. Muller K, Nahde T, Fahr A, Muller R, Brusselbach S. Highly efficient transduction of endothelial cells by targeted artificial virus-like particles. Cancer Gene Ther 2001;8(2):107-17.

36. Serke S, van Lessen A, Huhn D. Quantitative fluorescence flow cytometry: a comparison of the three techniques for direct and indirect immunofluorescence. Cytometry 1998;33(2):179-87.

37. Lenkei R, Gratama JW, Rothe G, Schmitz G, D'Hautcourt J L, Arekrans A, Mandy F, Marti G. Performance of calibration standards for antigen quantitation with flow cytometry. Cytometry 1998;33(2):188-96.

38. Hautala T, Grunst T, Fabrega A, Freimuth P, Welsh MJ. An interaction between penton base and alpha v integrins plays a minimal role in adenovirus-mediated gene transfer to hepatocytes in vitro and in vivo. Gene Ther 1998;5(9):1259-64.

39. van Hensbergen Y, Broxterman HJ, Elderkamp YW, Lankelma J, Beers JC, Heijn M, Boven E, Hoekman K, Pinedo HM. A doxorubicin-CNGRC-peptide conjugate with prodrug properties. Biochem Pharmacol 2002;63(5):897-908.

40. Smith RA, Giorgio TD. Quantitation and kinetics of CD51 surface receptor expression: implications for targeted delivery. Ann Biomed Eng 2004;32(5):635-44.

41. Mutin M, Dignat-George F, Sampol J. Immunologic phenotype of cultured endothelial cells: quantitative analysis of cell surface molecules. Tissue Antigens 1997;50(5):449-58.

42. Hallahan D, Geng L, Qu S, Scarfone C, Giorgio T, Donnelly E, Gao X, Clanton J. Integrin-mediated targeting of drug delivery to irradiated tumor blood vessels. Cancer Cell 2003;3(1):63-74.

43. Duenas-Gonzalez A, Cetina L, Mariscal I, de la Garza J. Modern management of locally advanced cervical carcinoma. Cancer Treat Rev 2003;29(5):389-99.

44. Albelda SM, Buck CA. Integrins and other cell adhesion molecules. Faseb J 1990;4(11):2868-80.

45. Curnis F, Sacchi A, Borgna L, Magni F, Gasparri A, Corti A. Enhancement of tumor necrosis factor alpha antitumor immunotherapeutic properties by targeted delivery to aminopeptidase N (CD13). Nat Biotechnol 2000;18(11):1185-90.

46. Curnis F, Gasparri A, Sacchi A, Longhi R, Corti A. Coupling tumor necrosis factor-alpha with alphaV integrin ligands improves its antineoplastic activity. Cancer Res 2004;64(2):565-71.

CHAPTER III

QUANTITATIVE MEASUREMENT OF MULTIFUNCTIONAL QUANTUM DOT BINDING TO CELLULAR TARGETS USING FLOW CYTOMETRY

RA Smith and TD Giorgio*

Department of Biomedical Engineering
Vanderbilt University, Nashville, TN

Correspondence:
Todd D. Giorgio
Vanderbilt University
Box 351620, Station B
Nashville, TN 37235
615-322-3756 (voice)
615-343-7919 (fax)
todd.d.giorgio@vanderbilt.edu

Key Terms: flow cytometry, fluorometry, quantum dot, nanocrystal, quantitative, calibration, NGR, PEG

This manuscript was prepared for submission in *Cytometry*

3.1 Abstract

Background**:** Semiconductor nanocrystals such as quantum dots (QDs) are a potentially powerful resource in the fields of flow cytometry and fluorescence microscopy. QD size and fluorescence characteristics offer attractive features for use in targeted delivery systems and detection by flow cytometry. While quantitative measurements of a variety of fluorescent molecules are routinely performed, fluorophores for which no calibration standards exist, such as QDs, pose a problem for quantitation in flow cytometry. Our goal was to develop a targeted nanoparticulate delivery system for therapeutic delivery as well as a method to accurately and quantitatively assess the performance of this system.

Methods: We synthesized surface-modified QD probes targeted to cellular surface receptors and measured the MFI of the resulting cell-probe conjugates by flow cytometry. MFI was converted to mean equivalent R-PE intensity (MEPE) using standard calibration microspheres. Known concentrations of both R-PE and QD probes were measured by fluorometry to relate R-PE and QD fluorescence. Fluorometry results were then used to translate MEPE measurements to the number of bound QD probes.

Results: The targeted probes we developed exhibited superior binding characteristics over unmodified and untargeted particles. This binding interaction was shown to be specific and mediated by the NGR targeting ligand. The calibration method developed to assess this system proved successful at converting raw fluorescence data to quantitative probe binding values.

Conclusions: We demonstrate the synthesis and performance of a highly modular nanoparticulate system capable of targeted therapeutic delivery and imaging. The calibration method implemented to quantify the performance of this system represents a potentially powerful tool to extend truly quantitative measurements to an array of fluorescent molecules.

3.2 Introduction

Recent advances in library screening and other methods have identified new cell-specific surface markers potentially suitable for drug and gene delivery. The NGR tripeptide is one such molecule identified as a tumor-homing sequence that selectively targets tumor vasculature *in vivo* (1,2). Additional studies identified CD13 as the receptor for this peptide motif (3). CD13 expression has been reported in a variety of tissues, and a recent study has revealed the existence of at least two distinct isoforms of this antigen (4). Further investigation confirmed that the isoform found in tumorigenic cells and angiogenic blood vessels functions as a receptor for the NGR motif, while the isoform expressed in normal counterparts of these cells does not appreciably bind NGR conjugates. CD13 overexpression has been measured in both tumor cells and angiogenic blood vessels (5,6), providing an appealing and accessible target for directed therapy.

Molecules targeting receptors such as these have been incorporated into liposomes (7-9), microparticles and nanoparticles (10,11), and directly conjugated to drugs or genes (2,12,13) to facilitate delivery of high concentrations of therapeutic agents to the cell surface. The use of nanoparticles for this purpose has the inherent advantage of a large surface area to volume ratio, allowing conjugation of multiple active

molecules. Stable covalent conjugation of bioactive molecules such as enzymes (14,15), mAbs (16), peptides (17), and DNA (18,19) to the surface of NPs has been reported. With small-molecule ligands, short peptides, and DNA probes, multiple copies of the ligand can be attached to the surface of the QD enabling multivalent binding to target cells.

QDs offer the typical characteristics of other nanoscale objects with the added benefit of intense fluorescence characteristics for straightforward and highly sensitive detection and imaging. These attributes impart the ability to integrate detection, imaging, and potential treatment characteristics (*e.g.* therapeutic payload delivery) into a single multifunctional nanoparticle. Particles such as these provide a stable and highly modular base for targeted delivery not offered by drugs or imaging materials alone. Intrinsic imaging capability enables detection and performance monitoring of these systems in a number of ways – qualitative fluorescence comparisons can be made in real time by fluorescence microscopy while more quantitative measurements can be performed by techniques such as flow cytometry. The current generation of QDs has been used successfully for both i*n vitro* and small animal *in vivo* imaging (20,21). Nanomaterials currently in development aim to extend this capability by providing the potential for medical imaging with particles such as reduced-toxicity near-infrared (NIR) emitting QDs and other nanoparticulate contrast agents.

Traditional fluorophores (*e.g.*, fluorescein isothiocyanate [FITC], R-phycoerythrin [R-PE], and enhanced green fluorescent protein [EGFP]) have been used extensively in conjunction with fluorescence microscopy and flow cytometry. Reliable fluorescence calibration standards have enabled users to move beyond basic sample detection and

visualization to quantitative measurements utilizing these reagents (22-24). Unfortunately, many fluorescent molecules (including QDs) currently lack the necessary standards to facilitate quantitative approaches. Without suitable calibration methods, measurements are often limited to qualitative comparisons and relative fluorescence intensities (*i.e.*, MFI) with little inherent connection to the biological structure or activity under assessment.

In this report we describe the synthesis and *in vitro* performance of a QD construct capable of multivalent targeted binding to cellular proteins and fluorescent labeling of targeted cells. These data provide a viable modular nanoscale platform capable of directed binding and payload delivery to target cells. Furthermore, we illustrate a method for fluorescence calibration of flow cytometry data capable of extending quantitative measurement to these molecules as well as to other fluorophores for which appropriate calibration standards are not available.

3.3 Materials and Methods

3.3.1 Cell Culture

HT-1080 cells (human fibrosarcoma, ATCC CCL-121) were maintained and subcultured in complete medium containing minimum essential medium (MEM) supplemented with 10% fetal bovine serum, 2mM glutamine, 1.5 g/L sodium bicarbonate, 0.1mM non-essential amino acids, 1mM sodium pyruvate, and 1% antibiotics of penicillin-streptomycin-amphotericin. All cells were maintained at 37°C, 5% CO_2, and 95% humidity for the duration of the study. For probe binding assays, cells

were grown to confluence in 12-well tissue culture plates (Becton-Dickinson) containing 1mL/well of supplemented MEM under the conditions described above.

3.3.2 Peptides and QD Probes

The cyclized PEGylated CD13-targeting peptide (HN-PEG-NGR) was synthesized and purified by AnaSpec (San Jose, CA), where HN-PEG is a 3400 Da PEG chain with functional groups suitable for subsequent synthesis reactions and NGR is the cyclized CNGRC targeting peptide. HN-PEG-NHS is the same PEG chain used in synthesis of the PEGylated CD13-targeting peptide described above and was obtained from Nektar Therapeutics (Huntsville, AL). The N-terminal amine group of the desired construct was conjugated to the surface of carboxylate QDs (585nm emission; Quantum Dot Corp., Hayward, CA) using 1-ethyl-3-(3-dimethylaminopropyl)carbodiimide (EDC; Sigma) to produce QD-PEG and QD-PEG-NGR probes. Briefly, 250μl of QDs (7.5μM) was diluted to 1μM with 10mM borate buffer, pH 7.4. 80μl from a 10mg/ml stock solution of HN-PEG-NHS or the HN-PEG-NGR targeting construct was then added to the solution. 57μl from a 10mg/ml stock solution of EDC was added and the mixture was stirred for 2h at room temperature to complete the conjugation. A representation of the final QD probe conjugates can be seen in Figure 3.1.

Following conjugation, the mixture was purified by spin filtration in a 50,000 nominal molecular weight limit (NMWL) cutoff device (Amicon Ultra-4, Millipore Corp.). Three buffer exchanges were performed with 50mM borate buffer (pH 8.3) and the final conjugate was stored at 4ºC. The concentration of the final purified product was

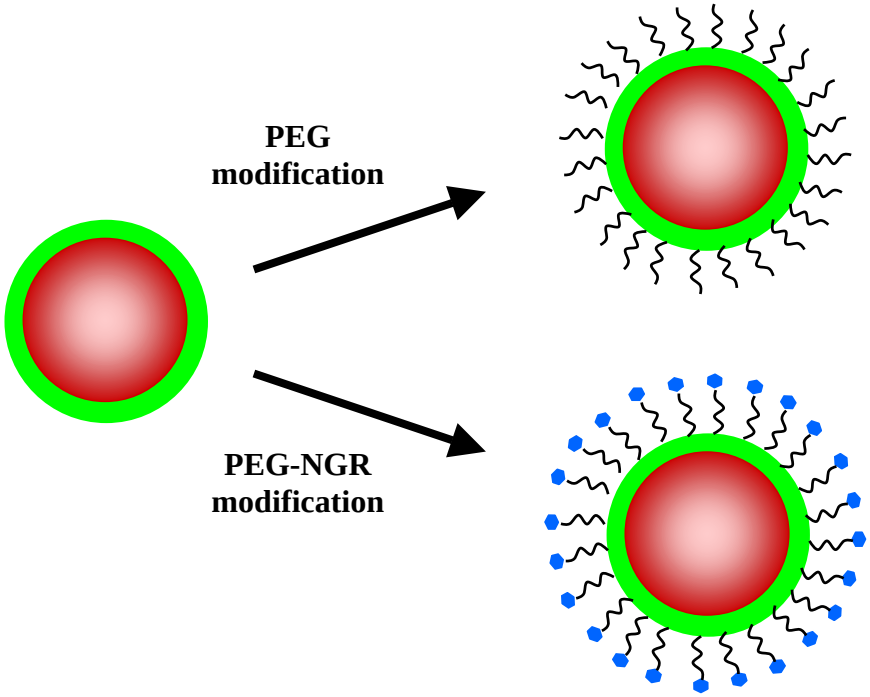

Figure 3.1. The capacity for cell binding of three distinct QD probes is characterized in this study. Representative structures of these probes are shown here. Unmodified QDs (left) consist of a semiconductor CdSe base (red) coated with an amphiphilic (AMP) polymer (green). QD-PEG probes (top right) are synthesized by modifying AMP QDs with multiple copies of PEG_{3400} polymer (black). QD-PEG-NGR probes (bottom right) are similar to QD-PEG probes with the addition of a distal NGR targeting peptide (blue). The conjugation of many identical PEG-NGR ligands enables multivalent interaction of the QD probes with targets on the cell surface.

determined by measuring the absorbance at 575nm using a QD extinction coefficient of $400{,}000 M^{-1}cm^{-1}$. As this value is a characteristic of the semiconductor core, the extinction coefficient is presumably unchanged by surface functionalization. However, conjugation of molecules to the QD surface does have an effect on the fluorescence emission (*i.e.* quantum yield) of the final construct.

3.3.3 QD Probe Binding to Cellular Targets *in vitro*

Ligand-target cell interactions were conducted in an *in vitro* cell culture model. Target HT-1080 cell samples were grown to confluence in 12-well tissue culture plates prior to biological experimentation. QD-PEG-NGR solutions (50 or 100nM) in OptiMEM supplemented with 1% BSA were introduced and incubated with cell samples for 1hr at 37ºC on a shaker plate to promote convective transport of the targeted probes. Blocking studies followed the same protocol, with the addition of a 10-fold excess of soluble NGR added to the QD-PEG-NGR solution.

Following incubation and probe binding, QD solutions were aspirated and cell monolayers were washed three times with fresh PBS to remove any unbound QD probes. QD binding to adherent cells was then documented by fluorescence microscopy. Culture wells were treated with a nonenzymatic cell dissociation solution (Sigma) to detach the cell monolayer from the surface. The resulting samples were centrifuged for 5min at 900×g, resuspended in 500μl of fresh PBS, filtered through a 70mm mesh, and immediately analyzed by flow cytometry.

3.3.4 Photomicroscopy

The fluorescence of adherent HT-1080 cells following incubation with QD probes was documented by fluorescence microscopy. After washing the cell monolayer surface, phase contrast and corresponding fluorescence photomicrographs were taken of each experimental well. Samples were analyzed on a Nikon TE2000U inverted microscope using a fluorescence filter cube specifically designed for 585nm emission QDs (Chroma Technology). Images were obtained with a Hamamatsu C7780 3 channel CCD cooled digital camera driven with Image-Pro Plus software (Media Cybernetics) and saved as individual JPEG files. Each experimental well was imaged at 10x magnification.

3.3.5 Quantification of QD Probe Binding

Flow Cytometry. Fluorescence of all samples was measured on a FACSCalibur flow cytometer (Becton-Dickinson). CellQuest software (Becton-Dickinson) was used for all data acquisition. Cell-associated QD probe fluorescence as well as R-PE calibration microsphere emission was measured in the FL2 channel (band pass filter 585/42 nm). Data on forward scatter was collected in linear mode while all other parameters were collected in log mode. Twenty thousand events were collected by list-mode data for all samples, and the mean intensity (MFI) from the histograms for each sample was used to analyze their fluorescence intensity. WinList software (Verity Software House) was used to further prepare and analyze the list-mode data following collection.

For data acquisition, the cell region was determined by utilizing FSC and SSC measurements. Samples were then analyzed and the MFI of the FL2 channel was recorded for each sample. HT-1080 autofluorescence (from cells untreated with QD

probes) was subtracted from these fluorescence intensities to arrive at a final measurement for further analysis. Quantum™ PE MESF microspheres (Bangs Labs) were analyzed by flow cytometry under the same conditions and settings used in biological experimentation.

Fluorometry. Fluorescence spectra of both QD probes and soluble R-PE were measured on an LS 50 B luminescence spectrometer (Perkin Elmer). For R-PE, 1667, 833.5, 250, 166.7 and 16.67nM concentrations as well as blank PBS were measured in a small-volume quartz cuvette. Samples were excited at 488nm (5nm slit) and emission profiles were recorded from 564-606nm (5nm slit). Emission intensities for each sample were integrated to determine the total intensity within the measurement range (integrated intensity). A standard curve was then prepared relating R-PE concentration to measured integrated fluorescence intensity. QD probe fluorescence was measured using the same settings and the integrated intensity of these samples was compared to the standard curve to determine the equivalent number of R-PE molecules (*i.e.* the number of R-PE molecules required to equal the fluorescence of a QD probe).

Cross-correlation. R-PE calibration microspheres were used to correlate fluorescence measurements on the flow cytometer to R-PE, producing a standard curve relating measured MFI to the number of equivalent R-PE molecules. A standard curve of calculated integrated intensities from fluorometry was used to determine the number of R-PE molecules per QD probe. Using this comparison, a new standard curve was produced relating MFI measured by flow cytometry to the number of QD probes. This

standard curve allows direct conversion of fluorescence measured by flow cytometry to the number of bound QD probes per cell in biological assays.

3.4 Results

3.4.1 Surface modification of QD probes

The surface of AMP QDs was successfully modified with the NGR targeting ligand. We characterized the electrophoretic mobility of our QD probes to determine the success of the surface modification reaction. Figure 3.2 shows the difference in mobility between AMP QDs and those modified with the NGR ligand. Conjugation of multiple targeting ligands to the QD surface results in a significant increase in molecular weight (MW) of the probe and a corresponding decrease in electrophoretic mobility.

3.4.2 Probe binding to target cells

Biologically active cell-targeting peptides retain the capacity for specific binding to target cells after attachment to the QD surface. We tested the binding of QD-PEG-NGR conjugates to HT-1080 cells expressing high levels of the target CD13 receptor (Figure 3.3). Fluorescence photomicrographs revealed significant QD binding to target cells when the NGR targeting ligand was attached to the surface (Figure 3.4A, B). This interaction is nearly completely inhibited by competitive binding with excess soluble NGR ligand (Figure 3.4C, D). These photos give a qualitative view of QD probe binding, but do not yield quantitative results.

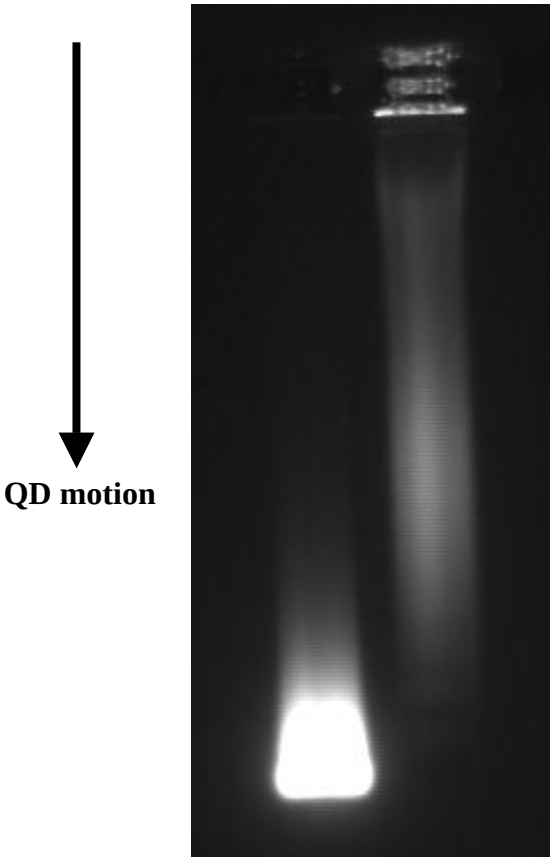

Figure 3.2. The surface of AMP QDs was successfully modified with the PEG-NGR targeting ligand. Electrophoretic mobility of QDs was assessed on a 1% agarose gel. Gels were run in 1X TAE buffer under a voltage of 150mV. Mobility of QDs exhibiting the PEG-NGR ligand (right lane) is reduced compared to that of unmodified AMP QDs (left lane), suggesting successful modification of the QD surface. The conjugation of multiple ligands to the QD surface increases the MW of the construct, resulting in reduced electrophoretic mobility. This image is representative of three independent measurements.

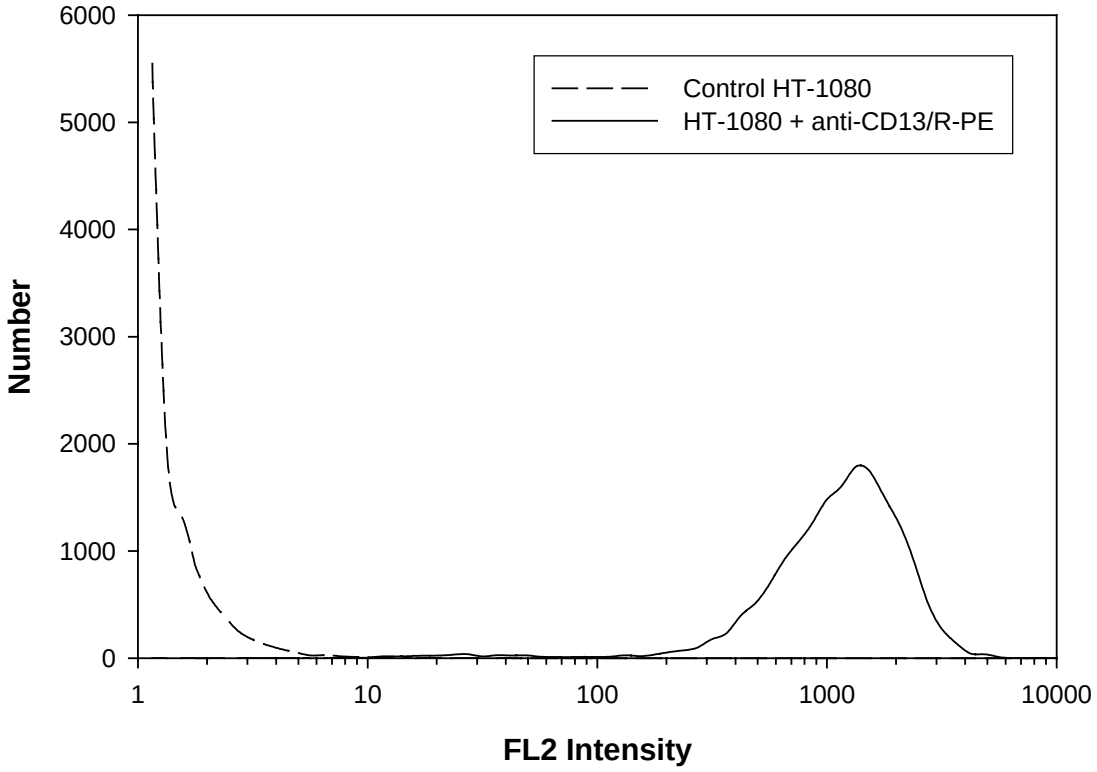

Figure 3.3. HT-1080 cells express high levels of the CD13 protein on their surface. Control, untreated HT-1080 cells generate low autofluorescence in the FL2 wavelength range when measured by flow cytometry. Incubation of the cells with an R-PE labeled anti-CD13 mAb (anti-CD13/R-PE) produces a unimodal cell population with an average FL2 intensity more than 1000-fold greater than that of untreated HT-1080 cells, presumably correlated with high expression levels of the CD13 antigen on the cell surface.

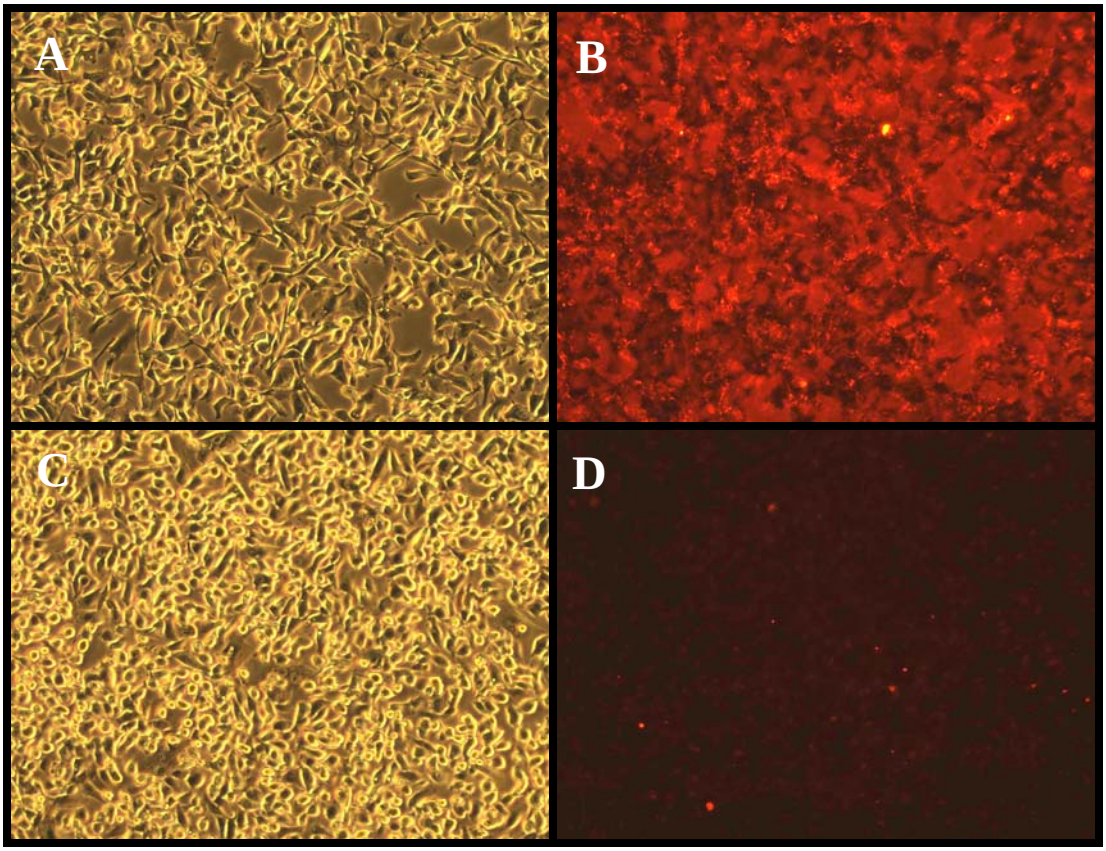

Figure 3.4. NGR surface functionalization specifically mediates QD binding to HT-1080 cells. Cells were grown to confluence in 12-well culture plates and incubated with a 50nM QD probe solution for 1h. Images are representative of $n \geq 3$ for all experimental cohorts. **B**. QDs functionalized with the NGR peptide interact extensively with the HT-1080 cell surface, resulting in a relatively high level of visible QD fluorescence in this photomicrograph. **D**. Addition of 10-fold excess NGR ligand concurrently with QD-NGR inhibited nearly all QD interaction with the cell surface, greatly reducing detectable fluorescence. **A, C.** Phase contrast images of cultured cells.

Flow cytometry confirms the trends observed in the photomicrographs for these studies and yields data for quantitative analysis of binding interaction (Figure 3.5). A distinct shift in cellular FL2 fluorescence was measured after incubation with QD-PEG-NGR probes, indicating a strong interaction of the probe with the cellular surface. Control HT-1080 cells had a mean FL2 of 2.7 a.u. while those treated with the targeted QD probes had a mean intensity of 101.5 a.u. This shift in fluorescence intensity suggests significant interaction of the probes with the cell surface, which can be further quantified by the calibration method described in this work.

Surface modification greatly influences QD association with the cell surface. We tested the binding of three 50nM solutions of QD probes (unmodified AMP QDs, QD-PEG, and QD-PEG-NGR) to HT-1080 cells expressing high levels of the target CD13 receptor. Flow cytometry revealed markedly different interactions among each of these cohorts (Figure 3.5). HT-1080 cells had a mean intensity of 95.9 a.u. after incubation with AMP QDs, revealing considerable interaction of the amphiphilic polymer coating with the cell surface. This intensity fell to 3.6 a.u. (a 96% reduction) when the surface of the QDs was modified with PEG, demonstrating the ability of the PEG coating to mask recognition of the amphiphilic polymer.

The specificity of QD-PEG-NGR probe binding was further tested by competition with free NGR peptide. Introduction of a 10-fold excess of this ligand reduced the mean FL2 intensity from 101.5 to 11.5 a.u., an 89% reduction in probe binding to the cell surface. Addition of soluble BSA, however, had no effect on QD binding (data not shown). These results suggest that QD-PEG-NGR probe binding is modulated primarily through specific binding of the NGR peptide to antigens on the cell surface.

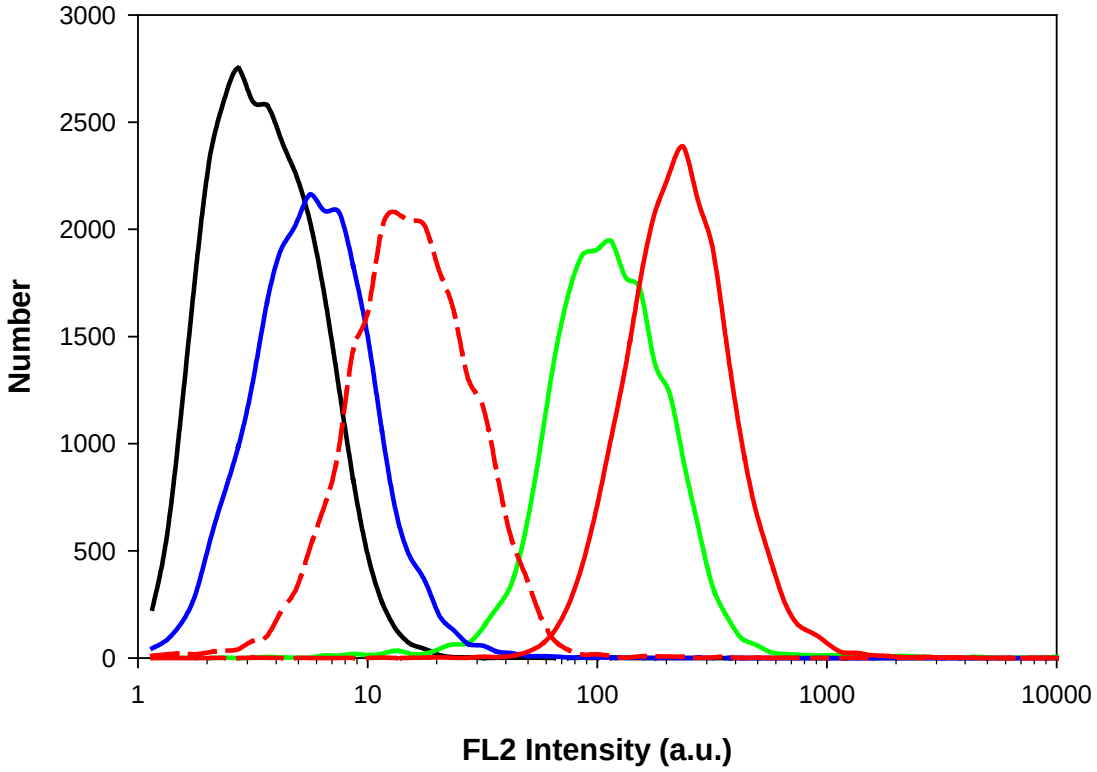

Figure 3.5. Surface modification influences QD probe interaction with cultured target HT-1080 cells as detected by changes in fluorescence intensity measured by flow cytometry. Cells were grown to confluence in 12-well culture plates and incubated for 1h with a 50nM QD probe solution. Control HT-1080 cells prior to incubation with QDs (black) exhibit low-level autofluorescence. QDs presenting the native AMP coating (green) are significantly associated with HT-1080 cells. The mechanism of unmodified QD association with cells is non-ligand mediated based on the binding inhibition provided by PEG modification of the QD surface (blue). Addition of the NGR targeting ligand to the QD-PEG, producing the QD-PEG-NGR construct (solid red), regenerates extensive interaction with the cell surface. Nearly all of the NGR-mediated interaction can be blocked by coincubation of the cells with a 10-fold excess of free NGR ligand (dashed red), providing evidence for specificity of QD-PEG-NGR interaction with cells. A quantitative analysis of these flow cytometric histograms appears in Figure 7. 20,000 cells were recorded during each trial. Histograms are representative of $n \geq 3$ for all experimental cohorts.

3.4.3 Calibration of fluorescence data

A linear relationship exists between QD concentration and fluorescence intensity. To perform QD binding quantitation, fluorescence measurements were made by both fluorometry and flow cytometry. Integrated intensities (564-606nm) of both soluble R-PE and QDs were measured by fluorometry (Table 3.1). Data was then used to generate standard curves for these molecules relating integrated intensity to molecule concentration (Fig 3.6A). The linear regression equations were then set equal to one another, producing a standard curve that directly relates AMP QD and R-PE concentrations (Equation 3.1).

$$[\mathrm{QD}] = [\mathrm{PE}] \times 0.2638 - 12.1005 \tag{3.1}$$

Fluorescence measurements made by flow cytometry were then calibrated to the number of equivalent R-PE molecules using standard calibration microspheres (Figure 3.6B). This standard curve was then combined with the fluorometry results to produce a new relationship capable of directly correlating FL2 intensity measured by flow cytometry to the number of equivalent bound AMP QDs (Equation 3.2). To obtain quantitative binding values for both QD-PEG and QD-PEG-NGR probes, the calculated number of AMP QDs was factored by their measured relative fluorescence to AMP QDs (Table 3.1).

$$[\mathrm{QD}] = (FL2 \times 438.72 + 1639.8) \times 0.2638 - 12.1005 \tag{3.2}$$

The particular relationships developed here are valid only for the particular system of fluorophores (AMP QD and R-PE), flow cytometer, and settings used in this

	Integrated Fluorescence Intensity	Relative Brightness (compared to AMP QD)
500nM AMP QD	36547.6	1
250nM AMP QD	21230.1	1
125nM AMP QD	10407.3	1
75nM AMP QD	9207.7	1
62.5nM AMP QD	3725.7	1
1667nM R-PE	32568.0	0.24
833.5nM R-PE	15693.6	0.24
250nM R-PE	3731.5	0.24
166.7nM R-PE	3554.6	0.24
16.7nM R-PE	195.4	0.24
600nM QD-PEG-NGR	35689.9	0.77
350nM QD-PEG	11457.4	0.43

Table 3.1. Integrated intensities of QD probes and R-PE were measured by fluorometry to produce calibration standard curves (Figure 3.6) for quantitative analysis. Curves for AMP QD and R-PE were then compared to develop a direct relationship correlating the numbers of AMP QD and R-PE molecules (Equation 3.1). Fluorescence settings were chosen to match the spectral excitation and emission characteristics of the FACSCalibur flow cytometer used in this study. These measurements confirm that QD fluorescence intensity is large relative to traditional fluorophores. Furthermore, these measurements reveal that surface modification of native AMP QDs significantly modulates fluorescence emission intensity of the QD probes. This modification can be compensated for by the calibration method described here.

A.

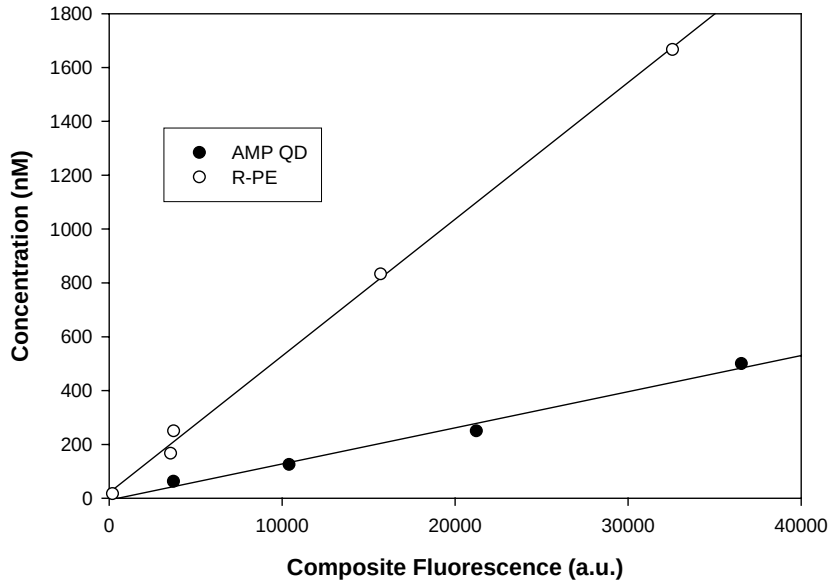

B.

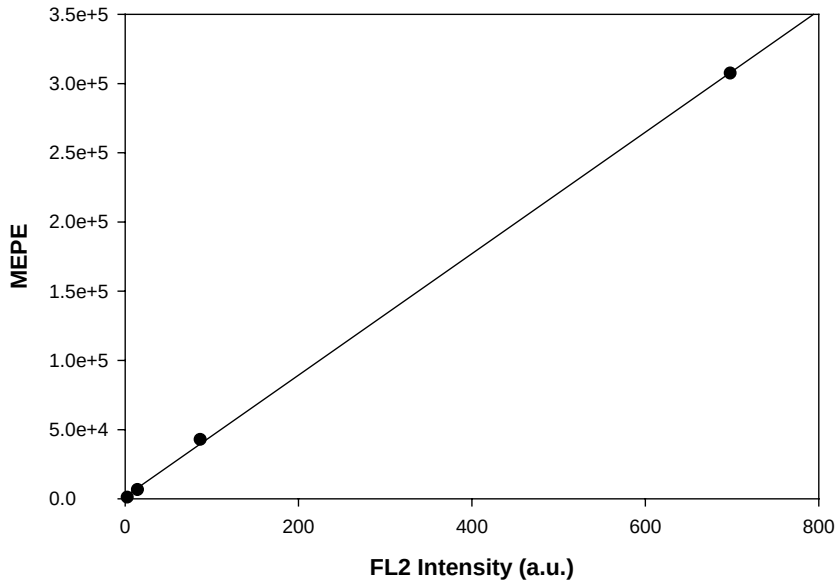

Figure 3.6. Indirect calibration must be performed to quantitatively analyze fluorophores for which no standards are available. **A.** Fluorometry measurements were used to develop standard curves illustrating measured fluorescence as a function of QD or R-PE concentration. These standard curves can be used to determine the relationship between R-PE and QD fluorescence intensity. **B.** Flow cytometry fluorescence intensity measurements were translated to the number of equivalent soluble R-PE molecules (MEPE) using commercially available calibration microspheres. Fluorometry and flow cytometry measurements were then combined to develop a direct relationship between flow cytometry fluorescence intensity and the number of equivalent QD probes.

calibration. In particular, measurements were conducted on the other two QD species used in this study (QD-PEG and QD-PEG-NGR) as the surface treatments modulated the QD fluorescence quantum yield. This modulated fluorescence behavior essentially created three unique 'orphan' fluorophores and resulted in three unique quantitative correlation relationships with the R-PE standards. The results, quantitative assessment of the number of QDs associated with each cellular event, are absolute values that can be directly compared among the three QD cohorts. The QD per cell results, but not the raw fluorescence intensities, can also be compared to quantitative results from other instruments, settings and reagents.

3.4.4 Quantitative measurement of QD probe binding to cells *in vitro*

Flow cytometry results, coupled with fluorometer-flow cytometer cross calibration, can be used to determine the number of QD probes bound to the cell surface. The standard curve obtained from the fluorometer-flow cytometer cross calibration was used to relate the measured FL2 intensity shift of cellular samples to the corresponding number of bound QD probes. The results for each QD surface coating are shown in Figure 3.7A. AMP QDs exhibited significant binding of 11,010 ± 490/cell to the surface of HT-1080 cells. Modification of the QD surface with PEG significantly reduced this interaction to 1090 ± 60/cell. Addition of the NGR targeting peptide produced the highest cellular interaction of 15410 ± 980/cell, while introduction of competitive binding with 10-fold excess NGR peptide blocked 88% of binding to 1870 ± 50/cell. Similar results were seen in experiments utilizing 100nM QD probes (Figure 3.7B).

A.

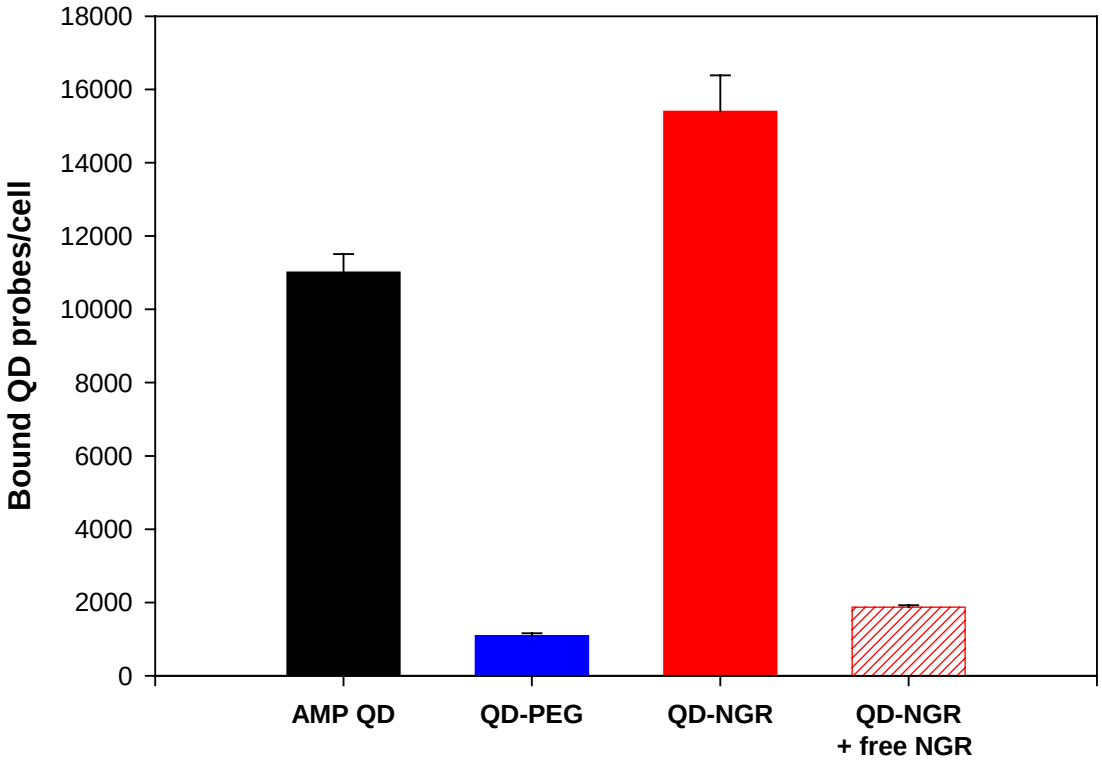

Figure 3.7. Flow cytometry fluorescence data was calibrated to quantitatively assess QD probe binding to target HT-1080 cells. **A**. Surface modification significantly modulates QD interaction with the cell surface. The interaction of 50nM QD probes with HT-1080 cells was measured. Unmodified AMP QDs exhibit a high level of binding (11014 ± 493 QD/cell) that can be overcome by surface modification with PEG (1094 ± 64 QD/cell). Addition of the NGR targeting ligand to QD-PEG-NGR results in extensive probe binding to the cell surface (15406 ± 980 QD/cell,). Nearly 90% of this NGR-mediated binding can be inhibited with the addition of a 10-fold excess of free NGR ligand (1867 ± 51 QD/cell). **B**. Increasing probe concentration results in higher levels of QD probe binding. QD-PEG-NGR probe binding nearly doubled to 28987 ± 602/cell with increased QD concentration. Minor increases in binding were measured at the increased concentration with QD-PEG (1182 ± 58 QD/cell) and QD-PEG-NGR inhibited with free NGR (2390 ± 39 QD/cell). $n \geq 3$ for all experimental cohorts. Bar height is the mean and error bars reflect standard deviation (standard deviation is too low to visualize error bars for QD-PEG-NGR + free NGR and QD-PEG samples on this scale).

B.

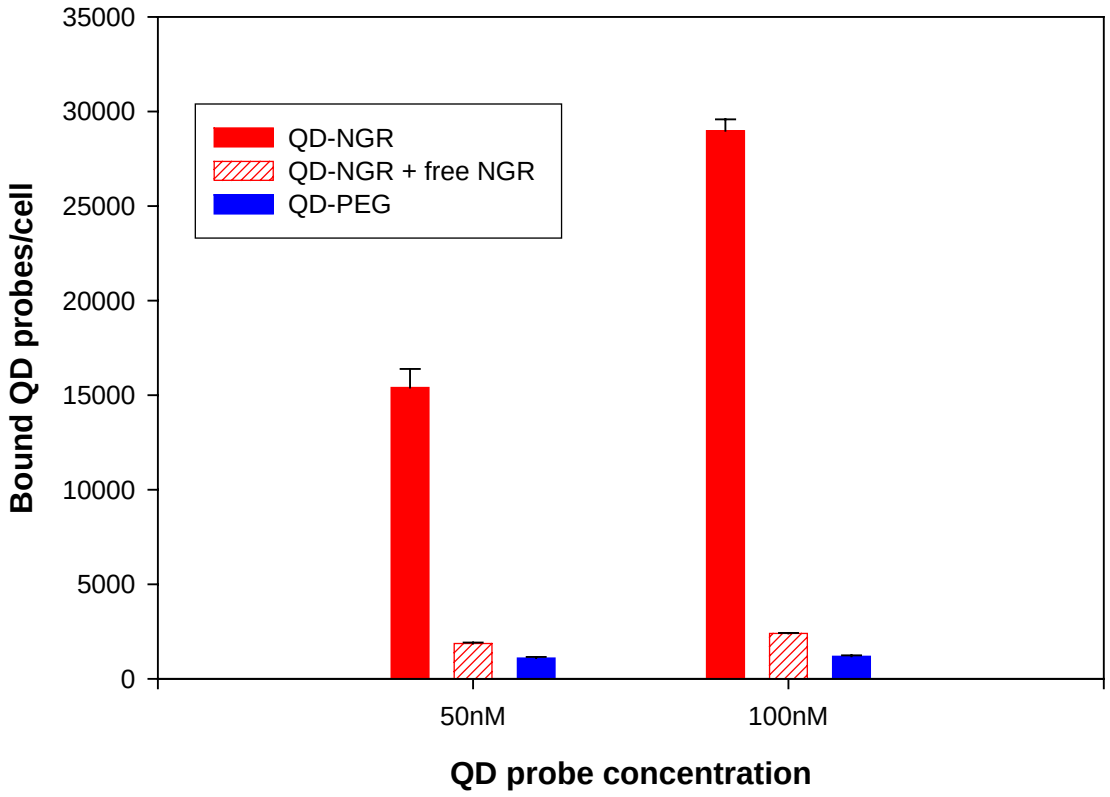

Figure 3.7. Flow cytometry fluorescence data was calibrated to quantitatively assess QD probe binding to target HT-1080 cells. A. Surface modification significantly modulates QD interaction with the cell surface. The interaction of 50nM QD probes with HT-1080 cells was measured. Unmodified AMP QDs exhibit a high level of binding (11014 ± 493 QD/cell) that can be overcome by surface modification with PEG (1094 ± 64 QD/cell). Addition of the NGR targeting ligand to QD-PEG-NGR results in extensive probe binding to the cell surface (15406 ± 980 QD/cell,). Nearly 90% of this NGR-mediated binding can be inhibited with the addition of a 10-fold excess of free NGR ligand (1867 ± 51 QD/cell). B. Increasing probe concentration results in higher levels of QD probe binding. QD-PEG-NGR probe binding nearly doubled to 28987 ± 602/cell with increased QD concentration. Minor increases in binding were measured at the increased concentration with QD-PEG (1182 ± 58 QD/cell) and QD-PEG-NGR inhibited with free NGR (2390 ± 39 QD/cell). $n \geq 3$ for all experimental cohorts. Bar height is the mean and error bars reflect standard deviation (standard deviation is too low to visualize error bars for QD-PEG-NGR + free NGR and QD-PEG samples on this scale).

3.5 Discussion

Traditional approaches to disease treatment often involve systemic doses of highly toxic drugs. These approaches are typically limited by nonspecific delivery to non-target cells, resulting systemic toxicity (25). Similarly, many imaging reagents are delivered in bolus systemic doses, effectively reducing overall detection sensitivity (by increasing background) or limiting their application to easily accessible compartments (*e.g.* vasculature). Many prior efforts have focused on targeted delivery of drugs, genes, or imaging agents directly to the target cell type(s) both *in vitro* (26-28) and *in vivo* (29-31). However, while offering improvements over nondiscriminant systemic therapies many of these approaches suffer from either suboptimal targeting or only a partial quantitative (or even qualitative) analysis of interaction with target sites.

The current study expands on these previous efforts by demonstration of the synthesis and *in vitro* performance of a versatile, modular nanoscale platform capable of targeted binding, sensing of biological events, and labeling of target cells. Furthermore, we describe a general method for calibration of flow cytometry fluorescence data capable of providing truly quantitative measurements of these constructs and other fluorophores for which appropriate calibration standards are not currently available. This method is implemented here to determine the number of QDs associated with cells *in vitro* as a function of surface characteristics.

Nanoparticulate systems offer a versatile platform with several distinct advantages in the realm of *in vitro* and *in vivo* targeted delivery and detection. Physical characteristics of the nanoparticle base impart features not available with molecular structures alone. These systems provide the opportunity for colocalization of molecular

species and the potential for multifunctional capability. Benefits such as these are limited in the absence of a particle, as molecular structures offer lower valency for functionalization and increased likelihood of functional changes following modification. Surface chemistry and three-dimensional particulate structure enable the use of NP systems to provide targeted or localized delivery, to improve bioavailability, to sustain the delivered effect in target tissues, to solubilize agents for intravascular delivery, to improve the stability of therapeutic agents against enzymatic degradation and clearance, and to allow manipulation of the release profile of the delivered therapeutic agent (32). Due to their small physical size, nanoparticles can also penetrate deep into tissues, through fine capillaries, and are generally incorporated efficiently by cells (33).

QDs offer all of the advantages of NP delivery systems previously described with the added benefit of an intrinsic imaging component. The intense fluorescence characteristics of QD probes relative to organic fluorophores facilitates sensitive detection of cell surface interaction not possible with traditional approaches. Qualitative fluorescence comparisons can be made by fluorescence microscopy while more quantitative measurements can be performed by techniques such as flow cytometry. Furthermore, the spectral characteristics of QD fluorescence lend themselves to the possibility of multiplexed detection of targets. Multiple colors of QD probes can be excited using a single light source while narrow emission bands enable simultaneous detection of multiple different QD colors (corresponding to multiple targets) with minimal crosstalk between detection channels.

Enhanced delivery and distribution of nanoscale structures to the desired cell population(s) can be achieved by both passive and active targeting principles. A common

approach to passive targeting, as utilized in this study, uses chemical modification, often applying PEG polymers directly onto the drug or delivery device (34-36). Passive targeting also refers to the preferential, size-based extravasation of nanomaterials through the relatively porous vasculature of many tumors. The small physical diameter of the QD nanoprobes utilized in this study allows them to retain many transport characteristics of molecular structures. Thus, these constructs have access to fine capillaries, are capable of extravasation, and can penetrate deep into tissues through size restrictive structures (34,37).

Active targeting is achieved by increasing the affinity of the delivery system for the target site(s). This is often accomplished by the introduction of ligands such as monoclonal antibodies (mAbs) or peptides (as in the current study) for specific recognition of a particular protein or cellular receptor. The effectiveness of some specific targeting ligands has been documented and incorporated into a handful of commercially available treatments (e.g. Glivec®, Herceptin®, Iressa). Thus, chemical modification of drugs or delivery devices can have a significant impact on affinity for both target and non-target sites.

Probe Binding

Our QD probe targeting studies conducted by flow cytometry (Figures 3.4, 3.5) confirm the dependence of nanoparticle surface modification on cell surface target interaction. PEGylation of the QD surface resulted in a significant decrease in binding over unmodified AMP QDs, with a nearly 90% reduction in nonspecific interaction. This is consistent with previous reports (34-36) detailing the ability of PEG polymers to passivate the surface and minimize undesired interactions with non-target sites.

PEGylated QDs serve as the control for specific binding experiments, as targeted probes are built from the same platform with an added NGR ligand on the distal end of the PEG. Addition of this peptide ligand to the PEG coating mediated a substantial increase in QD binding to the cell surface. Interactions between HT-1080 cells and QD-PEG-NGR increased by 1300% over PEGylated QDs and 40% over unmodified AMP QDs, suggesting significant specific recognition of the NGR targeting ligand by molecules on the cellular surface. These results also follow expected trends for traditional ligand-receptor interaction. Although no specific Km value is available to describe NGR/CD13 binding, QD-NGR concentrations used in binding experiments are well below values reported for other peptide-receptor pairs. Thus, QD-NGR binding is expected to be a function of QD-NGR concentration. This behavior is apparent when comparing results for 50nM and 100nM QD-NGR binding.

Competitive binding experiments were conducted to further examine the specificity of targeted QD probe binding. The addition of a 10-fold excess of free NGR ligand resulted in an 88% inhibition of targeted probe binding (100nM experiments saw a 92% reduction), thus actively reducing binding to levels approaching those of simple PEGylated QDs. Furthermore, the addition of 1% BSA during the binding assay had no effect on QD probe binding (data not shown), additional evidence that targeted probe interactions are not mediated by nonspecific interactions. These experimental results strongly suggest that increased targeted QD probe binding is a direct result of modification with the NGR targeting ligand, and that this binding is mediated by specific interactions of the NGR ligand with molecules on the cell surface.

While fluorescence shifts measured by flow cytometry indicate functional QD binding to the cell surface and enable “quantitative” comparisons and relative binding levels, they are not a direct quantitative measure of the number of probes present on the cell surface. Fluorescence intensity is modulated by multiple factors, ranging from the particular fluorophore used to specific instrument settings in use. Thus, direct comparisons of raw fluorescence data are not necessarily accurate indicators of the number of bound probes, especially across multiple systems, instruments and reagents. To ensure portability and reproducibility, FACS fluorescence intensity data must be correlated to physical values unaffected by experimental conditions.

Calibration

Photomicrographs (Figure 3.5) illustrate considerable modulation of QD probe binding by surface treatment modification. Photomicrographs support qualitative assessments, but are difficult to interpret in terms of fluorescence intensity per cell. Fluorescence intensities measured by flow cytometry have been employed in a number of studies, including the current work, to measure the effects of both passive and active targeting mechanisms (38-40). These approaches provide considerably more information for interpretation and enable simple quantitative comparisons. Nevertheless, fluorescence intensity measurements alone do not support quantitative analysis of probe binding due to a lack of calibration between probe number and fluorescence intensity.

Methods to provide calibrated fluorescence intensities for flow cytometry are limited by the availability of appropriate standards. In many cases, such as with QDs, no commercially available standards currently exist to provide reliable calibrations (‘orphan’ fluorophores). In these instances, alternative methods must be developed to allow

indirect calibration of measured fluorescence data. The calibrated flow cytometry methods utilized here are a principal component in this work.

A similar approach was previously used to analyze fluorophores for which commercial calibration standards were not available (41). This technique is based on comparison of the fluorescence (as measured by fluorometry) of the 'orphan' fluorophore (QDs) to that of a fluorophore with available calibration standards (R-PE). The resulting relationship between concentration of the two fluorophores and the measured fluorescence intensities can be presented as a type of calibration curve that, in this case, is linear (Figure 3.6A). This relationship can be used to make a direct comparison between AMP QD and R-PE concentration (Equation 3.1).

Accurate calibration of 'orphan' fluorophores by flow cytometry requires fluorometry measurements using excitation and emission settings that mimic the fluorescence characteristics of the flow cytometer. For example, the FACSCalibur used in our studies utilizes a single excitation laser (488nm) while the R-PE and QD fluorophores are maximally detected in the FL2 channel (585/42nm). Fluorometer settings were chosen to closely match these characteristics. Excitation was set to 488nm (5nm slit) while the emission intensities were measured from 564-606nm. Performing these measurements under the same conditions (e.g. pH, buffer components, etc.) minimizes the introduction of error due to environmental modulation of fluorescence.

Another potentially important factor is spectral matching in the choice of fluorescent markers. Ideally, the chosen fluorophores are sufficiently excited by the same laser line and detected by flow cytometry using the same fluorescence channel. This insures sufficient sensitivity for both fluorometry and flow cytometry measurements and

minimizes error due to spectral mismatch. An additional factor affecting fluorophore selection includes quenching, which may be an issue at high concentrations. In our case R-PE was chosen as the calibration fluorophore, as it is very bright and exhibits minimal self-quenching (42). Although R-PE is exceedingly resistant to self-quenching, the behavior of other fluorophores must be carefully considered when choosing a compatible marker to achieve quantitative results.

Translation of the fluorescence cross-calibration in Figure 3.6A to quantitative interpretation of flow cytometry data requires a calibrated scale for fluorescence intensity of one fluorophore. Such a calibration is routinely conducted using commercially available reagents (43,44) and appears here as Figure 3.6B for R-PE. Combining this calculated standard curve with the previously calculated QD to R-PE comparison provides a means for direct conversion of MFI to the number of bound QD probes (Equation 3.2).

By applying the calculated calibration equation (Equation 3.2) we were able to translate fluorescence intensity values into meaningful measurements of bound QD probes/cell. For targeted therapy or imaging studies, quantitative values such as these can provide important information such as probe binding efficiency, cellular susceptibility to targeted therapy, or expected therapy payload delivery – measurements not possible with traditional uncalibrated flow cytometry techniques. These values are also especially significant for imaging and detection applications, as contrast enhancement and labeling intensity are a direct function of the number of delivered contrast agents. Furthermore, these calibrated values provide a valuable real-world translation of arbitrary fluorescence values, enabling greater understanding and data

portability among instruments. It is possible that some QDs were removed from the cell surface during cell dissociation, resulting in an artificially low measurement of QD/cell. Thus, the values reported here serve as a lower bound for QD/cell. Any removal of QDs from the cell surface during the cell dissociation protocol would only serve to increase the effectiveness of QD-NGR conjugates synthesized in this work.

This technique unlocks the underlying power of flow cytometry to allow more detailed quantitative evaluations of probe binding as well as the ability to provide more detailed information on kinetics and efficiency not possible with traditional techniques. For example, measurements from traditional FACS analysis can yield only arbitrary fluorescence increases over time. A conversion to quantitative analysis enables these measurements to provide kinetic probe binding values revealing the *number* of probes bound per time, data which are especially useful for targeted delivery and dosage studies.

Additional analysis can also be performed on the data provided in this study. Fractional binding (total QD added/total QD bound) is nearly identical between 50nM and 100nM samples (0.20% and 0.19%, respectively). These very low values suggest that probe binding has not yet reached saturation at these concentrations and is limited by factors other than QD surface modification. Access to the cell surface is one probable cause, as the colloidal QD probes do not settle during incubation. Furthermore, incubation time (1h) is sufficiently short to limit significant passive motion of the nanoprobes to the cell surface.

Data on additional probe concentrations and incubation times would enable access to a range of supplementary quantitative characteristics including binding constants, kinetics of saturation, and the number of nanoprobe binding sites, among others. These

examples highlight the importance of quantitative data conversion to further analysis of existing FACS measurements. These evaluations have the ability to provide valuable detailed information not accessible with raw fluorescence data.

Conclusions

We describe the development and performance of a nanoparticle system capable of targeted binding and delivery, along with a method for providing quantitative performance analysis of this system and a range of other fluorescent molecules. This system offers several distinct advantages over traditional molecular delivery techniques to increase therapeutic efficiency and efficacy while offering a powerful imaging component, especially for *in vitro* analysis. The calibration method developed and employed in this work allows a straightforward conversion of relative fluorescence values into meaningful measurements not affected by experimental conditions. This method extends the capability of quantitative flow cytometry measurements to include fluorescent molecules (e.g. QDs) and fluorophores for which no reliable calibration standards currently exist.

3.6 References

1. Pasqualini R, Koivunen E, Ruoslahti E. Alpha v integrins as receptors for tumor targeting by circulating ligands. Nat Biotechnol 1997;15(6):542-6.

2. Arap W, Pasqualini R, Ruoslahti E. Cancer treatment by targeted drug delivery to tumor vasculature in a mouse model. Science 1998;279(5349):377-80.

3. Pasqualini R, Koivunen E, Kain R, Lahdenranta J, Sakamoto M, Stryhn A, Ashmun RA, Shapiro LH, Arap W, Ruoslahti E. Aminopeptidase N is a receptor for tumor-homing peptides and a target for inhibiting angiogenesis. Cancer Res 2000;60(3):722-7.

4. Curnis F, Arrigoni G, Sacchi A, Fischetti L, Arap W, Pasqualini R, Corti A. Differential binding of drugs containing the NGR motif to CD13 isoforms in tumor vessels, epithelia, and myeloid cells. Cancer Res 2002;62(3):867-74.

5. van Hensbergen Y, Broxterman HJ, Hanemaaijer R, Jorna AS, van Lent NA, Verheul HM, Pinedo HM, Hoekman K. Soluble aminopeptidase N/CD13 in malignant and nonmalignant effusions and intratumoral fluid. Clin Cancer Res 2002;8(12):3747-54.

6. van Hensbergen Y, Broxterman HJ, Rana S, van Diest PJ, Duyndam MC, Hoekman K, Pinedo HM, Boven E. Reduced growth, increased vascular area, and reduced response to cisplatin in CD13-overexpressing human ovarian cancer xenografts. Clin Cancer Res 2004;10(3):1180-91.

7. Oku N, Asai T, Watanabe K, Kuromi K, Ogino K, Taki T. Anti-neovascular therapy by use of liposomes targeted to angiogenic vessels. J Liposome Res 2003;13(1):25-7.

8. Hallahan D, Geng L, Qu S, Scarfone C, Giorgio T, Donnelly E, Gao X, Clanton J. Integrin-mediated targeting of drug delivery to irradiated tumor blood vessels. Cancer Cell 2003;3(1):63-74.

9. Mamot C, Drummond DC, Greiser U, Hong K, Kirpotin DB, Marks JD, Park JW. Epidermal growth factor receptor (EGFR)-targeted immunoliposomes mediate specific and efficient drug delivery to EGFR- and EGFRvIII-overexpressing tumor cells. Cancer Res 2003;63(12):3154-61.

10. Chenevier P, Delord B, Amedee J, Bareille R, Ichas F, Roux D. RGD-functionalized spherulites as targeted vectors captured by adherent cultured cells. Biochim Biophys Acta 2002;1593(1):17-27.

11. Hood JD, Bednarski M, Frausto R, Guccione S, Reisfeld RA, Xiang R, Cheresh DA. Tumor regression by targeted gene delivery to the neovasculature. Science 2002;296(5577):2404-7.

12. Harbottle RP, Cooper RG, Hart SL, Ladhoff A, McKay T, Knight AM, Wagner E, Miller AD, Coutelle C. An RGD-oligolysine peptide: a prototype construct for integrin-mediated gene delivery. Hum Gene Ther 1998;9(7):1037-47.

13. Hart SL, Collins L, Gustafsson K, Fabre JW. Integrin-mediated transfection with peptides containing arginine-glycine-aspartic acid domains. Gene Ther 1997;4(11):1225-30.

14. Phadtare S, Vinod VP, Mukhopadhyay K, Kumar A, Rao M, Chaudhari RV, Sastry M. Immobilization and biocatalytic activity of fungal protease on gold nanoparticle-loaded zeolite microspheres. Biotechnol Bioeng 2004;85(6):629-37.

15. Rossi LM, Quach AD, Rosenzweig Z. Glucose oxidase-magnetite nanoparticle bioconjugate for glucose sensing. Anal Bioanal Chem 2004;380(4):606-13.

16. Tang DP, Yuan R, Chai YQ, Zhong X, Liu Y, Dai JY, Zhang LY. Novel potentiometric immunosensor for hepatitis B surface antigen using a gold nanoparticle-based biomolecular immobilization method. Anal Biochem 2004;333(2):345-50.

17. Liu J, Zhang Q, Remsen EE, Wooley KL. Nanostructured materials designed for cell binding and transduction. Biomacromolecules 2001;2(2):362-8.

18. Zhang D, Chen Y, Chen HY, Xia XH. Silica-nanoparticle-based interface for the enhanced immobilization and sequence-specific detection of DNA. Anal Bioanal Chem 2004;379(7-8):1025-30.

19. Wang M, Sun C, Wang L, Ji X, Bai Y, Li T, Li J. Electrochemical detection of DNA immobilized on gold colloid particles modified self-assembled monolayer electrode with silver nanoparticle label. J Pharm Biomed Anal 2003;33(5):1117-25.

20. Medintz IL, Uyeda HT, Goldman ER, Mattoussi H. Quantum dot bioconjugates for imaging, labelling and sensing. Nat Mater 2005;4(6):435-46.

21. Alivisatos AP, Gu W, Larabell C. Quantum dots as cellular probes. Annu Rev Biomed Eng 2005;7:55-76.

22. Gerena-Lopez Y, Nolan J, Wang L, Gaigalas A, Schwartz A, Fernandez-Repollet E. Quantification of EGFP expression on Molt-4 T cells using calibration standards. Cytometry A 2004;60(1):21-8.

23. Schwartz A, Fernandez-Repollet E. Quantitative flow cytometry. Clin Lab Med 2001;21(4):743-61.

24. Smith RA, Giorgio TD. Quantitation and kinetics of CD51 surface receptor expression: implications for targeted delivery. Ann Biomed Eng 2004;32(5):635-44.

25. Frei E. Combination chemotherapy, dose and schedule. Cancer Medicine; 1997. p 817-837.

26. Colin M, Maurice M, Trugnan G, Kornprobst M, Harbottle RP, Knight A, Cooper RG, Miller AD, Capeau J, Coutelle C and others. Cell delivery, intracellular trafficking and expression of an integrin-mediated gene transfer vector in tracheal epithelial cells. Gene Ther 2000;7(2):139-52.

27. Moffatt S, Wiehle S, Cristiano RJ. Tumor-specific gene delivery mediated by a novel peptide-polyethylenimine-DNA polyplex targeting aminopeptidase N/CD13. Hum Gene Ther 2005;16(1):57-67.

28. Li H, Gray BD, Corbin I, Lebherz C, Choi H, Lund-Katz S, Wilson JM, Glickson JD, Zhou R. MR and fluorescent imaging of low-density lipoprotein receptors. Acad Radiol 2004;11(11):1251-9.

29. Keller G, Schally AV, Gaiser T, Nagy A, Baker B, Halmos G, Engel JB. Receptors for luteinizing hormone releasing hormone expressed on human renal cell carcinomas can be used for targeted chemotherapy with cytotoxic luteinizing hormone releasing hormone analogues. Clin Cancer Res 2005;11(15):5549-57.

30. Adams GP, McCartney JE, Tai MS, Oppermann H, Huston JS, Stafford WF, 3rd, Bookman MA, Fand I, Houston LL, Weiner LM. Highly specific in vivo tumor targeting by monovalent and divalent forms of 741F8 anti-c-erbB-2 single-chain Fv. Cancer Res 1993;53(17):4026-34.

31. Zhao M, Beauregard DA, Loizou L, Davletov B, Brindle KM. Non-invasive detection of apoptosis using magnetic resonance imaging and a targeted contrast agent. Nat Med 2001;7(11):1241-4.

32. Moghimi SM, Hunter AC, Murray JC. Long-circulating and target-specific nanoparticles: theory to practice. Pharmacol Rev 2001;53(2):283-318.

33. Vinogradov SV, Bronich TK, Kabanov AV. Nanosized cationic hydrogels for drug delivery: preparation, properties and interactions with cells. Adv Drug Deliv Rev 2002;54(1):135-47.

34. Akerman ME, Chan WC, Laakkonen P, Bhatia SN, Ruoslahti E. Nanocrystal targeting in vivo. Proc Natl Acad Sci U S A 2002;99(20):12617-21.

35. Gao X, Cui Y, Levenson RM, Chung LW, Nie S. In vivo cancer targeting and imaging with semiconductor quantum dots. Nat Biotechnol 2004;22(8):969-76.

36. Ballou B, Lagerholm BC, Ernst LA, Bruchez MP, Waggoner AS. Noninvasive imaging of quantum dots in mice. Bioconjug Chem 2004;15(1):79-86.

37. Pluen A, Boucher Y, Ramanujan S, McKee TD, Gohongi T, di Tomaso E, Brown EB, Izumi Y, Campbell RB, Berk DA and others. Role of tumor-host interactions in interstitial diffusion of macromolecules: cranial vs. subcutaneous tumors. Proc Natl Acad Sci U S A 2001;98(8):4628-33.

38. Zitzmann S, Ehemann V, Schwab M. Arginine-glycine-aspartic acid (RGD)-peptide binds to both tumor and tumor-endothelial cells in vivo. Cancer Res 2002;62(18):5139-43.

39. Kunath K, Merdan T, Hegener O, Haberlein H, Kissel T. Integrin targeting using RGD-PEI conjugates for in vitro gene transfer. J Gene Med 2003;5(7):588-99.

40. Nan A, Ghandehari H, Hebert C, Siavash H, Nikitakis N, Reynolds M, Sauk JJ. Water-soluble polymers for targeted drug delivery to human squamous carcinoma of head and neck. J Drug Target 2005;13(3):189-97.

41. James MB, Giorgio TD. Nuclear-associated plasmid, but not cell-associated plasmid, is correlated with transgene expression in cultured mammalian cells. Mol Ther 2000;1(4):339-46.

42. Glazer AN. Phycobiliproteins. Methods Enzymol 1988;167:291-303.

43. Iyer SB, Hultin LE, Zawadzki JA, Davis KA, Giorgi JV. Quantitation of CD38 expression using QuantiBRITE beads. Cytometry 1998;33(2):206-12.

44. Chance JT, Larsen SA, Pope V, Measel JW, Cox DL. Instrument-dependent fluorochrome sensitivity in flow cytometric analyses. Cytometry 1995;22(3):232-42.

CHAPTER IV

PROXIMITY-ACTIVATED NANOPARTICLES: ENZYME-SPECIFIC MODIFICATION FOR TARGETED DELIVERY AND BIOSENSING

RA Smith and TD Giorgio*

Department of Biomedical Engineering
Vanderbilt University, Nashville, TN

Correspondence:
Todd D. Giorgio
Vanderbilt University
Box 351620, Station B
Nashville, TN 37235
615-322-3756 (voice)
615-343-7919 (fax)
todd.d.giorgio@vanderbilt.edu

This manuscript was prepared for submission in *Nano Letters*

4.1 Abstract

We describe the development and *in vitro* performance of a modular nanoscale system capable of specific structural modification by enzymatic activity. Due to its small physical size and adaptable characteristics, this system represents a versatile option for utilization in targeted delivery systems and biosensing. Surface modification allows these proximity-activated nanoparticles to act as physiologically inert structures until activation and cleavage by tumor-specific enzymes. We synthesized probes containing two distinct fluorescent species including a quantum dot base particle and fluorescently labeled cleavable peptide substrate. Activity of these probes was monitored by gel electrophoresis with quantitative cleavage measurements made by fluorometric analysis. The model proximity-activated nanoparticles studied here exhibit significant susceptibility to cleavage by MMP-7 at physiologically relevant concentrations, with nearly complete cleavage of available substrate molecules after 24h. This response was shown to be specific to MMP-7 enzyme activity, as cleavage is completely inhibited with the addition of EDTA. Utilization of enzyme-specific modification is a sensitive approach with broad applications for targeted therapeutics and biosensing. The versatility of this nanoparticle system is highlighted in its modular design, as it integrates characteristics for detection, biosensing, targeting, and payload delivery into a single, multifunctional nanoparticle structure.

4.2 Introduction

4.2.1 Background

Localized or specific delivery of therapeutics to diseased cells represents a historic paradigm shift in the treatment approach toward many disease states, including various types of cancer. Traditional approaches utilize systemic administration of highly potent drugs in an attempt to eradicate neoplastic cells, often with significant toxic side effects. Initial attempts at targeted delivery of these drugs have focused on the incorporation of small ligands to direct the therapy to a specific target site (1-4). However, the current generation of targeted therapies has not yet achieved highly specific targeting of tumors and emerging neoplasia through a single recognition mechanism (5,6). Nonspecific binding and specific binding to nontarget cells compromise the therapeutic index of small molecule, ubiquitous cancer targeting ligands, and limit their applicability and efficiency as primary chemotherapeutic agents.

An alternative targeting approach involves the use of molecules capable of activation following cleavage by tumor-specific enzymes. These compounds have been incorporated into many structures ranging from *in vivo* imaging constructs (7-9) to chemically modified drug structures in the form of prodrugs (10-12). These studies demonstrate the feasibility of tumor-specific enzyme interaction as a means of modifying the physical structure of delivered drugs and imaging constructs, and potentially enables targeted delivery of nanoparticle (NP) and other particulate drug carriers.

A number of studies utilizing this approach have focused on the development of tumor-specific molecular imaging constructs cleavable by matrix metalloproteases

(MMPs) (9,13-16). These reports have detailed peptide sequences with cleavage activity specific to a number of different MMPs, and to MMP-7 in particular. The basis of the MMP-7 specific peptide substrate (RPLALWRS) utilized in one such report (15) is employed in this study to impart tumor-specific activity to our NP delivery system.

Literature citations of tumor-specific cleavable constructs focus mainly on molecular imaging of enzyme activity and drug activation *in vivo*. However, incorporation of these constructs into NPs or their application to target NP-based therapeutic delivery systems (forming proximity-activated (PA) NPs) has not yet been reported. The use of NPs for this purpose has the inherent advantage of a large surface area to volume ratio, allowing conjugation of multiple active molecules. Stable covalent conjugation of bioactive molecules such as enzymes (17,18), mAbs (19), peptides (20), and DNA (21,22) to the surface of NPs has been reported. With small-molecule ligands such as the PA construct used here, many copies can be attached to the surface of the NP enabling multivalent interaction with target cells. QDs offer the advantages seen in other NP systems with the added benefit of intense fluorescence characteristics for straightforward and highly sensitive detection and imaging. These attributes impart the ability to integrate specific delivery, detection, imaging, and treatment characteristics into a single, multifunctional NP delivery vehicle.

4.2.2 The role of MMP-7 in biological processes

MMPs (including MMP-7) are a family of extracellular, zinc-dependent proteases that have a role in tissue breakdown and remodeling during both normal (*e.g.* angiogenesis, gut innate immunity) and pathological (*e.g.* inflammation, tumorigenesis,

metastasis) processes. MMP-7 has been specifically implicated as an important facilitator of tissue remodeling due to its ability to cleave a variety of known substrates, including many ECM proteins and the latent forms of other MMPs (23). Overexpression of MMP-7 has been directly correlated with enhanced tumorigenicity and tumor cell invasion using *in vitro* model systems (24). It has been shown to be important in the progression of a number of tumors, notably those originating in the colon or in the breast (15). Furthermore, MMP-7 has proven to have diagnostic and prognostic value, as expression is associated with poor outcome in esophageal (25), colon (26), and pancreatic (27) cancers. The overexpression and significance of MMP-7 in the tumor cascade make this enzyme an attractive target for site-directed delivery vehicles.

For tumor systems in which MMP-7 activity is known to modulate the course of the disease, MMP-7 is secreted even in the earliest stages. Small, benign "precancerous" lesions, for example, exhibit MMP-7 secretion well before these lesions would be clinically detectable (28,29). Furthermore, analysis of MMP-7 expression in human neoplasia revealed that enzyme mRNA appeared in the surrounding normal tissue in only a few isolated cases (23), suggesting highly specific enzyme expression in the immediate tumor vicinity. The larger and more progressed these tumors become, the higher the MMP-7 levels tend to be. This focused source of abundant extracellular MMP-7 is expected to provide ample activity for the *in vivo* application of PA NPs to cancer targeting.

The utilization of MMP-7 activity represents a potentially powerful approach toward specific targeting. In this study, we describe the synthesis and *in vitro* performance of a NP probe capable of specific activation by MMP-7. In addition, the

importance of quantitative analysis of construct performance is described in the context of *in vitro* and *in vivo* application. These data provide the basis for a PA system capable of targeted delivery, detection, imaging, and therapeutic payload delivery from a single NP package.

4.3 Methods

4.3.1 Cleavable peptides and NP probes

A fluorescently labeled, PEGylated substrate for MMP-7 (HN-[Ahx]-PEG_{3400}-RPLALWRS-PEG_{5000}-K(5-FAM)-[Ahx]-NH2; PA construct) was synthesized and purified by Anaspec (San Jose, CA). This structure consists of the cleavable peptide substrate (RPLALWRS) flanked by polyethylene glycol (PEG) groups of 3400 and 5000 g/gmol (to prevent nonspecific interactions) and aminohexanoic acid groups ([Ahx]) to serve as spacer molecules, as well as a fluorescent tag (5-FAM) for fluorometric detection. To stabilize the substrate and prevent further modification at this site, C-terminal amidation was performed during synthesis.

The N-terminal amine group of the substrate was conjugated to the surface of carboxylate QDs (585nm emission; Quantum Dot Corp., Hayward, CA) using 1-ethyl-3-(3-dimethylaminopropyl)carbodiimide (EDC; Sigma). Briefly, 250µl of QDs (7.5µM) was diluted to 1mM with 10mM borate buffer, pH 7.4. 80µL from a 10mg/mL stock solution of the cleavable substrate was then added to the solution, yielding a PA:QD molar ratio of 10.0:1 (lower bound) and 28.4:1 (upper bound). 57µl from a 10mg/ml stock solution of EDC was added and the mixture was stirred for 2h at room temperature

to complete the conjugation. A schematic of the final QD-PA probe is shown in Figure 4.1.

Following conjugation, the mixture was purified by spin filtration in a 50,000 nominal molecular weight limit (NMWL) cutoff device (Amicon Ultra-4, Millipore Corp.). This process is expected to yield a QD probe product nearly free of unreacted components, as the intact PA structure is ~11,000 Da and any other fragments should be considerably smaller. Three buffer exchanges were performed with 50mM borate buffer (pH 8.3) and the final conjugate was stored at 4°C. The concentration of the final purified product was determined by measuring the absorbance at 575nm using a QD extinction coefficient of $400{,}000 M^{-1} cm^{-1}$. As this value is a characteristic of the semiconductor core, the extinction coefficient is presumably unchanged by surface functionalization. However, conjugation of molecules to the QD surface does have an effect on the fluorescence emission (*i.e.* quantum yield) of the final construct.

4.3.2 MMP-7 cleavage assay

Studies were conducted to determine the susceptibility of both the PA and QD-PA constructs to exogenous MMP-7. Active MMP-7 (Calbiochem) was added to 100µl of a 50nM PA or QD-PA solution in borate buffer supplemented with 50µM $ZnSO_4$. The total concentration of MMP-7 was varied in these samples from 100nM to 5nM to reflect expected concentrations *in vivo*. Samples were then incubated at 37ºC for various timepoints ranging from 1h to 48h. Control studies involving QD-PA with no enzyme and with inactivated enzyme (by addition of 30mM EDTA, a known zinc chelator) were carried out simultaneously for direct comparison. QD probes were purified from any

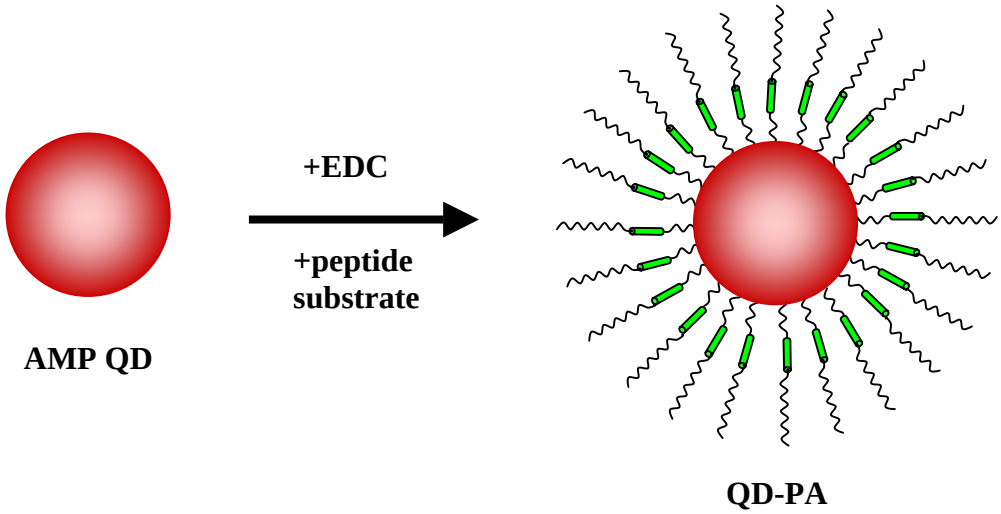

Figure 4.1. Enzyme sensitive QD-PA probes were synthesized by surface modification of AMP QDs. Carboxylate QDs (left, red) consist of a CdSe base with an amphiphilic (AMP) polymer shell containing multiple reactive carboxylate groups. 5-FAM labeled peptide substrate (green) was synthesized with proximal PEG_{3400} and distal PEG_{5000} polymers (black lines). AMP QDs were activated with EDC before addition of the soluble PEGylated substrate. The mixture was stirred for 2h and purified to remove any unreacted components, resulting in a modified, enzyme sensitive QD-PA probe (right). The conjugation of many identical substrate molecules to the QD surface increases probe specificity by necessitating multiple enzymatic cleavages to successfully activate the particle. Furthermore, this redundancy enables multivalent interaction of the activated probe with the target site.

cleavage products by spin filtration in a 50,000 NMWL cutoff device. Samples were then assayed by gel electrophoresis and spectrofluorometry to determine the extent of construct cleavage from the QD surface.

4.3.3 Cleavage measurement

Gel electrophoresis

Following the cleavage reaction, PA and QD-PA constructs were analyzed by gel electrophoresis to determine susceptibility to MMP-7. PA constructs were analyzed on a 10-20% gradient tris-tricine polyacrylamide gel (Life Gels). Samples were loaded in a buffer containing 10% glycerol in tris-tricine running buffer (Life Gels). Gels were then run under a 150mV voltage for ~1h to achieve optimal separation of the molecular species. Unconjugated PA constructs (free in solution) were compared to cleaved PA constructs to straightforwardly visualize and confirm enzymatic activity against the substrate.

Gel electrophoresis was also used to monitor the change in electrophoretic mobility of the QD construct. QDs subjected to the cleavage reaction were assayed against native AMP QDs, uncleaved QD-PA constructs, and QD-PA + EDTA on a 0.8% bufferless agarose gel (E-Gel, Invitrogen Corp.). Differences in electrophoretic mobility were used to qualitatively assess construct synthesis (the difference between AMP and QD-PA mobilities), construct cleavage (QD-PA and cleaved QD-PA), and cleavage specificity (cleaved QD-PA and QD-PA + EDTA). All gels were imaged for fluorescence on a BioDoc-It imaging system (UVP Inc.).

Fluorescence measurement

Fluorescence spectroscopy (Perkin-Elmer LS 50B) was used to monitor the progress of the cleavage reaction. Prior to experimentation, a fluorescence spectrum of the QD-PA construct was taken at 488nm excitation. This spectrum was used to quantify both the fluorescence intensity of the QD base (at 585nm) as well as the labeled PA molecules on the QD surface (at 519nm). As these spectra only minimally overlap, they are easily separated when present together in a single sample.

Following cleavage and purification, the fluorescence spectra of the cleaved QD-PA constructs were measured. The peak values at 519nm and 585nm were directly compared to the spectra of control, uncleaved QD-PA particles to estimate the extent of PA construct cleavage following MMP-7 treatment.

4.3.4 Quantitative fluorescence analysis

A quantitative determination of PA construct cleavage was made by digital analysis of gel electrophoresis images. Briefly, gel images were obtained on a BioDoc-It imaging system as JPEG files and visually analyzed in Doc-It LS software (UVP Inc.). This software platform was used to detect, define, and draw "gates" around individual bands. Each band was then electronically cut from the image, saved as a separate JPEG file, and loaded into MATLab.

For digital image analysis, these separate images were loaded into a MATLab script designed to calculate quantitative image parameters. The composite fluorescence intensity for each band (*i.e.* each individual image) was calculated by summing the measured intensity of each pixel contained in the image. These composite intensities

were then summed to determine the total fluorescence of all bands within each lane. The relative percentage contained in each band was obtained by comparing its composite fluorescence to that of the total for the lane. The MATLab code used to perform these calculations is shown in Appendix 4A.

Fluorescence measurements of QD-PA constructs were analyzed to quantitatively determine the extent of PA construct cleavage from the QD surface. Spectra measured by fluorescence spectroscopy were scaled to normalize QD peak fluorescence (~585nm) between all samples. The peak values for PA construct fluorescence (~519nm) were then recorded for each sample. Using samples with no enzyme as a control (defined as 0% cleavage), the extent of PA construct cleavage for each sample was determined by calculating the ratio of PA construct fluorescence between cleaved and uncleaved (control) samples. These quantitative measurements were then scaled to account for the percent of cleavable PA construct contained in the original sample (from values obtained by quantitative analysis of the polyacrylamide gels previously described).

4.3.5 Statistics

Statistical significance of experimental populations was assessed using an upaired t-test and determined by SigmaStat (Jandel Scientific Software). Differences were termed significant for $p < 0.05$.

4.4 Results

4.4.1 I*n vitro* cleavage of the PA construct

The PA construct is highly susceptible to cleavage by MMP-7. Prior to conjugation to the QD surface, PA constructs were assayed for susceptibility to enzymatic activity. Gel electrophoresis analysis of unconjugated PA construct confirms specific cleavage of these molecules by MMP-7 (Figure 4.2). Lanes 1 and 2 confirm the presence of the intact fluorescently labeled PA structure. These bright low mobility bands are nearly extinguished after 24h exposure to MMP-7. This cleavage also results in the generation of a very bright high mobility band corresponding to the low molecular weight labeled cleavage product (Figure 4.2, lanes 3 and 4). PA construct cleavage was completely abolished by the addition of 30mM EDTA (a known zinc chelator; Figure 4.2, lanes 5 and 6), as the band corresponding to the intact PA construct is present in these wells. These results are consistent with the near complete proteolysis of the PA construct at the site of the MMP target peptide and inhibition of the zinc-dependent MMP-7 enzyme by EDTA.

A quantitative analysis was also made of the gel electrophoresis images obtained from these samples. MATLab was used to calculate the composite intensity of all pixels within each band (the sum of individual intensities for each pixel), as well as the composite intensity within each lane. Table 4.1 contains representative values obtained from the gel pictured in Figure 4.2. From these values, we determined the percentage of PA construct contained in each sample. Control, uncleaved soluble PA construct contains $35.6 \pm 3.4\%$ intact PA structure ($n = 4$). After 24h exposure to 100nM MMP-7, $87 \pm 0.7\%$ of the initial PA construct was cleaved (statistically significant, $p < 0.001$) based on the residual $4.6 \pm 0.7\%$ intact PA construct, confirming the high susceptibility of the PA construct to MMP-7 proteolysis. MMP-7 mediated cleavage was completely

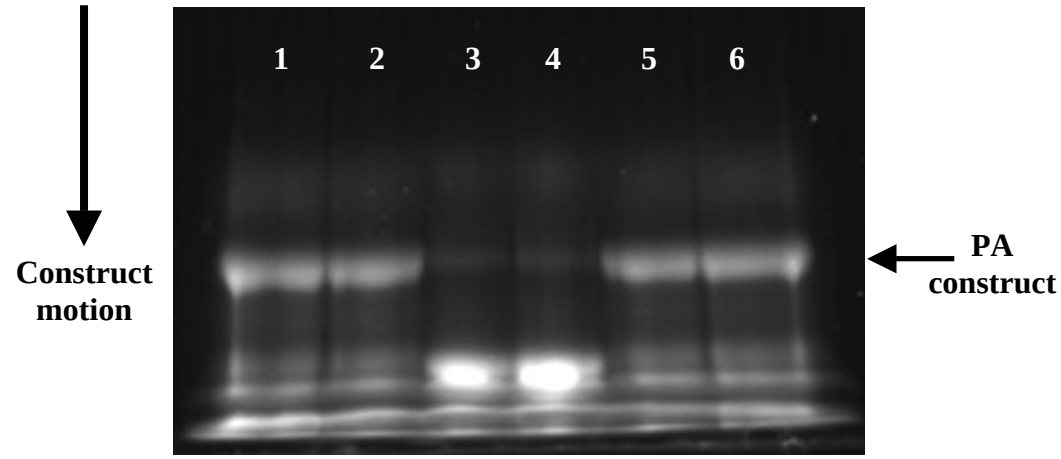

Figure 4.2. Cleavage of the soluble, unconjugated PA construct by MMP-7 was confirmed by gel electrophoresis. Samples of soluble PA construct were incubated for 24h with 100nM MMP-7 and analyzed on a 10-20% gradient tris-tricine polyacrylamide gel. Lanes 1 and 2 represent unconjugated PA construct prior enzymatic exposure as a control. The bright, low mobility band (identified by the horizontal arrow) represents the intact PA structure, while the other fluorescent bands presumably correspond to unreacted fluorescent species and intermediates not removed during purification. Nearly all of the PA construct is cleaved after 24h exposure to MMP-7 (Lanes 3 and 4), suggesting high susceptibility of the construct to MMP-7 activity. This activity is completely inhibited with the addition of 30mM EDTA (a zinc chelator) to the samples (Lanes 5 and 6). Inhibition of MMP-7 activity results in no measurable cleavage of the PA constructs. The gel pictured is representative of three independent measurements.

	PA Construct Fluorescence	Total Sample Fluorescence	% Intact PA Construct	% Cleavable PA Construct
Lane 1	0.5424	1.3707	39.5%	N/A
Lane 2	0.3094	0.9722	31.8%	N/A
Lane 3	0.0592	1.1591	5.1%	30.6%
Lane 4	0.0607	1.4803	4.1%	31.6%
Lane 5	0.3113	0.8443	36.9%	N/A
Lane 6	0.3354	0.9852	34.0%	N/A

Table 4.1. The PEGylated peptide substrate is highly susceptible to cleavage by MMP-7. Cleavage was measured by optical analysis of polyacrylamide gel images (Figure 1). Each band was identified as a region of interest, electronically cut from the image, and loaded into a MATLab script to calculate the fluorescence intensity for the band. The composite intensity of each well was then calculated by summing the intensities of each constituent band. These results correspond to the gel image in Figure 2. Control, uncleaved PA samples (Lanes 1 and 2) contain an average of 35.7% intact PA structure. 24h exposure to 100nM MMP-7 results in a reduction of intact PA structure to an average of 4.6%. The percentage of cleavable construct (31.1% average) was then calculated by subtracting the construct remaining after 24h MMP-7 exposure from the average percentage measured in the uncleaved samples. Addition of EDTA to the samples (Lanes 5, 6) results in strong inhibition of PA construct cleavage, as the percentage of intact construct (35.5% average) is nearly identical to that of control samples in the absence of MMP-7. Quantitative analysis for all experiments ($n \geq 3$) with statistical analysis appears in the Results.

blocked by the addition of EDTA. After 24 exposure to 100nM MMP-7 supplemented with 30mM EDTA, 35.5 ± 2.0% of the PA construct remained intact, a value nearly identical to the amount measured in control samples in the absence of MMP-7 ($p = 0.966$).

4.4.2 QD-PA construct synthesis

The surface of AMP QDs was successfully modified with the PA construct. We characterized the electrophoretic mobility of our QD probes to determine the success of the surface modification reaction. Figure 4.3 shows the difference in mobility between unmodified AMP QDs (lanes 3, 8) and those modified with the PA structure (lanes 4, 9). Conjugation of the PA construct to the QD surface results in a significant increase in MW of the probe and a corresponding decrease in electrophoretic mobility.

QD-PA synthesis was further confirmed by measuring the fluorescence spectra of the resulting conjugates. Following conjugation and purification, the fluorescence spectra of the QD-PA constructs were measured (Figure 4.4, control QD-PA). These spectra reveal fluorescence maxima at ~520 and ~590nm, corresponding to the emission maxima of the 5-FAM labeled PA construct (~519nm) and of the QD base (~585nm). The peak values measured at these wavelengths suggest a high level of PA construct conjugation to the QD surface. There was no significant photobleaching of either 5-FAM or QD over the course of the measurements. Furthermore, additional studies revealed no significant change in QD fluorescence intensity (at ~585nm) upon PA cleavage from the surface (data not shown).

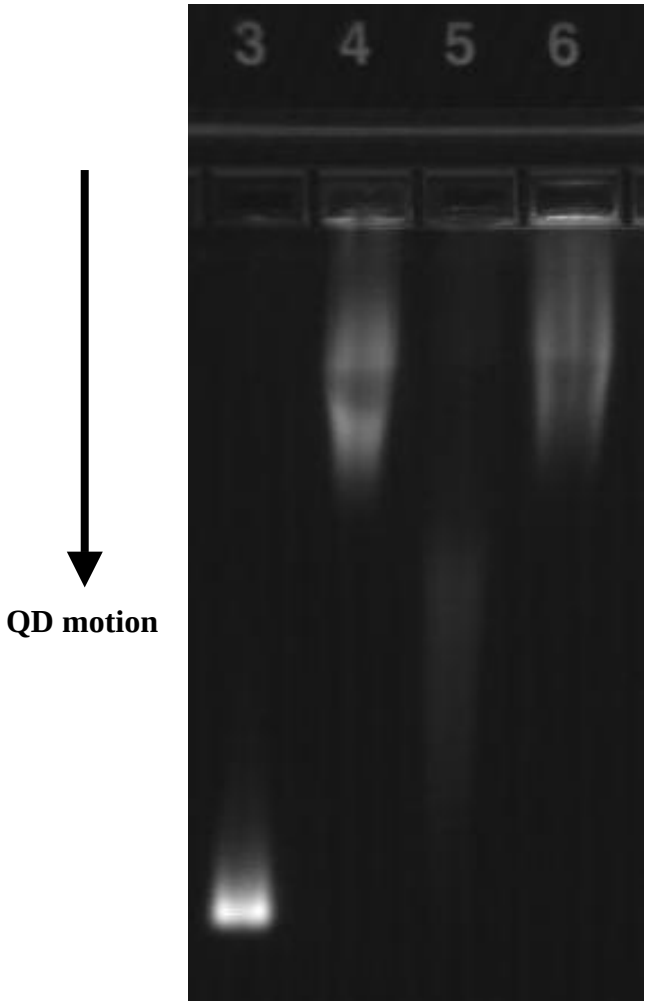

Figure 4.3. The surface of AMP QDs was successfully modified with the cleavable PA construct. Electrophoretic mobility of QD conjugates was assessed on a 0.8% bufferless agarose gel. Mobility of QDs modified with the cleavable PA construct (lane 4, diffuse band) is reduced compared to that of unmodified AMP QDs (lane 3). The conjugation of PA construct to the surface modifies the molecular mass and surface charge of the construct, resulting in reduced mobility. 24h exposure of the QD-PA conjugates to MMP-7 (lane 5) leads to a partial recovery of mobility, suggesting significant cleavage of the attached PA structure. Increased mobility after exposure to MMP-7 can be completely inhibited by the addition of 30mM EDTA (lane 6), suggesting the presence of intact PA construct on the QD surface. This image is representative of three independent trials.

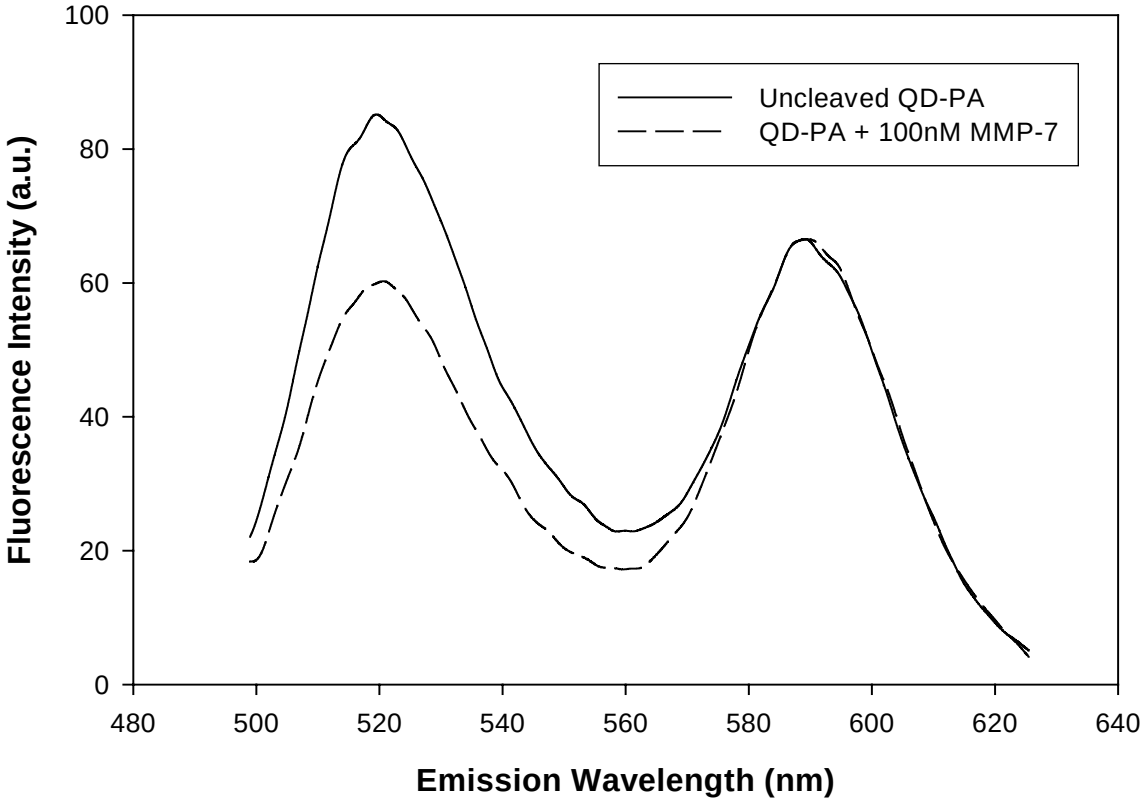

Figure 4.4. Fluorometric measurements reveal a significant PA cleavage from the QD surface after 24h exposure to 100nM MMP-7. The presence of two peaks in the uncleaved QD-PA also confirms conjugation of the PA construct to the QD surface. Fluorescence spectra of QD-PA constructs from 500-625nm were monitored by fluorometry, with an excitation wavelength of 488nm (5nm slit). Spectra were scaled to normalize QD fluorescence intensity (~585nm) among all samples. QDs reacted with PA construct and purified to remove unbound material possess two fluorescence emission peaks consistent with colocalized QD and PA construct fluorescence. Exposure to MMP-7 (dashed line) results in reduced 5-FAM fluorescence intensity at ~519nm when compared to control, uncleaved QD-PA samples (solid line), suggesting significant cleavage of the labeled PA construct from the QD surface at the site of the MMP-7 target substrate. Figure is representative of multiple independent measurements with varying MMP-7 concentrations and incubation times. Results shown are representative of $n \geq 3$ trials for all experimental groups.

4.4.3 QD-PA cleavage by MMP-7

PA constructs retain their enzymatic susceptibility after conjugation to the QD surface. Surface-functionalized QD-PA constructs were treated with 100nM MMP-7 under the same conditions as unconjugated PA constructs. Agarose gel analysis of these samples (Figure 4.3) reveals a partial recovery of mobility following MMP-7 treatment (lanes 5, 10), consistent with a reduction of surface-associated molecular mass mediated by proteolytic cleavage. Mobility recovery is not complete, consistent with persistence of the proximal portion of the PA construct on the QD surface after proteolytic cleavage of the distal PA component. MMP-7 mediated increase in electrophoretic mobility is reversed with addition of 30mM EDTA during the cleavage (lanes 6, 11), suggesting inhibition of MMP-7 activity by EDTA. Changes in relative mobilities provide evidence of successful QD surface functionalization, subsequent proteolytic degradation, and inhibition of enzyme activity expected in this system.

Enzymatic cleavage was also monitored by measuring changes to the fluorescence spectra of the QD-PA constructs after incubation with MMP-7. Following the enzymatic exposure, QD constructs were purified from cleavage products by spin filtration, and the fluorescence spectrum of purified QDs was measured (Figure 4.4). Relative to control, uncleaved QD-PA constructs, these spectra reveal a reduced fluorescence peak at 519nm corresponding to the labeled, intact QD-PA construct. This result is consistent with gel electrophoresis images and computed results, and suggests significant proteolysis of the PA construct at the site of the MMP-7 target peptide and subsequent removal of cleavage products, including the 5-FAM fluorophore from the QD surface.

Fluorescence measurements were used to produce a quantitative analysis of PA construct cleavage. These measurements (Figure 4.5) confirm significant cleavage of the PA construct from the QD surface. Treatment of the QD-PA constructs with 100nM MMP-7 resulted in steadily increasing cleavage with increased incubation time, reaching a plateau after 24h ($31.8 \pm 5.4\%$ cleavage, $n \geq 3$ for all timepoints). Measured cleavage values are highly dependent on incubation time, and follow an exponential rise to maximum curve describing traditional enzyme kinetics. These measured cleavage values were then scaled to account for the percentage of cleavable PA construct contained in the original sample (from quantitative analysis of gel electrophoresis). This scaling revealed nearly complete proteolysis of the cleavable PA construct on the QD surface after 24h ($90.9 \pm 15.4\%$ cleavage), consistent with cleavage of unconjugated PA constructs under the same conditions ($87.1 \pm 0.7\%$ cleavage).

Cleavage of the PA construct from the QD surface was also significantly influenced by initial MMP-7 concentration. Results from MMP-7 concentrations ranging from 100nM to 5nM are shown in Figure 4.5. Although the cleavage response measured for each MMP-7 concentration follows the same general trend, the extent of cleavage is markedly altered, as cleavage declined as MMP-7 concentration was lowered. Furthermore, additional analysis of these results (Figure 4.6) reveals that the initial cleavage rate ($t<6h$) plateaus at an MMP-7 concentration below 100nM, as no additional significant cleavage is measured as enzyme concentration is increased from 10nM to 100nM. A minimum of three independent trials was performed for each timepoint and MMP-7 concentration.

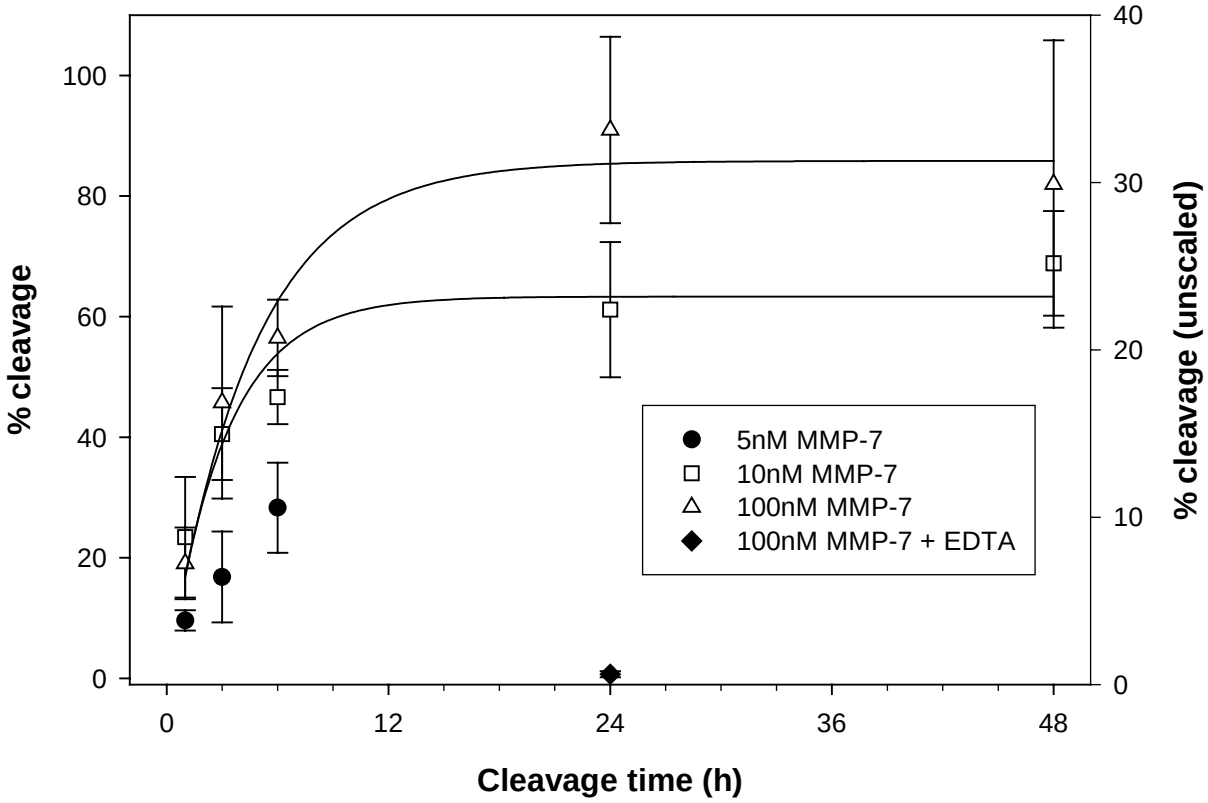

Figure 4.5. QD-PA probes are highly susceptible to MMP-7 activity. Fluorescence spectra of control, uncleaved QD-PA structures were compared to those of samples incubated with MMP-7. Fluorescence intensities corresponding to the QD and PA construct were then analyzed and scaled to quantitatively determine the extent of proteolytic cleavage of the PA construct from the QD surface. Measured cleavage was highly dependent on incubation time, steadily increasing to reach a maximum scaled value of 90.9 ± 15.4% after 24h incubation with 100nM MMP-7 (hollow triangles). Incubation with 10nM MMP-7 (hollow squares) resulted in reduced cleavage measurements for nearly all timepoints, although a statistically relevant difference compared to 100nM was only present at 24h. 5nM MMP-7 (solid circles) resulted in statistically reduced cleavage for all timepoints measured. Cleavage was completely inhibited with the addition of EDTA (solid diamond). The right vertical axis reflects the loss in 5-FAM fluorescence from the QD while the left vertical axis corrects that measurement to yield the percentage of surface-bound PA constructs cleaved. $n \geq 3$ for all concentrations and timepoints.

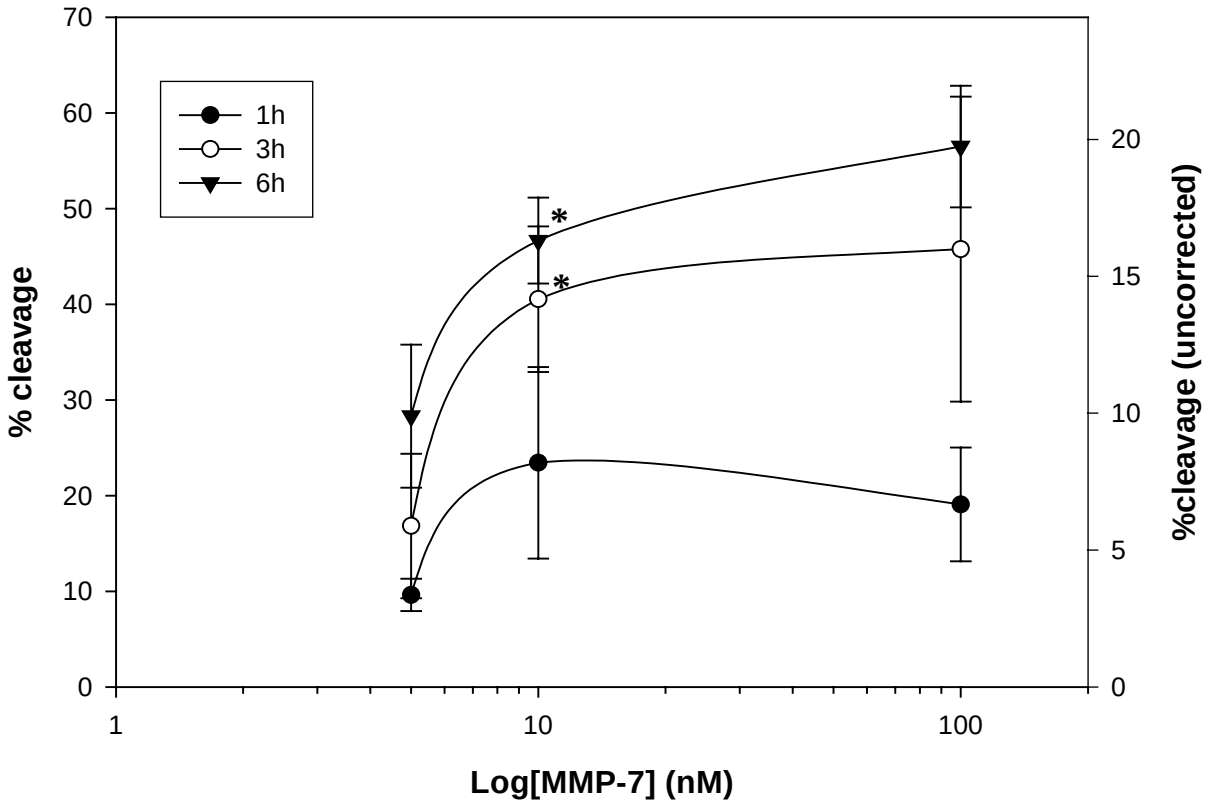

Figure 4.6. Cleavage of PA construct from the QD surface is modulated by MMP-7 concentration. Quantitative cleavage measurements were analyzed in the form of a dose response curve to highlight the influence of enzyme concentration on construct cleavage. MMP-7 concentrations used in this study correspond to the upper range of concentrations for the dose-response curve, as confirmed by the nearly quantitative cleavage at 100nM and the sharp drop in cleavage from 10nM to 5nM. PA construct cleavage increased at all timepoints after increasing initial MMP-7 concentration from 5nM to 10nM. However, the initial cleavage rate plateaus at an MMP-7 concentration ≥10nM, reaching a maximum value of 56.5 ± 6.3% after 6h. Statistical analysis was performed across concentrations for all timepoints (5nM compared to 10nM, 10nM compared to 100nM). Statistically significant values are denoted with a *****. There is no statistically significant change in cleavage at an increased MMP-7 concentration of 100nM (from 10nM) for any timepoint. These results are consistent with traditional enzyme kinetics and signify specific activity of the MMP-7 enzyme. $n \geq 3$ for all MMP-7 concentrations and timepoints.

4.5 Discussion

Although the importance of therapeutic targeting has been acknowledged for more than two decades, few viable options for targeted therapy have been successfully implemented. Many treatment regimens continue to rely on bolus systemic doses that compromise the drug concentrations delivered to target tissue based on systemic toxicity resulting form specific and nonspecific delivery to nontarget cells (30).

The power of effective *in vivo* drug targeting is exemplified by the astounding success of trastuzumab (Herceptin), a monoclonal antibody that targets the HER2 receptor that is overexpressed on the surface of some breast cancers. Other approaches have attempted to use small ligands to direct administered therapies specifically to the target site(s) that present the corresponding receptor. However, nonspecific binding and specific binding to nontarget cells often compromises the therapeutic index of small molecule targeting ligands, limiting their applicability and efficiency as primary targeting agents (31,32). These obstacles compromise the large investment in targeting ligand discovery and the availability of robust approaches for screening new molecular targeting ligands.

This study describes the development and *in vitro* performance of a new family of multifunctional nanoscale constructs capable of overcoming the obstacles that compromise *in vivo* small molecule drug targeting. The approach described here presumably enables display of the targeting ligand only in the immediate vicinity of the target tissue. Demonstrated in this work is the feasibility of nanoparticle activation by MMP-7, a proteolytic enzyme secreted by a number of tumors. With potential applications for targeted therapy as well as *in vitro* and *in vivo* biosensing, the ‘smart’ NP probes developed here represent a powerful, versatile platform combining detection,

biological activity sensing, targeting, and treatment characteristics into a single, multifunctional nanoscale construct.

The construct developed and assessed in this work initially presents as a PEGylated nanoparticle with low nonspecific binding as predicted from previous studies (33-35). PEGylation is provided by a PA construct, essentially composed of a PEG chain interrupted by the peptide target of MMP-7 proteolysis. Cleavage of the internal peptide liberates the distal PEG and part of the peptide (along with a fluorophore, in this work, for assessment of cleavage). Proteolytic modification can presumably be used to enable access to a small molecule ligand previously concealed near the nanoparticle surface. Effective proximity activated targeting will likely be modulated by many molecular factors, including the relative characteristics of the distal and proximal PEGs on the PA construct and the PEG (or other molecular spacer) that displays the ligand from the nanoparticle surface.

Proximity activated targeting requires the colocalization of the cleavable mask and the targeting ligand, necessitating a particulate approach. In the exemplar described here, the nanoparticle is a QD, used to provide a fluorescent beacon for performance assessment. Subsequent work will employ this construct, amended to include a targeting ligand, to assess proteolytically activated targeting *in vitro* and *in vivo* by quantitative fluorescence measurements and fluorescence imaging. The appropriateness of QDs for clinical applications remains unknown, but the proximity activated targeting approach described here can be applied to other nanostructures approved for use in humans. These nanomaterials include iron oxide nanoparticles for magnetic resonance (MR) image

contrast enhancement and drug delivery structures such as polymers, liposomes, polymersomes and gene delivery vehicles.

Successful delivery of therapeutics or particles to desired site(s) can, in principle, be accomplished by both passive and active targeting principles. Passive targeting reduces recognition by, and nonspecific interaction with nontarget sites such as healthy cells while active targeting mechanisms act to directly increase the affinity of the delivery system to the target site. The QD-PA systems described here minimize undesirable interactions with nontarget tissues via a passivating hydrophilic PEG surface coating. This coating has been used successfully in other *in vitro* and *in vivo* applications to reduce unintended nonspecific interactions of delivered drugs and particles (33-35). The novel approach described here also employs an active targeting mechanism (cleavage by MMP-7) to activate ligand display only in the vicinity of the target, thus presumably maximizing interaction with target cells. This two event requirement for targeting increases the effective sensitivity of the construct by keeping the passive PEG coating intact until the particle reaches the immediate proximity of the target. Thus, NP-PA constructs may be able to achieve much greater target selectivity over both conventional and single-modality targeted delivery systems.

PA and QD-PA cleavage

Our initial gel electrophoresis characterization of the PA structure reveals significant susceptibility of this molecule to specific MMP-7 activity. These results are consistent with previous reports detailing specific cleavage of the peptide substrate by MMP-7 (15). Furthermore these results establish that specific activity is retained after modification of the peptide with spacer ([Ahx]) and PEG molecules. Additional studies

demonstrate that PA constructs retain their MMP-7 susceptibility following conjugation to the QD surface.

While cleavage measured by gel electrophoresis can detect susceptibility of PA and QD-PA constructs to MMP-7 activity, these results are not direct quantitative measures of construct cleavage. Traditional gel electrophoresis typically yields results appropriate for straightforward qualitative comparisons. However, further analysis of this gel data is able to produce some quantitative results. Pixel by pixel optical analysis of polyacrylamide gel data (Figure 4.2) using MATLab provided additional insight unavailable by visual inspection alone (Table 4.1). This analysis revealed that only approximately one-third (~35%) of the original PA construct sample fluorescence is produced by intact PA structure. The remainder of the sample likely consists of unreacted fluorescently labeled starting material and labeled intermediates not removed during purification of the PA structure. These impurities are also expected to attach to the QD surface during the conjugation reaction, resulting in QD-PA conjugates with a significant level of non-cleavable substrate on the surface. In the current study, cleavage measurements were appropriately scaled to account for these labeled impurities. However, subsequent work will employ robust purification methods (e.g. HPLC) to remove these impurities prior to conjugation, thus maximizing construct activity and sensitivity.

Results of QD-PA cleavage obtained by agarose gel electrophoresis, however, are not capable of producing similar quantitative results. The polyacrylamide gels studied previously contain PA structures labeled by a single fluorophore (5-FAM). QD-PA constructs, on the other hand, contain both 5-FAM as well as QD fluorescence emissions.

Thus, the grayscale images obtained from these gels represent the composite fluorescence of both fluorophores contained in the QD-PA structure. A similar quantitative analysis of these images is not possible as these fluorescence emissions cannot be easily separated without simultaneous analysis of multiple images obtained using filters for each fluorophore.

Quantitative analysis of cleavage measurements

Results obtained by fluorometry, however, are able to easily separate 5-FAM and QD emissions based on wavelength and provide data appropriate for quantitative analysis. Fluorometric analysis (Figure 4.4) confirms the results obtained by gel electrophoresis, verifying both successful conjugation of the PA construct to the QD surface and subsequent cleavage by MMP-7. This data also reveals system characteristics not accessible through qualitative techniques. Analysis of uncleaved QD-PA samples reveals a high level of 5-FAM fluorescence associated with each QD. As each 5-FAM molecule results in lower fluorescence emission intensity than a single QD, this data suggests that multiple PA constructs are conjugated to the QD surface. Subsequent fluorescence spectra taken following MMP-7 cleavage confirm significant cleavage of the intact PA construct from the QD surface as well as cleavage inhibition by EDTA, singling out specific MMP-7 mediated activity as the source of reduced fluorescence intensity. Further analysis of these constructs by fluorometry and spectrophotometry reveal that the level of substitution ranges from 0.74 (lower bound) and 2.2 (upper bound) PA constructs per QD (data not shown). The current conjugation level may be too low to support effective masking of underlying ligands, however several

methods are being investigated to increase surface substitution. Nonetheless, the studies presented here demonstrate the viability of the PA approach.

The performance of the multifunctional NP system described here has some characteristics of conventional materials. Our studies also reveal several variables strongly modulating QD-PA cleavage. Initial cleavage measurements (Figure 4.5) reveal a strong dependence on enzyme concentration and exposure time. Furthermore, these results demonstrate the expected shape and saturation characteristics of traditional enzyme kinetics. In addition, the dose-response curve (Figure 4.6) shown here follows an apparently sigmoidal shape, representative of many well-known enzyme and ligand binding systems. These characteristics enable predication of the system response based on the MMP-7 concentration and exposure time, critical factors in establishing *in vivo* performance of the construct. Measurements such as these will be useful in future studies for optimization of the QD-PA structure, as they enable assessment of the contribution of alternate configurations to the proteolytic sensitivity of the construct.

From previous analysis in the literature, the K_m of the unmodified PA substrate is 26μM (36). Thus, at substrate concentrations below this value, PA cleavage is expected to be independent of MMP-7 concentration. Bulk PA concentrations used in the current study range from 37.5 – 100nM. However, these studies demonstrate the effect of MMP-7 concentration on construct cleavage. Additional analysis of experimental conditions reveals a likely explanation for these results. At the given substrate concentration, and at low MMP-7 concentrations (e.g. 5nM and 10nM), MMP-7 is the limiting reagent. At higher MMP-7 concentrations (e.g. 100nM), MMP-7 concentration meets or exceeds

substrate concentration. Thus, cleavage behavior transitions from a regime where MMP-7 is the limiting component to a regime where PA is the limiting component.

Additional characteristics affecting probe performance, including kinetic measures such as cleavage rate, can be obtained only from quantitative data. For example, results confirm that MMP-7 concentration significantly affects the overall cleavage and cleavage rate (average cleavage over the first three timepoints) of the QD-PA probes (Figure 4.6). Furthermore, these results suggest that proteolytic susceptibility saturates at MMP-7 concentrations above 10nM. Thus, at enzyme concentrations at or above this threshold, QD-PA probes are expected to demonstrate maximal activity.

Quantitative analyses such as this are especially important for predicting performance in *in vivo* applications where enzyme concentration is not under direct control. For example, MMP-7 concentration can vary widely, with overexpression noted in various tumor phenotypes (15). While few quantitative measures of MMP-7 concentration have been performed, previous studies have utilized MMP-7 concentrations of up to 100nM *in vitro* (37,38), while others have measured comparable concentrations of additional MMPs *in vivo* (39). This evidence suggests possible MMP-7 concentrations in tumor of at least 50nM, corresponding with the levels utilized in the current study. At these predicted MMP-7 concentrations, the QD-PA probes described here require <6h for activation (defined as 50% cleavage), with significant activity reached within 3h.

As particle activation time and tissue residence time (*i.e.* particle velocity) are competing factors, this ratio is an important consideration with potential for significant impact on *in vivo* utility of QD-PA constructs. If activation time is long compared to residence time (*e.g.* for vascular targets), then the NP will presumably be transported

away during activation and before specific binding can occur. In this case, PA delivery is no worse than current targeted approaches. However, the small size and surface passivation (PEGylation) of the QD-PA construct combine to create a construct likely capable of extravasation, enabling access to targets within the tissue. In this compartment, particle velocity is likely to be small, allowing ample time for particle activation.

The modular structure of the QD-PA constructs provides multiple parameters for performance optimization, with various factors presumably modulating the overall activity of the construct. PEG length is one variable with potential to significantly affect multiple characteristics including enzyme susceptibility (by limiting enzyme access to the substrate), nonspecific binding limitation, effective ligand concealment (in future structures), and particle mobility. Additional structural parameters including enzyme substrate configuration, ligand selection, and QD ligand surface density (number of molecules conjugated to the QD surface) can also directly affect probe performance. Thus, the relative importance of these factors must be taken into account during optimization. Performed correctly, tailoring of these multiple characteristics enables optimization of probe performance for the requirements of both *in vitro* and *in vivo* systems.

The use of NPs as a base for this system imparts multiple characteristics not available with molecular systems alone. Chief among these is a significant inherent surface area to volume ratio, presenting capacity for conjugation of multiple targeting molecules. Surface conjugation is further advantaged by the availability of a large number of functional groups on the NP surface, enabling the colocalization of multiple

functionalities as well as multivalent target interaction of the NP construct. Additional properties of the modular base particle can also be utilized to impart desirable characteristics to the NP construct, including significant particle mobility, payload delivery, and an array of imaging options ranging from fluorescence (as for QDs) to CT contrast (*e.g.* gold nanoclusters).

This study forms the basis for a new family of modular nanoscale constructs capable of both targeted therapeutic delivery and sensitive detection of biological phenomena (*e.g.* enzymatic activity). Taken together, our results demonstrate the successful synthesis of a sensitive PEGylated substrate for MMP-7 activity, and its incorporation into a versatile system displaying detection, sensing, targeting and treatment characteristics in a single nanoscale platform. These probes are sensitive to low, physiologically relevant MMP-7 concentrations and represent an alternative approach to small-molecule targeting and biosensing systems. Substitutions to the specific mechanism for activation in the proximity of the target site or the incorporation of additional targeting molecules enable an array of new nanoscale constructs with the potential to significantly impact targeted therapy.

4.6 References

1. Hallahan DE, Geng L, Cmelak AJ, Chakravarthy AB, Martin W, Scarfone C, Gonzalez A. Targeting drug delivery to radiation-induced neoantigens in tumor microvasculature. J Control Release 2001;74(1-3):183-91.

2. Mitra A, Mulholland J, Nan A, McNeill E, Ghandehari H, Line BR. Targeting tumor angiogenic vasculature using polymer-RGD conjugates. J Control Release 2005;102(1):191-201.

3. Pastorino F, Brignole C, Marimpietri D, Cilli M, Gambini C, Ribatti D, Longhi R, Allen TM, Corti A, Ponzoni M. Vascular damage and anti-angiogenic effects of tumor vessel-targeted liposomal chemotherapy. Cancer Res 2003;63(21):7400-9.

4. Sachdeva MS. Drug targeting systems for cancer chemotherapy. Expert Opin Investig Drugs 1998;7(11):1849-64.

5. Bogenrieder T, Herlyn M. Axis of evil: molecular mechanisms of cancer metastasis. Oncogene 2003;22(42):6524-36.

6. Kim R, Toge T. Changes in therapy for solid tumors: potential for overcoming drug resistance in vivo with molecular targeting agents. Surg Today 2004;34(4):293-303.

7. Tung CH, Mahmood U, Bredow S, Weissleder R. In vivo imaging of proteolytic enzyme activity using a novel molecular reporter. Cancer Res 2000;60(17):4953-8.

8. Weissleder R, Tung CH, Mahmood U, Bogdanov A, Jr. In vivo imaging of tumors with protease-activated near-infrared fluorescent probes. Nat Biotechnol 1999;17(4):375-8.

9. McIntyre JO, Matrisian LM. Molecular imaging of proteolytic activity in cancer. J Cell Biochem 2003;90(6):1087-97.

10. Liu C, Sun C, Huang H, Janda K, Edgington T. Overexpression of legumain in tumors is significant for invasion/metastasis and a candidate enzymatic target for prodrug therapy. Cancer Res 2003;63(11):2957-64.

11. Suzawa T, Nagamura S, Saito H, Ohta S, Hanai N, Yamasaki M. Synthesis and HPLC analysis of enzymatically cleavable linker consisting of poly(ethylene glycol) and dipeptide for the development of immunoconjugate. J Control Release 2000;69(1):27-41.

12. Suzawa T, Nagamura S, Saito H, Ohta S, Hanai N, Kanazawa J, Okabe M, Yamasaki M. Enhanced tumor cell selectivity of adriamycin-monoclonal antibody

conjugate via a poly(ethylene glycol)-based cleavable linker. J Control Release 2002;79(1-3):229-42.

13. Bremer C, Tung CH, Weissleder R. Molecular imaging of MMP expression and therapeutic MMP inhibition. Acad Radiol 2002;9 Suppl 2:S314-5.

14. Bremer C, Tung CH, Weissleder R. In vivo molecular target assessment of matrix metalloproteinase inhibition. Nat Med 2001;7(6):743-8.

15. McIntyre JO, Fingleton B, Wells KS, Piston DW, Lynch CC, Gautam S, Matrisian LM. Development of a novel fluorogenic proteolytic beacon for in vivo detection and imaging of tumour-associated matrix metalloproteinase-7 activity. Biochem J 2004;377(Pt 3):617-28.

16. Zucker S, Cao J. Imaging metalloproteinase activity in vivo. Nat Med 2001;7(6):655-6.

17. Rossi LM, Quach AD, Rosenzweig Z. Glucose oxidase-magnetite nanoparticle bioconjugate for glucose sensing. Anal Bioanal Chem 2004;380(4):606-13.

18. Phadtare S, Vinod VP, Mukhopadhyay K, Kumar A, Rao M, Chaudhari RV, Sastry M. Immobilization and biocatalytic activity of fungal protease on gold nanoparticle-loaded zeolite microspheres. Biotechnol Bioeng 2004;85(6):629-37.

19. Tang D, Yuan R, Chai Y, Liu Y, Dai J, Zhong X. Novel potentiometric immunosensor for determination of diphtheria antigen based on compound nanoparticles and bilayer two-dimensional sol-gel as matrices. Anal Bioanal Chem 2005;381(3):674-80.

20. Liu J, Zhang Q, Remsen EE, Wooley KL. Nanostructured materials designed for cell binding and transduction. Biomacromolecules 2001;2(2):362-8.

21. Wang M, Sun C, Wang L, Ji X, Bai Y, Li T, Li J. Electrochemical detection of DNA immobilized on gold colloid particles modified self-assembled monolayer electrode with silver nanoparticle label. J Pharm Biomed Anal 2003;33(5):1117-25.

22. Zhang D, Chen Y, Chen HY, Xia XH. Silica-nanoparticle-based interface for the enhanced immobilization and sequence-specific detection of DNA. Anal Bioanal Chem 2004;379(7-8):1025-30.

23. Wilson CL, Matrisian LM. Matrilysin: an epithelial matrix metalloproteinase with potentially novel functions. Int J Biochem Cell Biol 1996;28(2):123-36.

24. Rudolph-Owen LA, Chan R, Muller WJ, Matrisian LM. The matrix metalloproteinase matrilysin influences early-stage mammary tumorigenesis. Cancer Res 1998;58(23):5500-6.

25. Yamamoto H, Adachi Y, Itoh F, Iku S, Matsuno K, Kusano M, Arimura Y, Endo T, Hinoda Y, Hosokawa M and others. Association of matrilysin expression with recurrence and poor prognosis in human esophageal squamous cell carcinoma. Cancer Res 1999;59(14):3313-6.

26. Adachi Y, Yamamoto H, Itoh F, Arimura Y, Nishi M, Endo T, Imai K. Clinicopathologic and prognostic significance of matrilysin expression at the invasive front in human colorectal cancers. Int J Cancer 2001;95(5):290-4.

27. Yamamoto H, Itoh F, Iku S, Adachi Y, Fukushima H, Sasaki S, Mukaiya M, Hirata K, Imai K. Expression of matrix metalloproteinases and tissue inhibitors of metalloproteinases in human pancreatic adenocarcinomas: clinicopathologic and prognostic significance of matrilysin expression. J Clin Oncol 2001;19(4):1118-27.

28. Crawford HC, Scoggins CR, Washington MK, Matrisian LM, Leach SD. Matrix metalloproteinase-7 is expressed by pancreatic cancer precursors and regulates acinar-to-ductal metaplasia in exocrine pancreas. J Clin Invest 2002;109(11):1437-44.

29. Hulboy DL, Gautam S, Fingleton B, Matrisian LM. The influence of matrix metalloproteinase-7 on early mammary tumorigenesis in the multiple intestinal neoplasia mouse. Oncol Rep 2004;12(1):13-7.

30. Frei E. Combination chemotherapy, dose and schedule. Cancer Medicine; 1997. p 817-837.

31. van Hensbergen Y, Broxterman HJ, Rana S, van Diest PJ, Duyndam MC, Hoekman K, Pinedo HM, Boven E. Reduced growth, increased vascular area, and reduced response to cisplatin in CD13-overexpressing human ovarian cancer xenografts. Clin Cancer Res 2004;10(3):1180-91.

32. van Hensbergen Y, Broxterman HJ, Hanemaaijer R, Jorna AS, van Lent NA, Verheul HM, Pinedo HM, Hoekman K. Soluble aminopeptidase N/CD13 in malignant and nonmalignant effusions and intratumoral fluid. Clin Cancer Res 2002;8(12):3747-54.

33. Akerman ME, Chan WC, Laakkonen P, Bhatia SN, Ruoslahti E. Nanocrystal targeting in vivo. Proc Natl Acad Sci U S A 2002;99(20):12617-21.

34. Ballou B, Lagerholm BC, Ernst LA, Bruchez MP, Waggoner AS. Noninvasive imaging of quantum dots in mice. Bioconjug Chem 2004;15(1):79-86.

35. Gao X, Cui Y, Levenson RM, Chung LW, Nie S. In vivo cancer targeting and imaging with semiconductor quantum dots. Nat Biotechnol 2004;22(8):969-76.

36. Welch AR, Holman CM, Browner MF, Gehring MR, Kan CC, Van Wart HE. Purification of human matrilysin produced in Escherichia coli and characterization using a new optimized fluorogenic peptide substrate. Arch Biochem Biophys 1995; 324(1):59-64.

37. Kioi M, Yamamoto K, Higashi S, Koshikawa N, Fujita K, Miyazaki K. Matrilysin (MMP-7) induces homotypic adhesion of human colon cancer cells and enhances their metastatic potential in nude mouse model. Oncogene 2003;22(54):8662-70.

38. Wang FQ, So J, Reierstad S, Fishman DA. Matrilysin (MMP-7) promotes invasion of ovarian cancer cells by activation of progelatinase. Int J Cancer 2005;114(1):19-31.

39. Furuya M, Ishikura H, Ogawa Y, Kawarada Y, Shibata M, Fujimoto S, Yoshiki T. Analyses of matrix metalloproteinases and their inhibitors in cyst fluid of serous ovarian tumors. Pathobiology 2000;68(6):239-44.

4.7 APPENDIX 4A

MATLAB SCRIPT FOR QUANTITATIVE GEL ELECTROPHORESIS ANALYSIS

```
clear all

for i=1
   A=imread([num2str(i) '.tif']);
   A=double(A(:,:,2));
   C(i,:)=[max(A(:)) min(A(:)) mean(A(:)) std(A(:))];
end

background=C(3);
clear C
for i=2:300
    A=imread([num2str(i) '.tif']);
    A=double(A(:,:,2));
    A=A-background;
    B=A(find(A>0));
    pixels=length(B);
    C(i,:)=[max(B(:)) min(B(:)) mean(B(:)) std(B(:))
pixels sum(B)];
    disp('Max')
 disp(C(:,1))
  disp('Min')
 disp(C(:,2))
  disp('Mean')
 disp(C(:,3))
  disp('Standard Dev')
  disp(C(:,4))
  disp('pixels')
  disp(C(:,5))
  disp('composite intensity')
  disp(C(:,6))
 end
```

CHAPTER V

CONCLUSIONS AND FUTURE DIRECTIONS

5.1 Summary

The work presented here traces the path of a specific targeting approach from the in-depth analysis of a specific cell surface protein to the design, synthesis, and *in vitro* performance of a targeted nanoscale construct. Complete characterization of any targeting system must begin with a comprehensive analysis of the target molecule. The current study utilizes fluorescently labeled mAbs to probe the surface of target cells in an *in vitro* environment to locate and quantify relevant target molecules (the CD13 protein). Studies were successful in quantifying the target concentration on these cells, as well as assessing the modulatory effects of several stimulating factors – exposure to low-dose ionizing radiation and incubation with the cytokines TNF-α and TGF-β1. Cell targets in an *in vivo* environment, however, are subjected to a range of possible modulatory factors. While the current study is unable to fully explore these options, it does reveal the significant effects these factors can evoke, and highlights the importance and utility of quantitative target analysis

By combining the features of nanoscale constructs with fluorescence detection, we were able to design a versatile multifunctional probe compatible with detection and imaging techniques readily available in many biological laboratories (e.g. fluorescence microscopy, fluorometry, flow cytometry). Work contained in this dissertation demonstrates the sensitivity and intense fluorescence emission of the QDs utilized as the

base of the targeting construct; a characteristic that facilitates detection of these probes at concentrations well below those required for conventional fluorophores. This ability presumably extends the capability of this system to detect rare event populations not detectable by traditional fluorescence techniques. Furthermore, the modularity conferred by the nanoparticle base enables customization of the construct for compatibility with a range of available detection methods from fluorescence (*e.g.* with QDs) to CT (*e.g.* with gold nanoclusters).

While presenting appealing characteristics, these native nanostructures do not possess any inherent activity. Surface functionalization was assessed as a means to mediate specific interaction with the *in vitro* environment. We were able to successfully conjugate multiple ligands to the surface of these nanoparticles, conferring a range of functionalities including reduced nonspecific interaction, targeted binding to cellular proteins, and specific susceptibility to enzymatic activity. *In vitro* analysis of these constructs reveals the capacity of surface functionalization to impart specific activity and significantly alter the characteristics of the entire nanoscale construct. Combining the functionality of surface-conjugated ligands with the physical and chemical characteristics of the underlying nanoparticle provides the basis for a versatile multifunctional probe capable of specific interactions with the immediate environment.

While only a handful of interactions are studied here, this work reveals the utility of small molecule ligands to impart specific activity and highlights the potential of nanoparticles as a base for these interactions. These studies trace the development of a targeted nanoscale probe from characterization of the target protein through synthesis and *in vitro* performance analysis of the targeted constructs. The strategies put forth in this

dissertation are highly effective in providing specific activity at target sites. Individually, these approaches can provide significant utility for both targeted delivery and biosensing. While these studies do not describe the characteristics of the complete PAT construct, individual elements assessed here lay the groundwork to achieve this goal. In addition, multiple levels of construct modularity enable customization of the targeting system to adapt to different targets, detection modalities, and delivery strategies. These advancements have the potential to provide a versatile system capable of providing features for targeted binding, imaging, biosensing, and therapeutic payload delivery in a single nanoscale particle, with the sensitivity, efficacy, and modularity not available in similar targeting strategies.

5.2 Future Work

While the studies toward the specific aims here comprise the entirety of this dissertation, the ultimate vision is the creation of a multifunctional NP with both tumor targeting and PA capability. In many cases, effective specific delivery requires more than a single recognition mechanism. The work outlined in this dissertation describes the components necessary to achieve this goal – design and implementation of a multifunctional proximity activated, targeted (PAT) system. Steps toward the realization of such a multifunctional surface-modified NP are described below.

5.2.1 Optimization

Before the success of a PAT system can be realized, each component targeting approach must be optimized to ensure maximal sensitivity and efficacy. One major

variable in targeting performance is the length of the PEG chains utilized for both specific targeting (*i.e.* PEG-NGR) and in the PA component (*i.e.* PEG-peptide$_{MMP7}$-PEG). Initial PEG lengths were chosen to minimize steric effects (spacing from the nanoparticle surface) and to achieve surface passivation. Variation of PEG chain length has the potential to significantly modulate both specific binding and enzyme susceptibility. However, as overall particle size is expected to significantly affect construct mobility *in vivo*, optimization of PEG chain length should be performed to maximize targeting efficiency while minimizing overall construct diameter.

A second major variable subject to optimization is the surface density of each targeting component. In the studies presented here, reaction conditions were chosen to maximize ligand conjugation. However, modulation of ligand surface density is expected to be a considerable factor for overall targeting efficiency. The effects of ligand density must be analyzed in the context of specific binding effects and susceptibility to enzyme cleavage. These results can then be used as the basis to optimize ligand density in the composite PAT system.

Molecular modeling of these characteristics has the potential to streamline the optimization process. Detailed molecular modeling of the contributions of each variable (*e.g.* PEG, enzyme substrate, ligand density) has the potential to predict performance, enabling optimization of structural characteristics while minimizing the experimental burden.

5.2.2 PAT synthesis

While the efficacy of each targeting strategy (*i.e.* specific homing to target cells and cleavage by a tumor-specific enzyme) has been characterized, the composite PAT structure has not yet been synthesized or analyzed. Colocalization of both targeting elements on the surface of a single nanoparticle can be accomplished by combining elements described in this dissertation. To facilitate construct synthesis, the linking chemistry (N-terminal primary amine) has been conserved between both the targeting and PA components. Attachment of these constructs to the QD surface can occur by mixing the desired amounts of targeting ligand and PA construct and following the attachment protocol outlined in the current studies. As both constructs utilize the same reaction chemistry and protocol, attachment to the QD surface is expected to occur with similar efficiency. The difference in molecular masses of the two classes of molecular surface conjugates may modulate reaction kinetics and require adjustment to the vision of translating solution stoichiometry to relative surface concentrations. Purification of the final PAT structure can be conducted by size exclusion using spin filtration as previously described.

5.2.3 Assessment of PAT construct cleavage and binding properties

Validation of QD-PAT synthesis is not possible by the methodology utilized for either QD-PEG-NGR or QD-PA constructs, as these techniques are not capable of simultaneous measurement of both targeting and PA structures. Thus, these proposed studies serve both as a validation of QD-PAT synthesis, as well as a functional validation of both the cleavage and binding properties of the construct.

In initial studies, the cleavage and binding properties of PAT QDs can be measured independently. Construct susceptibility to exogenous MMP-7 can be assessed as described earlier for QD-PA constructs. After exposure to MMP-7, gel electrophoresis can be performed to qualitatively assess construct cleavage. QD constructs can then be purified by spin filtration and their emission profiles measured by fluorometry. Fluorometric measurements taken prior to and after cleavage are then compared to quantitatively determine the extent of construct cleavage from the QD surface.

Once the PA structures have been cleaved from the surface, the binding properties of the resulting targeted QDs can be determined. A solution containing these pre-cleaved constructs can be added above a monolayer of target cells as previously described in Aim II. Following incubation and washing, fluorescence microscopy can be used to visualize construct binding to the cell surface. Flow cytometry can then be performed on the dissociated cell samples to quantitatively determine the extent of QD binding.

This method effectively decouples the cleavage and binding processes, as each can be measured quickly and independently. Furthermore, pilot studies reduce the complexity of the system by removing the intricate processes and variables associated with cellular experimentation. Once the success of each process is verified in the PAT structure, additional cleavage and binding studies can be performed.

Once PAT construct cleavage and binding has been confirmed and validated in pilot studies, these properties can be assayed in *in vitro* cellular environments. Construct cleavage can be assessed as described in Aim III. Briefly, PAT QDs are added to cell monolayers in culture. Following incubation, culture medium is sampled. MALDI-TOF may potentially be used to determine the presence of cleavage products in the culture

medium samples. QD particles remaining in solution can be purified by spin filtration and cleavage assessed by fluorometry and gel electrophoresis.

Cellular binding of the cleaved PAT QDs can be assessed as described for QD-PEG-NGR particles in Aim II. Culture media is aspirated and the cell monolayers are washed thoroughly with fresh PBS to remove any unbound QDs. Adherent cells are removed from the surface via treatment with a nonenzymatic dissociation solution and analyzed by flow cytometry. QD binding is assessed quantitatively by application of standard curves for conversion of measured fluorescence values.

5.2.4 Possible limitations

As this anticipated work is a combination of Specific Aims II and III of this dissertation, all limitations described in those sections are applicable here. In addition, the cleavage and binding characteristics of PAT QDs may differ significantly from those of QD-PEG-NGR and QD-PA constructs, and may be insufficient for effective NP targeting. Once the cleavage and binding properties of these particles are determined, PAT QD functionality can be optimized to maximize both processes. PEG length can be varied to modulate both enzyme access and binding characteristics, materially affecting the performance of the particle. Furthermore, QD surface density and ratio of both PEG-NGR and PA constructs can be varied to optimize performance of the final construct.

5.3 Protection of Research Subjects

No live animals were required for the completion of this work, and all animal-derived tissue use has been minimized. Animal-derived tissue was utilized in a fashion to

minimize the total number of animals necessary. Primary and immortalized human cell lines were purchased directly from established vendors that comply with legal standards for collection and use of these cell lines.

Appropriate training on general lab safety, standard chemical, biological and radiation safety, and animal techniques and procedures was performed for personnel involved in this study in compliance with institutional guidelines.

5.4 Societal Implications

Legal and ethical concerns of this work are minimal, as it extends prior work to target established therapeutics to a major source of worldwide morbidity and mortality. Successful development of the nanoparticulate constructs envisioned here has the potential for significant economic results, including the production of intellectual and physical property of substantial value to both the developing institution and any potential industrial partners.